UNIVERSITY OF SOUTHAMPTON

FACULTY OF NATURAL AND ENVIRONMENTAL SCIENCE

School of chemistry

Molecular dynamic studies of the antimicrobial peptide Dermaseptin B2 and its derivative Dermaseptin DS01

by

Malaz Elhussein

Thesis for the degree of Master of Philosophy

September 2015

UNIVERSITY OF SOUTHAMPTON

ABSTRACT

Rapid development of resistance to antimicrobials and the lack of new therapy development are critical issues facing infectious disease treatment globally. Over the past two decades, antimicrobial peptides (AMPs) have been extensively researched and shown to exhibit broad-spectrum activity against various microbes, viruses, fungi and even cancerous cells, thus they are thought to have the solution to the increasing resistance problem. Understanding the role that antimicrobial peptides play in preventing infections is essential if these peptides are to form a new class of clinically effective antimicrobial agents and for them to be used therapeutically in humans.

This research will look at a family of antimicrobial peptides known as Dermaseptin that are secreted by an Amazonian frog species. These peptides have shown potent activity against Gram-negative and positive bacteria, viruses, fungi and cancer cells. They exhibit bacterial colony inhibition effect at the micromolar concentration level with minimal effect on host cells. For its high potency and lack of toxicity to host cell, the Dermaseptin family appears to have therapeutic potential and this thesis will attempt to understand how they interact with membranes at the molecular level using coarse-grained computational models and simulations.

FACULTY OF NATURAL AND ENVIRONMENTAL SCIENCE

Chemistry

Thesis for the degree of MPhil

MOLECULAR DYNAMIC STUDIES OF THE ANTIMICROBIAL PEPTIDE DERMASEPTIN B2 AND ITS DERIVITATVE DERMASEPTIN DS01

Malaz Elhussein

Table of Contents

List of Tables

List of Figures

List of graphs

DECLARATION OF AUTHORSHIP

I, Malaz Elhussein declare that this thesis and the work presented in it are my own and has been generated by me as the result of my own original research.

Title of thesis:

Molecular dynamic studies of the antimicrobial peptide Dermaseptin B2 and its derivative Dermaseptin DS01

I confirm that:

1. This work was done wholly or mainly while in candidature for a research degree at this University;

2. Where any part of this thesis has previously been submitted for a degree or any other qualification at this University or any other institution, this has been clearly stated;

3. Where I have consulted the published work of others, this is always clearly attributed;

4. Where I have quoted from the work of others, the source is always given. With the exception of such quotations, this thesis is entirely my own work;

5. I have acknowledged all main sources of help;

6. Where the thesis is based on work done by myself jointly with others, I have made clear exactly what was done by others and what I have contributed myself;

7. Parts of this work have been published as:

Interaction between the NS4B amphipathic helix, AH2, and charged lipid headgroups alters membrane morphology and AH2 oligomeric state — Implications for the Hepatitis C virus life cycle

Signed: .....

Date:.....

Acknowledgements

This research project was a draining yet educationally rewarding journey that I have thoroughly enjoyed. In full gratitude, I would like to acknowledge the following individuals who encouraged, inspired, supported and assisted me in my pursuit of a postgraduate degree.

Firstly, I would like to thank my supervisor, Dr Syma Khalid, for the continuous support throughout my Masters study and related research, in particular, for her patience, motivation, and immense knowledge. Her guidance was much appreciated throughout this endeavor and she has been a great mentor and adviser during the academic year.

Besides my supervisor, I would like to thank my colleagues and friends for their help in understanding and using GROMACS and the various other programs and their insightful comments and encouragement that incentivized me to widen my research from various perspectives. Without their precious support, it would have been impossible to conduct this research.

I also thank them for the stimulating discussions; for their encouragement through many sleepless nights that I spent working and trying to meet deadlines; and for all the fun we have had over the year.

Last, but by no means least, I would like to thank my parents to whom I dedicate this thesis as a small token of appreciation for their unconditional love, support and encouragement. If not for their backing and confidence in my abilities, it would have been impossible to achieve anything in life. They provided me with a loving and optimistic home that has enabled every step of my life and I am eternally indebted to them.

I am deeply grateful to you all, and forever appreciative.

Definitions and Abbreviations

POPC: 1-palmitoyl-2-oleoyl-sn-glycero-3-phosphocholine

POPG: 1-palmitoyl-2-oleoyl-*sn*-glycero-3-phospho-glycerol

POPE: 1-palmitoyl-2-oleoyl-*sn*-glycero-3-phosphoethanolamine

PIP2: Phosphatidylinositol 4,5-bisphosphate

PI4P: Phosphatidylinositol 4-phosphate

MRSA: Methicillin-resistant Staphylococcus aureus

NMR: Nuclear Magnetic Resonance

MIC: Minimum Inhibitory Concentration

WHO: World Health Organization

LL-37: only human member of the cathelicidin family of antimicrobial peptides

AMR: Antimicrobial resistance

VMD: Visual Molecular Dynamics

PBP: penicillin binding peptides

PABA: para-aminobenzoic acid

AMP: antimicrobial peptides

ATP: adenosine triphosphate

LPS: Lipopolysaccharide

Ara4N: 4-amino-4- deoxy-T-arabinose

SH: sulfhydryl groups

Chapter 1: Dermaseptin – The next class of Antibiotics?

1.1 Introduction

In 1928, Alexander Fleming found that mould contaminated his Petri dishes. Upon examining the Petri dishes, he discovered that the mould produced a substance (now known as penicillin) that had killed off the bacteria which he was studying (1). In time, Fleming, with help from the scientific community, turned this fortunate coincidence into the penicillin class of antibiotics that has revolutionised healthcare and has saved the lives of many (approximated at 200 million by the new world encyclopaedia) (1). As research into antibiotics intensified, further groups and classes of medication were discovered that varied in efficacy, potency and mechanisms of action and which were pushed into the healthcare market to combat infectious diseases (2). Penicillin and the vast other classes of antibiotics that followed have been effective for many decades and, without fail, have rendered once deadly infections to be completely treatable (2). Unfortunately, the effectiveness of antibiotics has now become questionable as disease-causing organisms have started to develop various mechanisms of resistance to avoid eradication. As science advanced, more targets through which organisms can be eradicated were found, but the microorganisms have evolved and developed new mechanisms of resistance. These methods of resistance, usually acquired either through genome mutation or the acquisition the resistance gene, coupled with the evolutionary incentive to survive, have been passed down bacterial colonies and slowly, over time, widespread multiple drug resistant strains of microorganisms have dominated the microbial kingdom (1).

Given the lack of novel antimicrobial discovery and the desperate demand for new effective antimicrobial drugs, resistance is threatening rapidly modern science's best medicinal advancement in combatting infectious diseases. With the continued emergence of new antimicrobial resistant bacterial colonies and the widespread sharing of the resistance genes, it seems that doing nothing could send humanity back towards the pre-antibiotics era (3) whereby simple microbes causing once treatable infections can once again become life threatening. Infections, such as pneumonia,

tuberculosis and bacterial meningitis that were once treatable and had a high survival rate once again could become deadly in many cases (4, 5).

This possibility of all currently available antibiotics becoming obsolete is now driving intense research into other potential sources of antimicrobials. Science is now exploring nature as a potential source of possible compounds since, for quite some time, there has been no discovery of synthetic antibiotics. Naturally secreted antimicrobial peptides by animal and plant kingdoms seem to have high potential in some studies and, consequently, at present, these are being explored further (6).

Currently, the Carbapenems is one class of antibiotics used when all other therapies are ineffective in the treatment of multidrug-resistant infections such as MRSA.

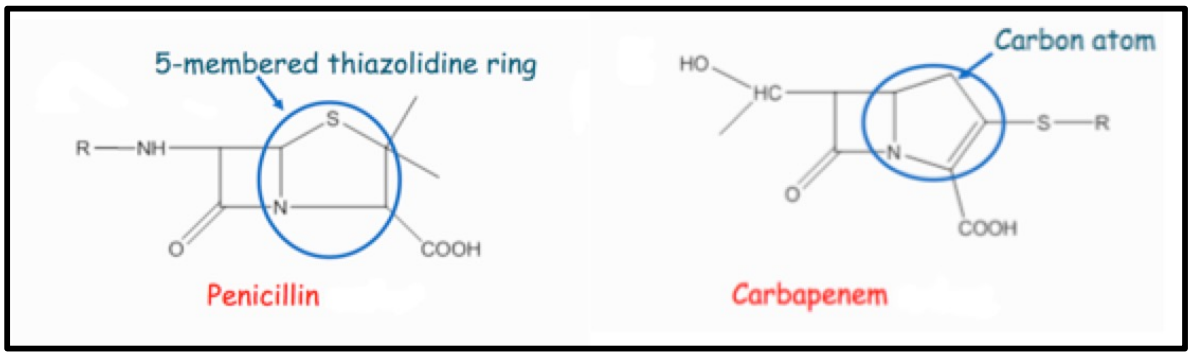

Figure 1 Core Structures for Penicillin and Carbapenem.

Carbapenems is a class of antibiotics that falls amongst the β-lactam ring group of antibiotics. It works by binding to Penicillin-Binding Peptides (PBPs) and inhibiting cell wall synthesis. They have a broader spectrum of activity when compared to other similar antibiotics in the classes (Penicillin and Cephalosporin) and, unlike most antibiotics in this class, they can resist hydrolysis by most β-lactamases produced by bacteria (7).

Figure 1 above shows the core structures for Penicillin and Carbapenem. As shown, the fundamental difference between the two structures is that Carbon 1 in the Carbapenem ring substitutes the sulphur group in the Penicillin ring, namely the β-lactam ring, which creates a fused ring in the Carbapenem structure. There is, also, a double bond between carbons 2 and 3 in Carbapenem that makes it an unsaturated ring structure which is not present in the Penicillin structure. There is, also, a significant difference between the side chains of the two antibiotics, the stereochemistry of the hydroxyethyl side chain in Carbapenem that produces both an

antimicrobial effect and resistance to β-lactam hydrolases produced by bacteria (7). The changes in the β-lactam ring in Carbapenem are significant enough for the β-lactamase not to recognize the structure and, consequently, are not hydrolysed as in the case of Cephalosporin and Penicillin.

When considering the amounts of funds a pharmaceutical company would need to invest into developing new antibiotics and the limited incentives to invest due to the projected lack of returns from sales (due to scarcity of use in preventing resistance), there has been a drastic reduction in the development of antibiotics. This has resulted in a large void of discovery spanning from the 1980s to the present day (8).

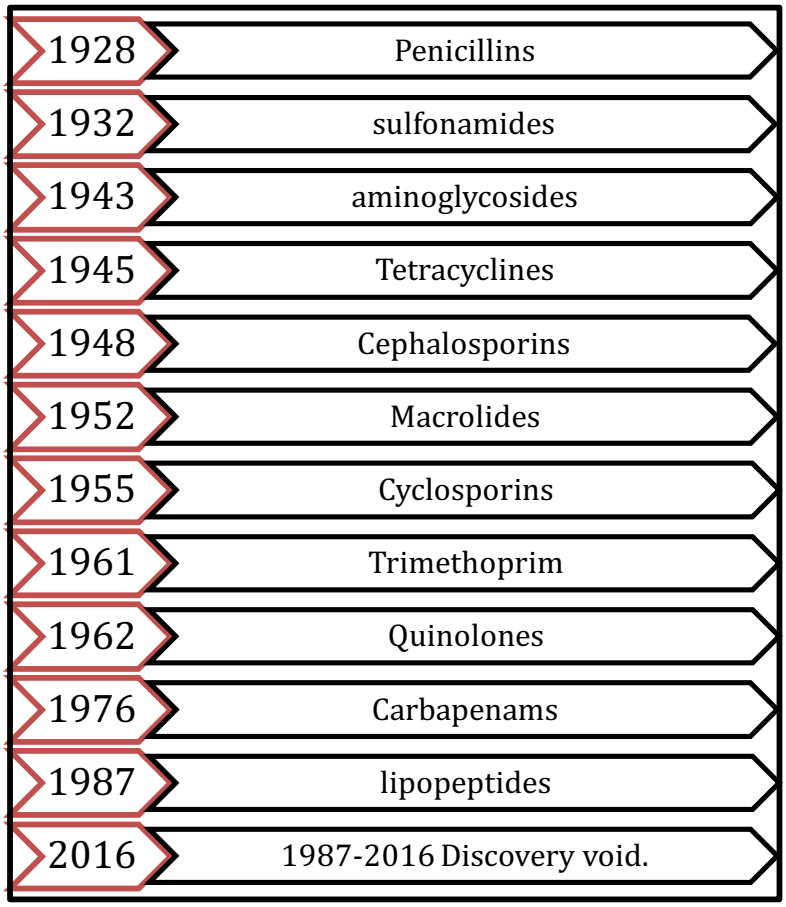

Figure 2 Brief timeline depicting the discovery of various antibiotic classes. The timeline shows a discovery void from the year 1987 to the present day.

Antibiotic resistance spreads from organism to organism through the sharing and transfer of genes that code for resistance amongst a bacterial colony. Incorrect use of antibiotics within the industrial, agricultural and healthcare sectors facilitate this transfer of resistance gene from one bacterial colony to another (9).

The agricultural industry uses antibiotics to boost their yields both in crops and livestock. Antibiotics are added to animal feeds at low doses to act as growth factors by preventing (and not curing) infections that can potentially halt the livestock's growth (9). Antibiotics are also added to water used for watering plants (which animals may drink) for the same purpose. By always abusing antibiotics in this way, the industry is exposing bacterial cells continuously to low sub-therapeutic doses of antibiotics and this gives bacterial cells an opportunity to develop and pass on resistance. Humans expose themselves to the new resistant strain of bacteria through exposure to low doses of antibiotics either in the meat, fruits and vegetables that they consume or through drinking contaminated water and, thus, giving rise to resistant strains of endogenous bacteria (natural micro-flora) (10,11).

The WHO in 2014 states the health sector's contribution to the problems is via the inappropriate prescribing of antibiotics and the lack of patient adherence to their courses of antibiotics (12).

In an infective bacterial colony, there will be some bacterial cells that are resistant (either naturally resistant or have acquired the resistance gene) to the used antimicrobial compound (9). Consequently, when an antibiotic course is prescribed and used, the susceptible bacteria are killed off leaving behind the resistant strain. The few remaining resistant bacteria are now in a nutrient rich environment with minimum competition and begin to divide and flourish and create a new colony of resistant bacteria that is now the dominant strain. This is an evolutionary phenomenon known as the survival of the fittest (12). This concept is illustrated in figure 3 below.

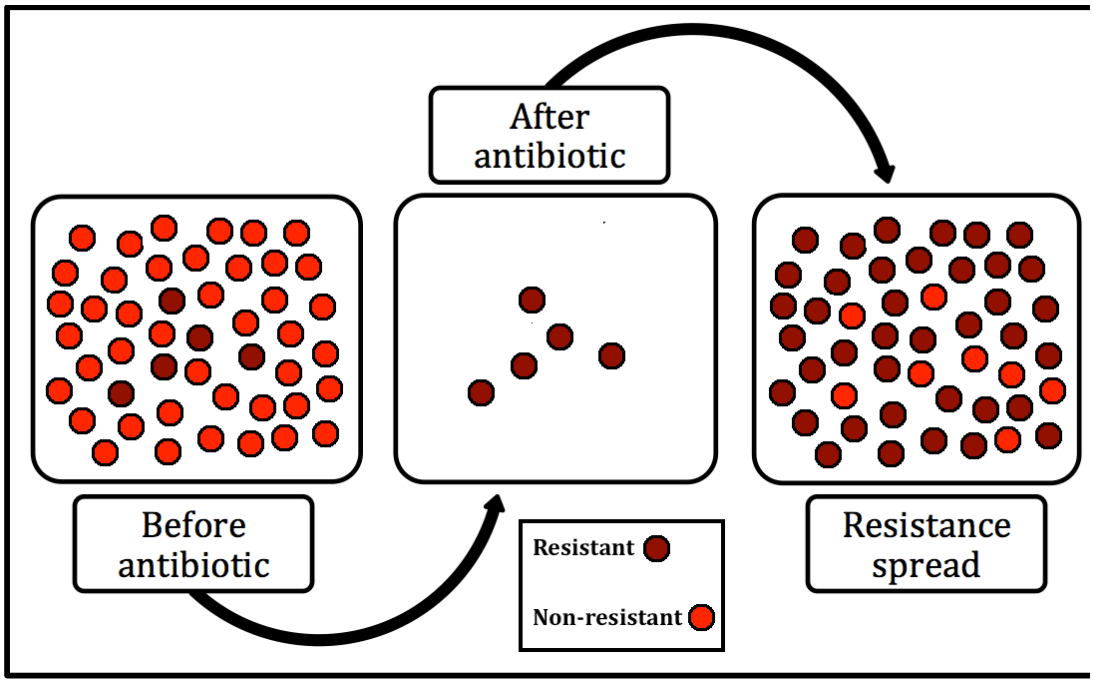

Figure 3 **Illustration showing how inappropriate prescribing or incompletion of antimicrobial course can cause antibiotic resistance. The before prescribing box shows a bacterial colony with few resistant bacteria amongst them, the after-antibiotic box shows how all the non-resistant bacteria have been killed off leaving the resistant bacteria to grow and multiply. The last box shows the resistant bacteria dominating the bacterial colony.**

Some steps have been taken towards the reduction of the spread of antimicrobial resistance but, in no way, do these take the pressure off the need to discover new antibiotics. In the EU, the agricultural regulatory office has banned the regular use of antibiotics in animal feeds (13). Widespread public awareness (in the form of posters and leaflets) targeting doctors and patients explaining the importance of finishing an antimicrobial course and only prescribing antimicrobials, when necessary, have flooded health care providing organisations (14). Doctors are also encouraged, where possible, to determine whether an infection is viral or bacterial and to carry out susceptibility testing where bacteria is involved to aid antimicrobial selection (9). Ultimately, all measures, currently in place, aim to contain the spread of resistance until an absolute solution can be found in the form of a new class of antibiotics that is

cheap to both produce and distribute along with the ability to resist antimicrobial resistance (14).

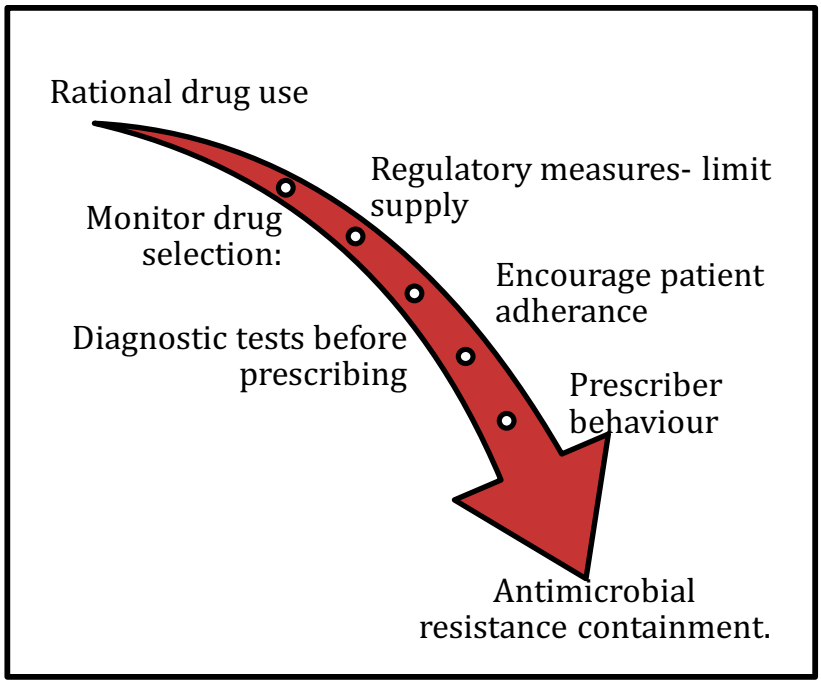

Figure 4 Steps that are currently taken to contain the spread of antibiotic resistance.

1.2 Antibiotic resistance

There are several mechanisms through which a microorganism can acquire resistance; all of which are facilitated by human intervention (15). Microbes have remarkably complex genetic makeups that allow them to evolve as fast as their surroundings permit. They are, also, incredibly unselfish organisms that share genetic information to achieve a dominant survival trait and this makes it tough to contain resistance.

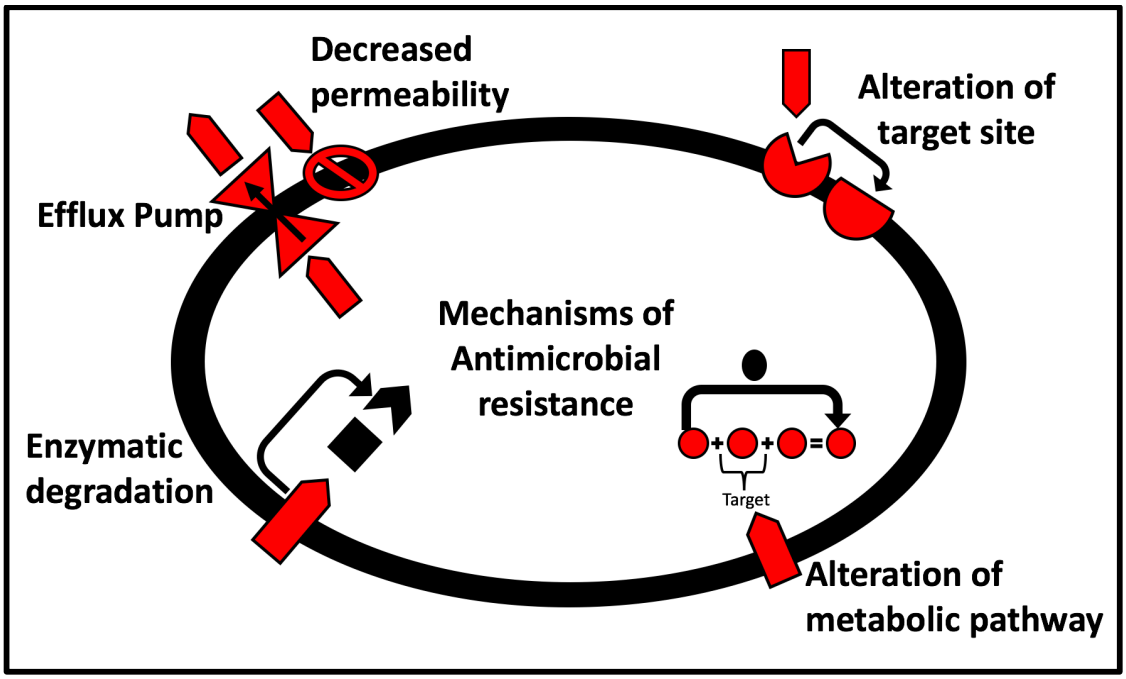

Figure 5 Diagrammatic representations of the various methods of the methods of antimicrobial resistance.

Antibiotic resistance occurs through one of the three mechanisms shown diagrammatically in Figure 5 above. As shown, most of the mechanisms are mediated by the bacterial plasmid which contains a variety of genes that code for many resistance mechanisms ranging from enzymes to degrade drug molecules to genes that result in the formation of efflux pumps, drug target modifiers and the modification of metabolic pathways used by the bacteria (16).

Table 1 shows the most common antibiotics and the primary means of resistance in the bacterial population.

Antibiotic	**Method of resistance**
β-lactams (Penicillin, Cephalosporin)	Inactivation via enzymatic action (β-lactamase)
Aminoglycosides	Inactivation by Acetyltransferase enzyme
Macrolides	Ribosome protection/target site modification (methylation of target site)
Quinolones	Mutation/alteration of target site
Tetracycline	Ribosomal protection enzyme/modification of active site.
Trimethoprim	Mutation of binding site (mutation of target enzyme)

Table 1 Table indicating the major classes of antibiotics and the methods of resistance microorganisms acquire to avoid eradication by them.

1.3 Methods of antimicrobial resistance:

It is thought that bacteria can resist eradication by antibiotics through either one or a combination of two or three of the methods described below.

1.3.1 Changing drug target:

This method of resistance develops usually through a genetic mutation that changes the drug target within the organism. Through these mutations, the bacterium can modify proteins, receptors or even metabolic pathways that are targeted by antimicrobials so that they are unable to recognise, bind to and act on their target

(15). Often, changing a drug target can render whole classes of antibiotics ineffective, since they frequently have one common mechanism of action.

There are two ways in which bacteria can alter the antibiotic target:

Alteration of the target site:

This can include either changing an enzyme active site or modifying cell wall proteins or modifying the drug target. An example of this mechanism at work is the alteration of the penicillin-binding pocket on the penicillin binding peptides within MRSA bacterium that makes them unable to recognize and bind penicillin molecules. Another example is the presence of ribosomal protection proteins that protect the bacterial cell from antibiotics, which target the cell's ribosomes to inhibit protein synthesis. Tetracycline is thought to inhibit protein synthesis by binding to the 30S subunit of the ribosome with high affinity and inhibiting protein synthesis. Ribosome protection proteins (Examples of which include Tet(O) and Tet(M)) can increase the dissociation factor of tetracycline. It is unclear how they do that, however, a proposed mechanism suggests that Tet (O) triggers the dissociation of tetracycline through an allosteric conformational change that alters the shape of the ribosome and, thereby, dislodging tetracycline from it (17).

Alteration of metabolic pathway:

Sulfonamides in a bacterial cell act as competitive inhibitors of the enzyme dihydropteroate synthase (DHPS), which is involved in folate synthesis (18). By binding to this enzyme, they prevent the substrate para-aminobenzoic acid (PABA), an important precursor in the synthesis of folic acid and nucleic acids, from binding and, thus, inhibit folate and nucleic acid synthesis. When sulfonamides bind to DHPS enzyme, they only inhibit the growth of the bacteria rather than killing it and clearing it from the body. However, they still control the infection and give the body's immune system time to eliminate it. Sulfonamide-resistant bacteria have modified their folate synthesis metabolic pathway and, consequently, they do not require para-aminobenzoic acid (PABA) and, even in the presence of the antibiotic, can go on making folic acid and nucleic acids (19).

These types of resistance often take some time to develop. However, the process has been accelerated by over-prescribing of antimicrobials, particularly when they are not needed, and inadequate patient adherence to the course of treatment (12).

1.3.2 Drug inactivation:

Drug inactivation is where bacterium develops a mechanism, enzymatic or otherwise, through which they inactivate the antibiotic molecules. The most common example is the hydrolytic deactivation of the β-lactam ring by β-lactamase that abolishes the effectiveness of the Penicillin and Cephalosporin. This resistance, like the previous example of changing drug target, takes some time to develop and can be transferred amongst colonies via gene acquisition (20).

1.3.3 Reduced drug accumulation:

This type of resistance is notably unspecific and can render many classes of antibiotics ineffective. Reduced drug accumulation can be caused by either cell wall or membrane modification resulting in a lack of membrane permeability to the antimicrobial agent or by the development of a recognition mechanism for toxic molecules triggering their removal via an efflux pump. This method is very effective against a wide variety of antibiotics and, potentially, can become disastrous if applied to any new class of antibiotic discovered and introduced into the healthcare market (21).

Microorganisms are rapidly developing new means of resistance to combat antimicrobials. These took several hundred years to find and several decades to increase in variety and, for years, have been used successfully to save lives. It seems that the need to update Fleming's efforts is rapidly becoming a necessity. With that in mind and the lack of possibilities of discovering a new synthetic chemical compound with antimicrobial properties, attention has turned to naturally occurring immune proteins for the next class of antibiotics.

1.4 Immune system

The human immune system is a complex network of cells and peptides that work together to defend efficiently against invading organisms.

With the lack of discovery of new antimicrobial compounds, the loss of antimicrobial potentials in currently used antibiotics and rapidly developing resistance to current antimicrobials, it is possible that the answer to the antimicrobial resistance crisis can be occurring naturally. All living organisms have some defensive mechanisms capable of mounting a chemical or physical attack against invading organisms so that they can survive. It could be possible to extract an antimicrobial from such an organism and use it in a therapeutic setting.

The human immune system is incredibly complex and efficient in dealing with invading organisms. It can differentiate between self and non-self-cells which it encounters and can react quickly and initiate an attack against non-self- cells and destroy them. It is split into two main branches both summarised in Table 2 (shown below) (22).

Adaptive immune system	**Innate immune system**
Pathogen and antigen specific response	Response is non-specific
Lag time between exposure and maximal response	Exposure leads to immediate maximal response
Cell-mediated and humoral components	Cell-mediated and humoral components
Exposure leads to immunological memory	No immunological memory
Found only in jawed vertebrates	Found in nearly all forms of life

Table 2 Table summarising the main differences between the adaptive and innate immune systems.

1.4.1 Adaptive immunity

Adaptive immunity develops over time, during which the body is exposed to many pathogens and defends itself accordingly. It is highly specific in its responses that are usually chemical based. It uses the various white blood cells of the body to generate antibodies against an invading organism and uses those antibodies to either kill the microorganism directly or to recruit other immune cells (such as phagocytes, natural killer cells and lymphocytes) into the destruction procedure. This method of defence has the advantage of immunological memory and, thereby, faster response in cases of re-infection by the same pathogen (22).

1.4.2 Innate immunity

Innate immunity is a nonspecific defence mechanism that comes into play immediately or shortly after an antigen appears in the body. It is the immunity one's born with and it is relatively unspecific in its responses which often are physical rather than chemical. It relies upon barrier protection (for example the skin) to physically prevent microorganisms from entering the body and cells that destroy infected host cells (phagocytes, natural killer cells, etc.). When using phagocytes or natural killer cells, the response is usually mechanical, whereby cells, identified as non-self, are destroyed via phagocytosis (where a cell is taken up and digested by phagocyte cells) rather than an antibody-based procedure.

The innate system also uses basic peptides known as antimicrobial peptides; that rapidly form pores in bacterial membranes and bring about cell lysis. The antimicrobial peptide part of the innate immune system was relatively unexplored until recently where peptides extracted from various insects, plants and amphibians were shown to act potently against viruses, bacteria, fungal and have gone as far as promoting apoptosis of cancerous cells (22). These are the peptides that the body creates naturally and releases in response to an infection to defend itself. Being a part of the innate immunity, they form a first line defence mechanism and, therefore, they need to be synthesised in areas of the body that are exposed continuously to pathogens for rapid response i.e. in humans the skin has the highest possibility of encountering and recognising pathogenic cells and, thus, it is mainly responsible for antimicrobial peptide secretion. These peptides are typically short and have an

amphipathic structure that allows them to penetrate and exit cells easily as well as giving them a desired non-specificity when it comes to attacking foreign cells (22).

1.5 Phospholipid containing membranes

Membranes are fundamental to maintaining healthy cellular function. Most living organism's cellular membranes are composed of a lipid bilayer in the form of a continuous barrier surrounding the cell. A cell membrane acts as a barrier to the free movement of molecules including water, ions, and proteins; this is vital to maintaining normal cellular function. The lipids in the bilayer are partially hydrophobic and, therefore, they limit movement of water (water is still able to get through the membrane slowly via embedded water channels or by osmotic diffusion to regulate concentrations across the membrane) and water-soluble molecules and the tight packing of lipids obstruct movement of larger molecules such as proteins.

Most lipid bilayers are made of phospholipids. These lipids are composed of a hydrophilic head group and two hydrophobic fatty acid tails (as shown in Figure 6 below). When these lipids are placed in an aqueous environment, they arrange themselves into two layers with the tails of all the lipids surrounded by the hydrophilic headgroups, the latter being exposed to the environment.

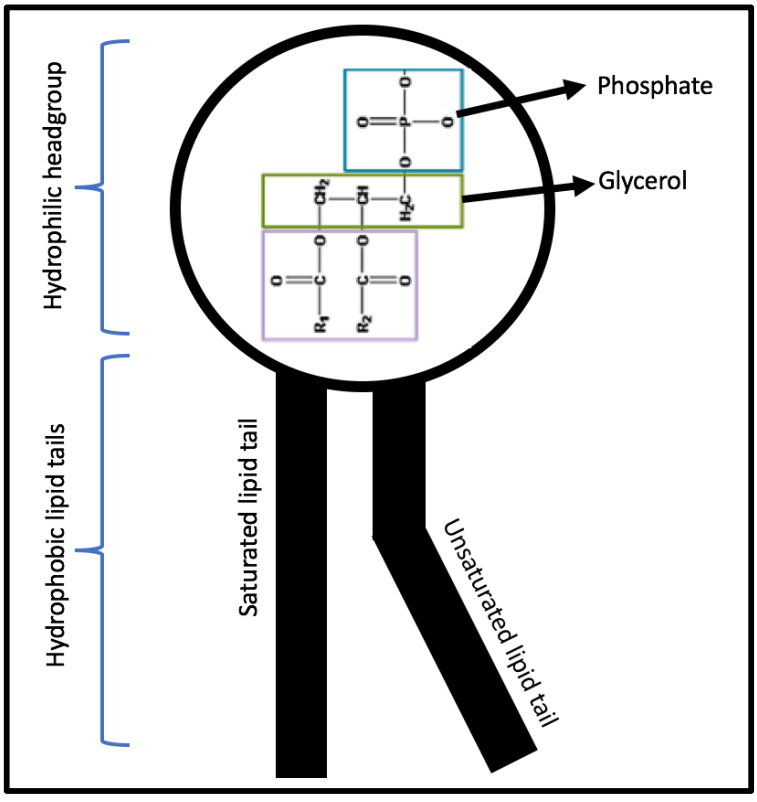

Figure 6 **Diagram of a phospholipid, the building block of cellular membranes. The diagram shows the hydrophilic headgroup with its phosphate group and the hydrophobic fatty acid tails.**

The headgroups on a phospholipid can affect the overall charge of the membrane. POPC (1-palmitoyl-2-oleoyl-sn-glycero-3-phosphocholine), which is present in most mammalian cells, is a neutral lipid with a headgroup having a negative charge on phosphate group and a positive charge the choline group. Another lipid that has no overall charge is the zwitterionic POPE (1-palmitoyl-2-oleoyl-*sn*-glycero-3-phosphoethanolamine).

There are some lipid headgroups that are charged and depending on the overall membrane phospholipid composition they can influence the membrane's overall charge. An example of such lipids is POPG (1-palmitoyl-2-oleoyl-sn-glycero-3-phosphoglycerol). The phospholipid headgroups can have, also, either individual anchoring or signaling properties that have biological significance and, in the case of charged lipids, they can affect the electrostatic interactions of the bilayer with small charged molecules (23).

The ratios of phospholipids affect the overall properties of the lipid bilayer; including the phase transition temperature. This is the temperature at which the lipid bilayer adopts a solid gel state from the original fluid state of a membrane. The bilayer is held together in part by Van der Waals forces between the tails of adjacent lipids. Thus, the size of the lipid tails influences the number of interactions that can occur and, in turn, the mobility/fluidity of the bilayer. Longer tails provide a large surface area for interactions; this increases the strength of interactions and, thereby, reduces the overall mobility or fluidity of the bilayer. This means that, at any given temperature, bilayer, composed of long-tailed phospholipids, are less fluid than those consisting of short-tailed phospholipids. (24).

The phase transition temperature of the bilayer also depends on the saturation of the lipid tails. Phospholipids with many unsaturated tails have a lower phase transition temperature when compared to ones with saturated tails. This is because unsaturated lipids have double bonds between some carbons in the lipid tail that produce a kink. The presence of the kink in the tails disrupts the packing of the lipids in the bilayer. This kinking leads to a loosely packed bilayer with free space within the bilayer for the lipid tails to move, break and form loose Van der Waals connections with neighboring lipids and to form a more fluid bilayer with a low phase transition temperature.

Saturation of the lipid tails is a very influential determinant of phase transition temperature and, as shown in Table 3, has more of an effect on the temperature than the length of the fatty acid tails (24).

As shown in Table 3, the addition of one carbon atom to the lipid tail carbon backbone increases the phase transition temperature by about 10 °C while adding a single, double bond to the fatty acid tail reduces the phase transition temperature by 50°C. This is a significantly more powerful influence (24).

Tail Length	Number of double bonds	Phase transition temperature (°C)
12	0	-1
14	0	23
16	0	41
18	0	55
20	0	66
22	0	75
24	0	80
18	1	1
18	2	-53
18	3	-60

Table 3 Phase transition temperature (in °C) as a function of tail length and saturation (24).

Lipid bilayers are difficult to study and to explore via experimental means. The presence of phospholipids in them creates an environment that is both hydrophobic and hydrophilic in nature. This makes these bilayers difficult to study experimentally and, therefore, they are often studied computationally. Since this limitation of environment does not apply to computational methods, looking at bilayers computationally has helped understand these structures and appreciate their functions in more detail (25). Experimentally, there are many methods that study lipid bilayers, examples include fluorescence microscopy, crystallography (which provides a detailed atomic structure of various lipid structures), electron microscopy (which offers higher resolution imaging) and NMR (which can potentially provide a wide range of information about the bilayer packing, phase transition, and lipid headgroups etc.) (26, 27).

1.6 Bacterial cell membranes

There are two types of bacteria, Gram negative and Gram Positive (classification is based on the Gram stain test). There are two types of bacteria; Gram negative and Gram Positive (classification is based on the Gram stain test) which differ in cell structure (difference summarized in table 4 below and illustrated in figure 7). Gram-Positive bacteria has a thick peptidoglycan layer whereas Gram-Negative bacteria have a smaller peptidoglycan later but have an outer membrane as well as the inner membrane (30). In general Gram-Negative bacteria is more resistant to antimicrobials compared to Gram-Positive (30).

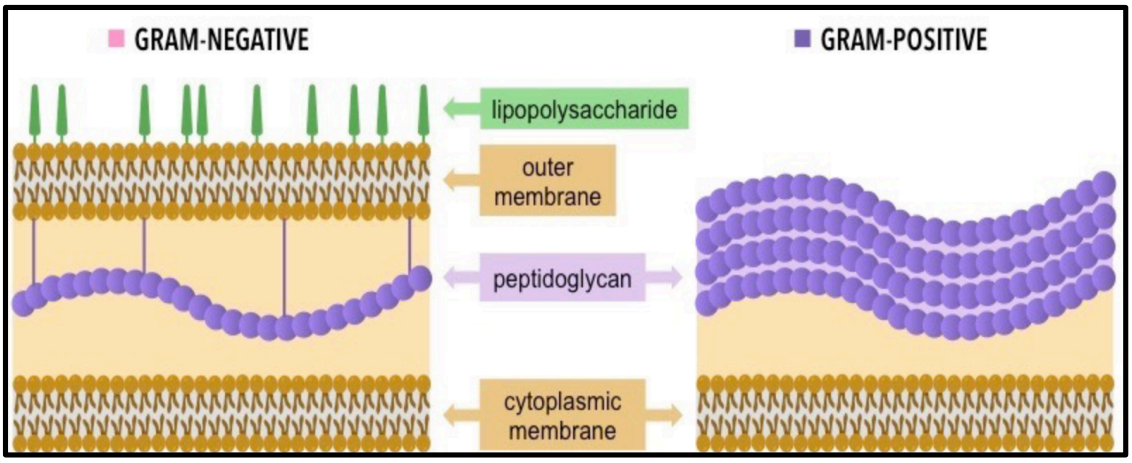

Figure 7 **Gram-positive and Gram-negative bacteria. A Gram-positive bacterium has a thick layer of peptidoglycan (20-80 nm) (left). A Gram-negative bacterium has a thin peptidoglycan layer (7-8 nm) and an outer membrane (right) (30).**

	Gram-negative Bacteria	Gram-positive Bacteria
Peptidoglycan layer	Thin (single-layered)	Thick (multilayered)
Periplasmic space	Present	Absent
Outer membrane	Present	Absent
Lipopolysaccharide (LPS) content	High	Virtually none
Lipid and lipoprotein content	High (due to presence of outer membrane)	Low (acid-fast bacteria have lipids linked to peptidoglycan)
Toxins produced	Primarily Endotoxins	Primarily Exotoxins
Resistance to physical disruption	Low	High
Cell wall composition	The cell wall is 70-120 Armstrong thick two layered.	The cell wall is 100-120 Armstrong thick, single layered.
Antibiotic Resistance	More resistant to antibiotics.	More susceptible to antibiotics

Table 4 Comparison of Gram-negative and Gram-positive bacteria.

The lipid composition of bacterial membranes differs from that of the human cells. Bacterial cell membranes tend to be charged, a characteristic which can be used to target bacterial cells specifically and not causing any harm to the host cells.

Since POPE and POPG lipids are commonly found in most inner membranes of Gram-negative bacteria, they form the basis of the membrane used in this series of simulations to try and understand how antimicrobial peptides attack bacterial membranes. The last lipid, used in the membrane, was 1-palmitoyl-2-oleoyl-sn-glycero-3-phosphocholine (POPC) (also shown in Figure 8 below). POPC was used because it formed the basis of most mammalian cells. The use of those three lipids in the simulation membranes allows for extrapolation of targeting towards each of the three lipids from which it is possible to understand why antimicrobial peptides target and destroy bacterial cells while leaving host cells unaffected (29).

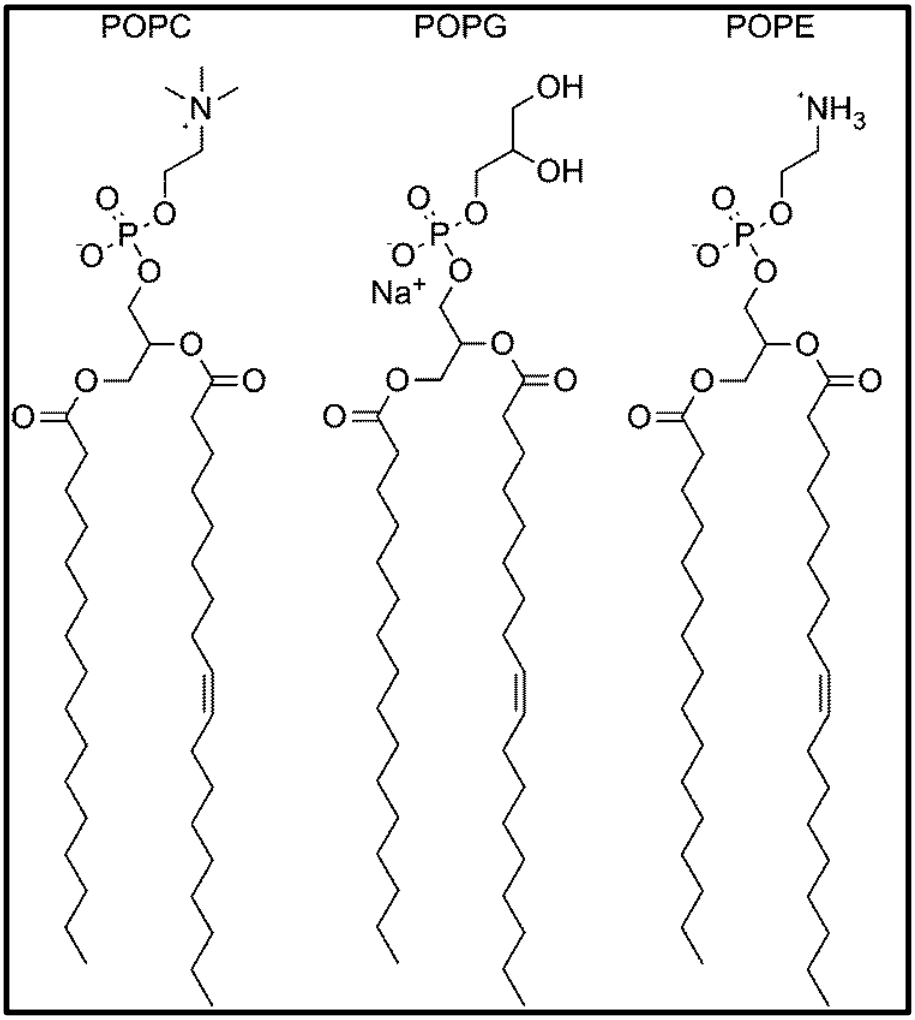

Figure 8 **Structures of POPG and POPE lipids that make up the inner membranes of Gram-negative bacteria. This Figure features, also, POPC lipid that is found in mammalian cell membrane. Picture taken from: (28).**

Chapter 2: Antimicrobial peptides.

Antimicrobial peptides, like penicillin also have a Sir Alexander Fleming background. In 1921, seven years before the penicillin era, Fleming found that mucus, tears and other bodily secretions contained a substance (which he named Lysozymes) that could inhibit the growth of some bacterial colonies (nowadays, we know lysozymes as antimicrobial peptides). At the time, Fleming saw that those lysozymes had limited efficacy against harmful bacteria and, while appreciating the idea of natural biological antibiotics, moved on with his research. Of course, this knowledge took a backseat as the penicillin era closely followed (31).

Many decades on, antimicrobial peptides have been studied and are known to be small proteins (usually less than 50 amino acids long) secreted by virtually all-living organisms as a defence mechanism. They have potent broad-spectrum activity against a vast range of microorganisms. These peptides are all cationic (due to the presence of many Lysine and Arginine residues) and have amphipathic properties; but differ vastly in sequence, length, structure and functional groups. Antimicrobial peptides are so diverse in structures, amino acid content and features; the only way to group them is based loosely on their secondary structures. Regardless of this diversity, all antimicrobial peptides have hydrophobic, hydrophilic and cationic residues structured in a way whereby the polar and non-polar regions of the peptides are separated to create the amphipathic structure common to all these peptides (32). It seems the sequence or length of these peptides do not govern the peptide's functionality (although they may alter potency). An antimicrobial peptide is active if the positive charge and amphipathicity are maintained (16, 33).

Antimicrobial peptides form a pivotal part of the innate system that is activated as soon as an antigen is detected and before the slower more specific adaptive immunity branch of the immune system as the first line defence against trauma or infection.

2.1 Structure-activity relationship

As discussed previously, antimicrobial peptides differ vastly and are therefore grouped per secondary structures. Classifying them in that way creates four major classes: namely β-sheet; α-helical; loop; and extended peptides. The first two form the bulk of peptides commonly found in nature (34, 8). Besides different secondary structures, peptide length, amino acid sequences, net charge, and either presence or absence of disulphide bridges may contribute to the activity or potency of antimicrobial peptides (35).

Group 1: β-sheet peptides

Antimicrobial peptides, which form β-strands are connected usually by intramolecular disulfide bridges and, therefore, are restrained in terms of their conformation (36). Tachyplesins, human defensin-2, protegrins and lactoferricin are a few examples from this group of peptides (37). Of these examples, the defensins are thought to be the best characterized β-strand peptides. Nuclear Magnetic Resonance (NMR) structure of α- defensin shows that these peptides are made up of three-stranded antiparallel beta-sheets (38). To understand the importance of structure related activity, analogous of tachyplesin were studied. In these studies, the sulfhydryl (SH) groups were protected chemically (to prevent cyclization) and they suggested that the cyclic structure was essential for antimicrobial activity (39).

Group 2: α-helical peptides

This group of peptides is the most abundant in nature. They are characterized by their α-helical conformation that often contains a slight bend in the center of the peptide. Giangaspero's study (26) proved that this bend was crucial for the selection of membranes and the suppression of hemolytic activity. Interactions of these helical peptides with the negatively charged phospholipid headgroups of bacterial membranes appear to be driven electrostatically. Many structure/activity relationship studies used α-helical peptides to understand their mechanism of action and to design therapeutically useful peptides (40, 41). These studies have shown that the size, sequence, charge, helicity, overall hydrophobicity,

amphipathicity, and the angles, subtended by hydrophobic and hydrophilic surfaces in helical molecules, are all in one way or another correlated with potency and antimicrobial activity (42).

Group 3: Loop peptides

This class of antimicrobial peptides cannot form an amphipathic structure as they contain a single disulphide bond forming a loop. They contain two cysteine residues linked by a disulfide bond to form a loop of nine amino acid residues. A study of structure-function relationships showed that the loop of these peptides was essential for its antimicrobial activity (19). An example of loop antimicrobial peptides is bactenecin which adopt a loop formation with one disulfide bridge (43).

Group 4: Extended peptides

This class of peptides contains a high concentration of an amino acid such as proline, tryptophan, arginine, and histidine and lack the conventional secondary structure associated with antimicrobial peptides (43). There are minimal constraints via intermolecular bonds and, consequently, they adopt an extended structure after which they are named (44). They may adopt a structure once they encounter a membrane but that is not common to all these peptides (43). Examples of extended peptides include:

- Histatins, (isolated from human saliva) are rich in histidine residues (45).
- Cathelicidins are rich in proline, arginine, and phenylalanine and have irregular structures (45).

Antimicrobial peptides have different structures, sizes, and sequences and they show a general trend of amphipathicity and positive charge. It appears these peptides' chemical and structural properties are crucial to understanding their mechanism of action. Without sufficient understanding of this and the lack of sequence or structural homology, it is difficult to predict these peptides' activity and, thereby, it is challenging to design a model antimicrobial peptide with predictable *in vivo* activity and of therapeutic benefit (45).

2.2 Mechanism of action of antimicrobial peptides

Antimicrobial peptides use the fundamental differences in overall charge between the membranes of microorganisms and those of multicellular organisms to target microbial membranes. Microbial membranes are rich in negatively charged phospholipid headgroups that the cationic antimicrobial peptides target and use to bind to the membrane surface, where the amphipathic properties facilitate membrane penetration and, thereby, destruction. Animal and plant cell membranes consist of zwitterionic phospholipids that are unattractive to the cationic peptides (33). They also contain high amounts of cholesterol which is, also, amiphatic in nature and can embed itself within the fatty acid tails of the membrane bilayer. By embedding within the lipid tails, they interfere with the tight packing of the bilayer and make it more fluid in nature. Their presence makes the bilayer less permeable to small water-soluble molecules. Cholesterol's presence in a lipid bilayer provides it with mechanical stability through the planar steroid ring in its structure. This reduces the effects of the antimicrobial peptides and provides protection from them (46, 33).

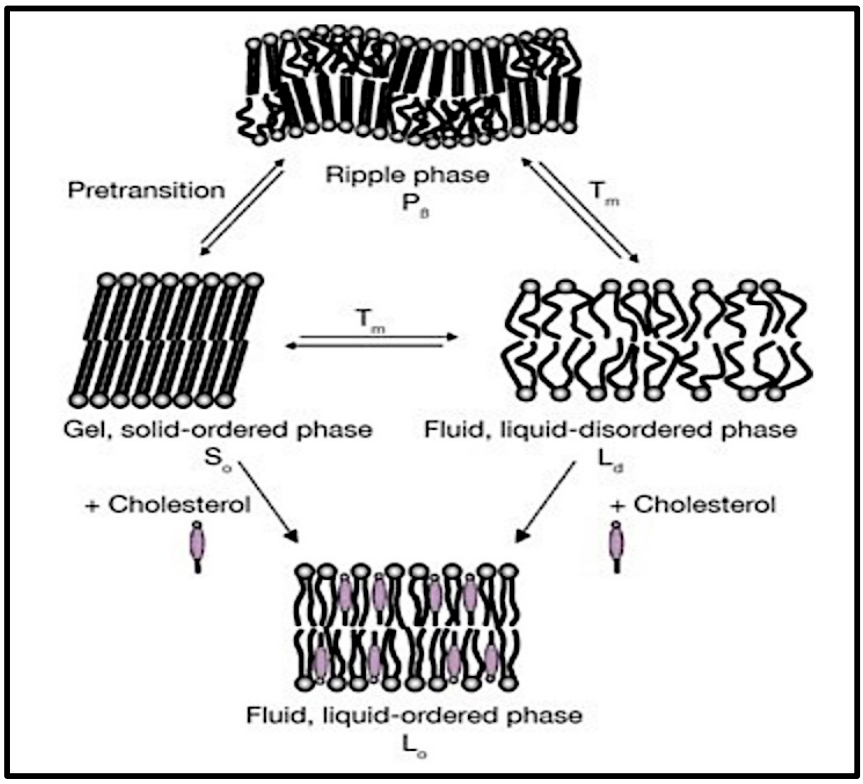

Figure 9 The role of cholesterol in a membrane (47).

Antimicrobial peptides are membrane-active proteins and, therefore, target the cell membrane and kill by either disrupting its structure or increasing its permeability (36). It is agreed that binding of the peptide to the membrane surface happens via electrostatic attraction to the negatively charged headgroups of the bacterial membrane lipids (36).

Despite extensive study, both experimentally and using computational methods, the mode of action of these peptides remains unknown. However, the agreed upon theory is that they form transmembrane pores that allow water to flow into cells and, thereby, destroy the osmotic balance and cause cell lysis via swelling (33).

2.2.1 Mode of action

As discussed above, the mode of action is thought to be membrane pore formation for which the specifics remain unknown. However, there are a few agreed widely accepted models. They are observed to frequently target the bacterial cell membrane whereby they form transmembrane pores allowing water to flow into cells and destroy the osmotic balance and promote cell lysis via swelling. Antimicrobial peptide contact with these membranes appears to happen electrostatically, i.e. the negative charge carried by most bacterial membranes attracts these cationic peptides whose size allows them to attach easily and penetrate the cell membrane to form pores (37, 33).

They are known to do this via one of three pathways mentioned below:

2.2.2 The Carpet model

The carpet model suggests that these peptides cluster together and form oligomers before attaching to the membrane. Once the concentration of peptides exceeds that of the membrane threshold (which depends on the peptide and type of lipids in the membrane and the bacterial species) either a transient membrane pore is formed or as shown in Figure 10 below complete membrane disintegration is observed (33).

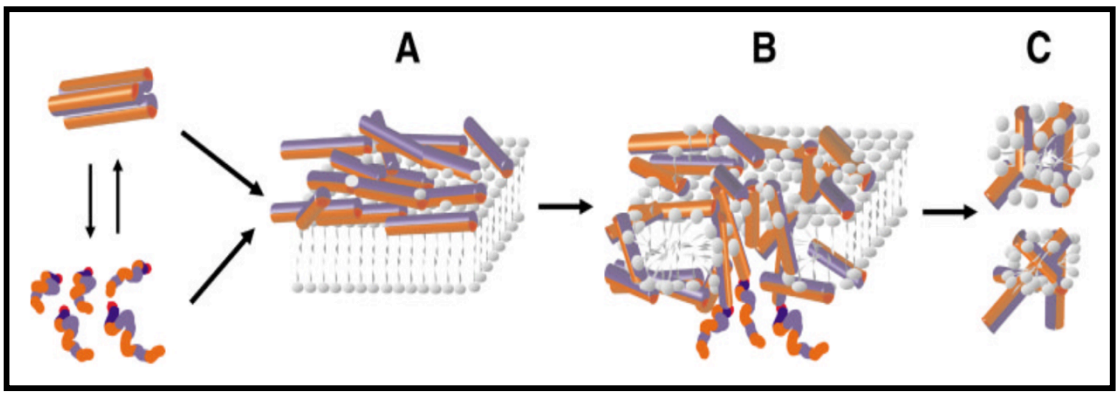

Figure 10 Diagrammatic representation of the carpet model: diagram A shows a cluster of proteins attaching to the membrane. B represents a threshold concentration having been reached and shows a membrane pore being formed and diagram C shows membrane disintegration. The diagram is taken from (33).

2.2.3 Barrel-stave model

In the barrel-stave model once an antimicrobial peptide immerses itself into the lipid core of a membrane, it recruits other peptides and, as shown in Figure 11 below forms systematically a peptide cluster based membrane pore (33).

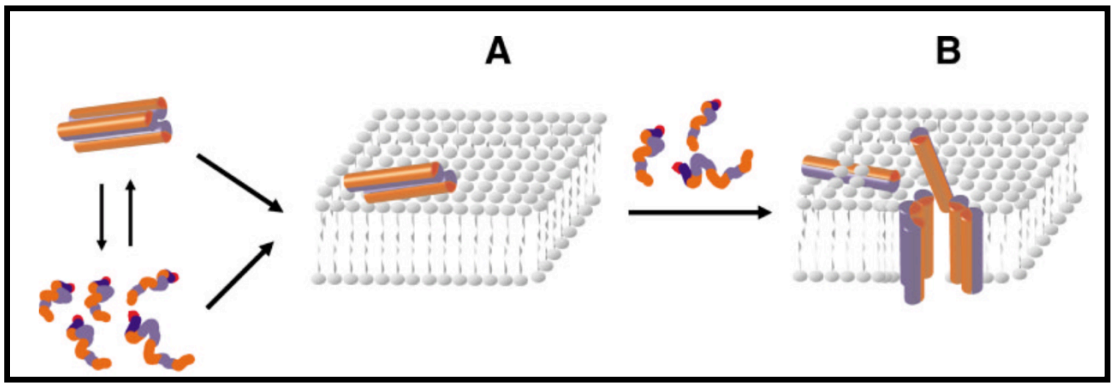

Figure 11 Diagrammatic representation of the barrel-stave model. Picture A shows a cluster of peptides attached to the membrane surface. In picture B, membrane immersed peptides attract other peptides and start to form a pore through the membrane. The diagram is taken from (33).

2.2.4 Toroidal pore model

Like the carpet model, this model also depends on a threshold concentration (This depends on the antimicrobial peptide in question and the lipids making up the membrane) of antimicrobial peptides to be reached before its effect can be seen. Antimicrobial peptides, acting via the toroidal pore model, create a well-ordered structure whereby the pore is lined by the lipid headgroups and the peptide helices. Peptides forming toroidal pores absorb onto the surface of the membrane and cluster. In doing so, they thin the membrane and expand the headgroups of its lipids causing the membrane to bend. By bending the membrane and expanding it, they form the toroidal pore that, classically, is larger in size at either ends and smallest in the middle (48). This model is represented diagrammatically in Figure 12 below.

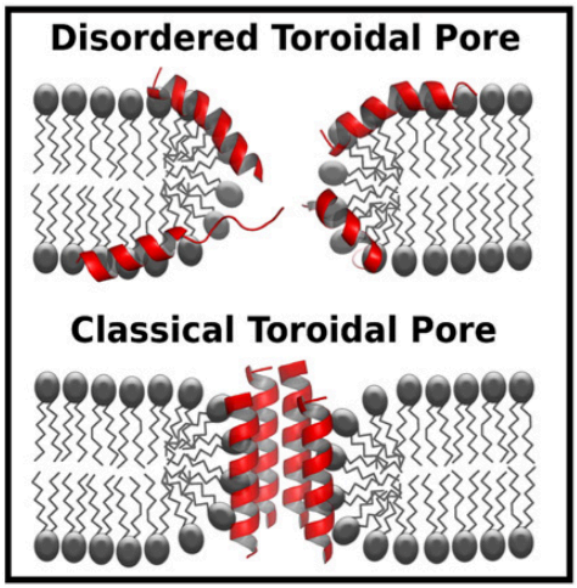

Figure 12 Diagrammatic representations of toroidal pores. Picture taken from (48).

2.2.5 Cellular based mechanisms

Other modes of actions with which these peptides are associated, include inhibition of cell division, interfering with DNA and protein synthesis/protein folding, alteration of membrane permeability, inhibition of essential enzymes and cell wall synthesis that all can lead to cell death. Although all these methods have been observed in various peptide bacterial cell interactions, the exact mode of action is not as well understood as the physical pore formation mechanism (33).

2.2.6 Immunomodulation

As well as directly killing invading organisms, antimicrobial peptides are involved in immunomodulation. They can act as either cytokines (essential cellular signalling proteins) or promote the production and release of cytokines. In doing so, they include the various cells of the adaptive immune system into the defence mechanism. With this function, they link the innate and adaptive branches of the immune system forming a well-integrated defence system that is crucial for both clearance and prevention of infections (49).

Antimicrobial peptides form a pivotal part of the immune system that has been shown to have far more significant alternative roles than just first line defence against infections.

Unlike chemical based antibiotics, which can be either bactericidal or bacteriostatic (i.e. inhibit growth but not kill the bacterial cell), these peptides appear to be only bactericidal and have a relatively low Minimal Inhibitory Concentration (MIC) which desirable in a novel antimicrobial agent (44, 50).

2.3 Resistance to antimicrobial peptides

Antimicrobial peptides have been very versatile in killing microbes by various mechanisms but, unfortunately, resistance to their effect is starting to emerge within bacterial colonies. Several studies have shown that a natural and induced resistance arising against antimicrobial peptides in several bacterial species (51). The most common mechanism of resistance is modifications to the cell membrane; this prevents the peptides from binding to the membrane. This section discusses changes to the cell membrane and other mechanisms of resistance.

2.3.1 Surface remodeling

Gram-negative and Gram-positive bacteria modify their cell wall by reducing the net negative charge on the surface that the antimicrobial peptides frequently target. Reducing the negative charge in the Gram-negative bacterial membrane is achieved by adding an amine-containing group (such as ethanolamine and 4-amino-4- deoxy-T-arabinose (Ara4N)) to the LPS lipids to mask the negative charge (52). It has been shown that this surface lipid modification can occur in response to the presence of an antimicrobial peptide (52).

Some Gram-negative bacteria (such as *Escherichia coli, Salmonella enterica and S. Typhimurium*) maintain a two-component (PhoP-PhoQ and PmrA- PmrB) system to sense the presence of antimicrobial peptides in their environment and, in response to activate LPS modifying enzymes response. Operon enzymes, such as operons VraSR cell-wall regulon and the vraDE operon catalyze the attachment of Ara4N group to the lipid A of the bacterial membrane (53).

Gram-positive bacteria reduce the negative charge of their surface by D-alanylation of teichoic acids triggered by dlt operon (54, 55, 56). Dlt operon facilitates the esterification of D-alanyl esters with teichoic acid from the cell membrane. There is, also, the MprF membrane protein that transfers enzymatically L-lysine group to POPG lipids changing their overall charge from negative to positive (54).

Mutations in genes relevant to both pathways were shown to drastically increase the susceptibility of several Gram-positive strains to antimicrobial peptides in all the following studies (57, 58).

Interestingly, Saar-Dover et al (56) suggested that the primary mechanism, involved in the AMP resistance mediated by the D-alanylation, displayed an increase in the cell wall density impairing the penetration of AMPs rather than a major effect on the AMP binding to bacterial surface (56). However, further studies with other species are necessary to confirm if this mechanism is common to the entire microbial kingdom.

2.3.2 Modulation of AMP genes expression

This method depends on regulating the expression of the gene that leads to AMP release. For example, *Shigella flexneri* is shown to down regulate the expression of genes coding for cathelicidin LL-37 and the human β-denfensin-1(59). This down-regulation of genes results in lower concentrations of AMP being produced. This allows for the bacteria to invade host cells and barrel deeper, unopposed by the body's defences, and makes infections more difficult to treat (59, 60).

2.3.3 Biofilms

Biofilms are biotic or abiotic surfaces consisting of an outer polymetric matrix that surrounds the bacterial cell. These biofilms are resilient and protect the bacteria from chemically and physically harmful environments as well as protecting them from biological antimicrobial agents. Biofilms provide resistance against antimicrobial peptides when specific genes are expressed that modify the polymetric structure and the architecture of the biofilm making it more robust and resistant to antimicrobial peptides. An example of this is in the *Pseudomonas aeruginosa* biofilm that contains alginates that are thought to be the reason behind

its antimicrobial peptide resistance (61). Alginate mimics a microbial membrane and, in doing so, the biofilm can bind AMPs and induce a conformational change (required for the effectiveness of an AMP when entering the membrane bilayer). They can also prevent the antimicrobial peptide's diffusion through the biofilm to the bacterial membrane as well as inducing peptide aggregation. This abolishes the effectiveness of antimicrobial peptides (61).

2.3.4 Proteolytic degradation

Both Gram-negative and Gram-positive bacteria can produce protease enzymes that hydrolyze antimicrobial peptides. They target linear peptides because their cleavage site is more exposed. For example *P. aeruginosa and S. aureus* are both able to make enzymes that break down the human antimicrobial peptide LL-37 and abolish completely their antimicrobial function (62, 63).

2.3.5 Efflux pumps

These are energy driven ATP (Adenosine triphosphate) transporters embedded in the cell membrane that are used to remove toxic molecules which include antibiotics and antimicrobial peptides. Efflux pumps are one of the primary methods of antimicrobial resistance; it is quite unspecific in nature and can provide resistance to many classes of antibiotics (64). An example of an efficient efflux pump is the Mrt pump found in the membrane of *Neiseria gonorrhea* and *N. Meningitides* bacteria. This pump recognizes and pumps out antimicrobial peptides (including Protegrins (such as PG- 1) a β-sheet AMP, human Cathelicidin LL-37 which is an α-helical AMP, and TP-1 which is a β-hairpin AMP) providing resistance against their activity (65,66). As mentioned, each of these examples has a different structure and, consequently, the Mrt pump can recognize antimicrobial peptides from various groups and can provide resistance against them (67).

2.3.6 Trapping

Some bacterial cells secrete molecules that bind to antimicrobial peptides and neutralize them. An example of such compounds is SIC proteins secreted by *S. Pyogenes* that binds many different antimicrobial peptides suppressing their activity (68). SIC has a higher affinity towards LL-37 than to human neutrophil

peptide HNP-1 as shown by the heightened sensitivity of SIC deficient mutants of the bacteria to LL-37 (68).

It is known that microbes can develop resistance to antimicrobial therapy that targets either a metabolic pathway, protein, or those that target a specific enzyme since these are easy targets to mutate and change (50).

Recently, antimicrobial peptides have shown increasing promise to becoming the alternative to antibiotics in the fight against pathogenic microorganisms due to their broad spectrum of activity (69).

Although some pathogens have evolved and developed resistance, their resistance to antimicrobial peptides is less common than other types of antibiotics. It seems a better understanding of the mode of action of antimicrobial peptides and finding a way to oppose the resistance mechanisms developed now can lead to potential peptides being used effectively as a therapeutic drug in place of conventional antibiotics (69).

2.4 Groups of antimicrobial peptides

All living organisms, plants, microorganisms and vertebrates alike are susceptible to infections and, therefore, secrete antimicrobial peptides to defend themselves and to ensure their survival. There are currently over 5000 known peptides secreted by all organisms in the five kingdoms of life, a number that is increasing rapidly. Antimicrobial peptides are vastly diverse in their sequences and structures to the extent that they are broadly classified based on their secondary structures. They can belong to one of four groups: β-sheet; α-helix; extended; and loop. Amongst these four groups, the most abundant are the β-sheet, α-helix with the latter being the most likely to be active against bacterial membranes. Hence, to date, the α-helix is the most studied group (70, 71).

Antimicrobial peptides are secreted by cells situated in areas where there is a high probability of exposure to microbes. In humans, those cells are in the dermis and epidermis of the skin, although there have been antimicrobial peptides isolated from tears, mucus and other moist surfaces of the human body. The release of these antimicrobial peptides is regulated by a bacterial macromolecule or cytokine stimuli that lead to the degranulation of the cells producing them and the release of peptides (49).

Three groups of antimicrobial peptides dominate the peptides secreted by humans; these are, namely, the defensins, cathelicidins and histatins.

2.4.1 Cathelicidins

The cathelicidins are named after their conserved cathelin precursor domain. In humans, there is only one peptide from this group, known as LL37, and it is derived from the C-termini of CAP18 protein usually found in leukocytes, skin, and the gastrointestinal and respiratory tracts. While the protein consists of 37 amino acids and has a relatively linear structure, it adopts a coil conformation in hydrophilic environments and an alpha-helix structure in hydrophobic environments. Cleaving of the CAP18 protein to obtain the LL37 protein is activated by the presence of an infectious stimuli and the resulting LL37 antimicrobial peptide is active against both Gram-positive and negative bacteria.

Further to this function, LL37 contributes, also, to the degranulation of mast cells and acts as a chemo-attractant to T-cells and other cells of the adaptive immune system. This chemo-attractant represents the ability of antimicrobial peptides to act as antimicrobial agents and mediators of the adaptive immune system (34, 35).

2.4.2 Histatins

The histatins is a family of small cationic peptides rich in histidine residues that are secreted mainly by sublingual glands into the saliva. Structure wise, they are found to coil randomly in aqueous environments, and in lipid environments, they form an a-helix typical of antimicrobial peptides. They have high fungicidal activity and are essential to preventing infections in the oral cavity (34, 35).

2.4.3 Defensins

The defensins are known for their 6-cysteine groups forming intramolecular disulphide bridges that usually form a three strand β-sheet structure. The two types of defensins, found in humans, are, namely, α-defensins and β-defensins; both are found in neutrophils where they are thought to play a role in phagocytosis. It is thought that the C-terminal of these peptides is responsible for their antimicrobial activity. The defensins are known to inhibit the growth of both Gram-negative and positive bacteria as well as some fungi. Alongside their antimicrobial activity, the defensins are thought to also attract immune cells, stimulate cytokine release and, more recently, they have shown some antitumor activity (34, 35).

2.5 Cell membrane penetration

When thinking about antimicrobial peptides killing microbes via membrane pore formation, the first question that comes to mind is how do they manage to penetrate such robust barriers? Two pathways for this process have been suggested, one of them being a mere attraction between the positively charged peptide to the negatively charged lipid membrane of the microorganism (known as non-receptor mediated). The second pathway is more complex and is usually a highly targeted one in which a peptide targets a specific receptor on the membrane to start off the destruction process (known as receptor-mediated) (37).

2.5.1 Non-receptor mediated

Most antimicrobial peptides work via non-receptor mediated interactions that allow them to have a broad spectrum of activity. They target the negative charge of microorganism membranes to which they are attracted and begin to cluster around them. It is through these clusters that the peptides can cause antimicrobial actions either via barrel-stave, the carpet mechanism or toroidal pores discussed above (37).

2.5.2 Receptor mediated

Receptor-mediated active antimicrobial peptides are secreted usually by microorganisms to kill other microorganisms. They secrete defensive antimicrobial peptides to kill off colonies competing for nutrients to ensure their growth and survival. Antimicrobial peptides, secreted by microorganisms, usually have a species exclusive target and are often highly bactericidal to that specific species. These peptides differ structurally to the non-receptor mediated peptides in that they don't have the classic cationic charge. They consist of a receptor binding domain that is essential to activity and a secondary pore-forming domain. Although they have a different targeting method, they work ultimately by forming a pore in the membrane forcing the cell to lyse; this is common to all antimicrobial peptides (37).

Despite fundamental differences between plants and animals, they do share some elements in their defence against pathogens in the form of antimicrobial peptides. Mammalian antimicrobial peptides are similar to those isolated from plants and insects. Mammalian defensins have a β-sheet structure with between 29 and about 40 amino acid residues and three intramolecular disulfide bonds between cysteine residues. Cathelicidin, a family of polypeptides, are found in leukocytes of many mammals. Other kinds of antimicrobial peptides, found in most mammals, include protegrins, granulysin, and histatins (71, 72).

Due to the growing interest in antimicrobial peptides and demand for antimicrobial agents, an antimicrobial peptide database was established in 2003. Now, this contains structural information of more than 2600 naturally occurring antimicrobial peptides (http://aps.unmc.edu/AP/main.php).

This thesis considers the Dermaseptin superfamily of peptides. Existing studies have shown they possess many properties and activity that have biological significance against bacteria, viruses, and fungi. Dermaseptin B2, a peptide within that group, has been shown to have broad-spectrum activity against many microbes, viruses, and fungi but little is known about its mode of action. This thesis aims to learn how Dermaseptin B2 and its analogue Dermaseptin DS01 bind to membranes and how they go about causing disruption to the membrane. The thesis also looks at HCV NS4B peptide and its considers its potential as a drug target in the treatment of Hepatitis C.

.

Chapter 3: Dermaseptin

Of the various types of antimicrobial peptides which have been discovered, this thesis focuses on Dermaseptin B2 and a shorter analog Dermaseptin DS01; both belong to the Dermaseptin superfamily. This family of antimicrobial peptides is very versatile in effectiveness and shows no specificity towards any species of invading organisms. Experimental biochemists found micromolar concentrations of Dermaseptin can be highly bactericidal, virucidal, fungicidal and can be even selectively toxic to cancerous cells with very low toxicity to host cells (73). The Dermaseptin family shows high medicinal potential and does seem to fill the gap in antimicrobial therapy. Unfortunately, it is a family that is secreted only by the skin cells of an Amazonian frog species and not much is known about its mode of action or toxicity potentials. This thesis uses computational methods to find out more about the Dermaseptin family and attempts to understand how they bring about cell death or how they target microbial cellular membranes (73).

3.1 The Dermaseptin superfamily

The skin of Hylidae and Ranidae Amazonian frogs secretes this family of antimicrobial peptide. All peptides in the family are related genetically but have markedly different structures and functionality (73, 74).

Dermaseptin peptides undergo coil-to-helix transformation upon encountering a membrane before causing any damage. A 34-residue peptide, named Dermaseptin S1, was the first peptide of this family to be studied and it was found to have lytic activity against both Gram-negative and positive bacteria as well as some yeast and protozoa while having no effect on mammalian cells (75).

As more peptides from this family were isolated and studied, it became apparent that most of them had broad-spectrum activity against microbes. However, despite their sequence similarities, they differed vastly in potency (73, 74, 76). It appears that shortening the length of the peptide chain does not impact majorly on antimicrobial activity with peptides, with sequences as short as 10-12 residues, showing a fully uncompromised antimicrobial effect against a wide range of bacterial colonies (42).

Table 5 below, taken from (73), shows the minimum inhibitory concentration of peptides required to inhibit the growth of a bacterial colony.

Microorganism	DRS B1	DRS B2	DRS B3
Mollicutes			
Spiroplasma apis	0.3 (1.8)	0.3 (12.5)	3.1 (12.5)
Spiroplasma citri	0.4 (3.1)	0.4 (3.1)	3.1 (12.5)
Spiroplasma floricola	25 (100)	12.5 (R)	6.2 (50)
Spiroplasma melliferum	1.5 (6.25)	1.5 (6.25)	6.2 (25)
Acholeplasma laidlawii	3.1 (6.25)	3.1 (6.25)	3.1 (6.25)
Mycoplasma galliepticum	R[a]	R	25 (100)
Mycoplasma mycoides	R	R	R
Gracilicutes			
Escherichia coli K12	1.5 (1.5)	1.5 (1.5)	1.5 (1.5)
Pseudomonas aeruginosa	6.2 (12.5)	12.5 (12.5)	3.1 (6.2)
Salmonella typhimurium	3.1 (3.1)	3.1 (3.1)	3.1 (3.1)
Rhizobium meliloti	0.3 (3.1)	0.3 (3.1)	0.8 (0.8)
Pasteurella multocida	25 (100)	12.5 (50)	25 (50)
Firmicutes			
Staphylococcus aureus	12.5 (25)	12.5 (25)	3.1 (3.1)
Enterobacter faecalis	50 (50)	50 (50)	12.5 (50)
Bacillus megaterium	0.3 (0.3)	0.3 (0.3)	0.8 (0.8)
Corynebacterium glutamicus	1.5 (1.5)	1.5 (1.5)	1.5 (1.5)
Yeasts			
Saccharomyces cerevisiae	5.5 (15)	5.5 (15)	
Candida albicans	10 (25)	5 (15)	
Cryptococcus neoformans	0.3 (15)	1.5 (1.5)	

Fungi			
Microsporum canis	0.8	1.5	
Tricophyton mentagrophytes	10 (25)	15 (30)	
Arthroderma simii	3.1 (3.1)	5 (15)	
Aspergillus fumigatus	3.1 (6.2)	3.1 (6.2)	
Protozoa			
Leishmania Mexicana	3.1 (3.1)	3.1 (3.1)	
Leishmania major	5.5 (15)	1.5 (10)	
Hemolysis			
Human erythrocytes	>250	>250	>100

Table 5 The antimicrobial activity is expressed as MIC (μM), the minimal peptide concentration required to kill or totally inhibit cell growth. This table is taken from (73).

Although a detailed mechanism of action for Dermaseptin is yet to be found, data using simple artificial membranes and molecular dynamic simulations (77) have suggested they bind to membranes through a carpet-like mechanism of action and that the N-terminal region of these peptides is mainly responsible for their membrane effects (75, 76, 78, 79). Planar lipid bilayers studies suggested that Dermaseptin B2 tetramers form mixed lipid-peptide toroidal pores (80). NMR studies show Dermaseptin B2 can adopt different helical structures depending on their environment (81). Thus, a unifying model that correlates the structural and physicochemical parameters of Dermaseptin's with their antibacterial properties is still lacking, but in literature the most agreed upon theory is that Dermaseptin B2 works via a carpet like mechanism (79, 81, 82).

Fluorescence studies of the binding pattern of these peptides showed that preferred binding to negatively charged lipids and, therefore, it was assumed that binding was driven electrostatically. NMR studies of their structure showed that these peptides were in the presence of a polar solvent from an amphipathic α-helix. Residues 11-33

of Dermaseptin B2 form the amphipathic helical structure while residues 3-8 seem to create a loose helical segment. The two segments are joined by a hinged region consisting of a valine and glycine residues. It appears the flexibility of this hinge dictates and facilitates the potential of the peptide's membrane penetration (79, 83).

These cationic peptides are attracted to and bind to negatively charged lipids on a membrane surface and gradually cover the surface in more peptides. Following the binding process, these peptides next align themselves so that the hydrophilic portion is facing the phospholipid headgroups before rotating to orientate the hydrophobic groups into the hydrophobic membrane core. In doing so, the peptide can insert itself into the membrane bilayer. Dermaseptin B2 does not insert itself deep into the membrane bilayer due to the loosely helical segment of the peptide anchoring it to the membrane surface. As these peptides cover the surface of the membrane, they form small transient membrane pores that allow water and other low molecular weight molecules in and out of the membrane leading to cell lysis (84).

3.1.1 Peptide oligomerisation

Macroscopic conductance and concentration dependence studies as well molecular simulations suggest that tetramers of Dermaseptin peptides form mixed peptide and lipid pores (82, 85). Planar lipid bilayers studies and molecular simulations have shown the pores formed by Dermaseptin have ion specificity that is mediated by lipid headgroups, supporting the mixed peptide-lipid pore theory (45, 85, 86).

Dermaseptin shows potent antimicrobial activity but this activity depends upon the lipid composition of the bilayer upon which they are acting. Since Dermaseptin seems to work via the carpet mechanism, they form small transient pores that are smaller than those made by the barrel-stave mechanism. Both pores tend to be lined by positively charged residues within the side chains (87).

3.1.2 Peptide-lipid contact

Fluorescence studies of Dermaseptin binding patterns show that Dermaseptin has a higher affinity for anionic lipids as compared to zwitterionic ones (86, 88), which is the reason for their lack of toxicity to mammalian cells. Dermaseptin assumes its

helical membrane active structure in the presence of a membrane containing anionic lipids. This feature can be the reason for the high potency of antimicrobial activity and further explains the lack of toxicity to mammalian cells. Since mammalian cells contain mainly zwitterionic lipids, Dermaseptin does not form a helical structure that is fundamental to its antimicrobial activity. It is noteworthy that Dermaseptin also shows selectivity for lipids with low phase transition temperatures such as POPG. This is particularly true for analogues of Dermaseptin with a shorter amino acid sequence (86, 88).

3.1.3 Peptide orientation

In the presence of a lipid membrane, Dermaseptin peptides assume a helical structure that is not seen in the absence of a membrane. As mentioned earlier, in the presence of zwitterionic membrane lipids (as is the case of the mammalian cell membrane), Dermaseptin lacks its helical structure and, thus, has no cell lysis effect. This added degree of specificity makes this peptide a viable investigative option for use in antimicrobial therapy (83, 89).

Dermaseptin peptides tend to attach themselves to a membrane at a negatively charged lipid headgroups, following which they modify their orientation so that the hydrophilic portion faces the head groups before rotating to bring their hydrophobic groups towards the membrane core (81, 86).

3.1.4 Anticancer properties

Antimicrobial peptides can exploit the fact that cancer cell membranes are more fluid than healthy cell membranes (except for some breast and prostate tumours), and so that makes them a viable target to these peptides (90, 91,92).

The net negative charge of cancer cells, a property, shared with bacterial cell membranes, also makes cancerous cells a viable target for antimicrobial peptides (91).

Antimicrobial peptides lyse cancerous cells via a similar mechanism (carpet model) as they do a microbial cell.(90).

Dermaseptin B2 has been shown to have significant activity against prostate cancer cells. (93).

Dermaseptin tends to have a cytotoxic and inhibitory effect on cancerous cells. They inhibit tumour cell proliferation and, in some cases, angiogenesis, a process via which tumour cells make new blood vessels to feed their expanding metabolic requirements and growth (92, 93).

3.1.5 Dermaseptin DS01

Dermaseptin DS01 is shorter than Dermaseptin B2 and shows highly potent antimicrobial activity with very little toxic effects to mammalian cells (20). DS01 is formed by 70% non-polar amino acids that facilitate their binding onto anionic membranes. Sequence wise, Dermaseptin DS01 is related more structurally to the Dermaseptin S group as compared to Dermaseptin B. Like all other Dermaseptin peptides, Dermaseptin DS01 brings about antimicrobial activity via the carpet model for which the ability to form helices is essential. DS01 forms long uniform helices that are very membrane active even at very low concentrations (20).

Chapter 4: Computational methods

Molecular dynamics is the method used to generate computer simulations of complex biological systems to gain a new dimensional insight into their functionality. Molecular simulations have become an indispensable tool in medical research. It validates experimental results easily and is used consistently to confirm theories. It is a cheaper and effective way of accurately (depending on the accuracy of the parameters used) predicting protein activity and protein-membrane interactions. Although a highly useful method of research, significant limitations prevent it from reaching its full potential usefulness; the big one being the length of simulations possible halting progress.

All atoms simulations are extremely expensive to compute and require a long time to produce results. Consequently, it was evident that, to save time and resources, to look only at interactions relevant to the problem in question and cut down the number of atoms in the system. This was the basis for the development of the coarse-grained method of simulations.

4.1 Coarse-grained simulations

Coarse-grained simulations disregard the hydrogen atoms in the system since there are so many of them forming and disbanding hydrogen bonds irrelevant to either biological systems or the question (95). Coarse-graining maps out the properties of several atoms onto a large bead that represents adequately the group of atoms in reactions. In doing so, the number of particles is reduced, therefore, longer simulation times can be achieved in shorter real times and with lower computational costs (95). While this seems an excellent and effective way of addressing the problem, it does depend on a lot of assumptions that need to be validated.

For a coarse-grained model to have any meaning, it is vital to know which interactions or atoms to consider and which to disregard. In practice, it is very difficult to do so accurately. To date, the computational power available to be exploited in simulations, has increased several folds with supercomputers making easy work of huge calculations, the time issue remains the main limitation to molecular simulations (95). Where, in experimental terms, it is possible to monitor

reactions and interactions over extended periods of time in molecular simulations terms, it is only possible to simulate in the microsecond time regions.

There is a significant gap between the two methods that a coarse-grained approach attempts to bridge by reducing the size of the particles in the system to be simulated and by focusing the computational energy to those interactions relevant to the question being asked. By removing the hydrogen interactions from the system and combining atoms, one focuses the computational power where it is most needed and increases significantly the efficiency of simulations. Thereby, this manages to increase the time scale to the millisecond regions but comes at the cost of loss of detail. As with all research, compromises must be made and with biological systems coarse-grained simulations provide enough detail to make it possible to figure out what is happening at the interaction face without the requirement for hydrogen bond representation. It is necessary, also, to use coarse-grained methods when modelling a biological system because, more so than the detail, the longer time scale is essential to attaining meaningful descriptions of the system in question (95).

The Levitt group was the first group to employ this method successfully (96). Arguably, the Levitt group created the first coarse-grained model as they attempted to understand protein folding. They researched the essential elements of a protein that related to protein folding and expressed them in a simple model (coarse-grained) to increase their computational efficiency and to use their power to answer their questions. Also, they managed successfully to build and simulate a phospholipid bilayer to attain results that were comparable to the atomistic and experimental data of the same system. Although efficient, their systems were highly dependent on water and, when it came to proteins, did not allow for accurate predictions. Consequently, Marrink (97) attempted to improve upon it. He managed to build a system that had significantly higher efficiency and, thereby, managed to achieve longer time scales in significantly larger systems by reducing the number of degrees of freedom and by using only short-range potentials.

Following in those footsteps Tanaka & Scheraga (98) embarked on a new knowledge based system. They used the information from the protein data bank and other reliable sources, which they found to create their coarse-grained protein model. Miyazawa & Jernigan's (99) subsequent attempts by introduced the quasi-chemical knowledge based model. This model attempts to incorporate experimental data into a

physics based coarse-grained model for proteins. The problem with their system was the weak predictive power of the system's protein structure. Tirion (100) was first to introduce the elastic network model. These models describe the proteins by using a simple ball and spring theory with the spring representing the elastic bond with a constant cut-off length. The system describes small proteins relatively accurately but, due to the constant cut-off for the bond length, it is unable to model large conformational changes in a structure without requiring significant modifications.

Following these models, Marrink and his group (101) came up with their coarse-grained model, named MARTINI CG, which is used in this project. Their system attempts to fit simple, functional forms such as Lennard-Jones potential to fit experimental data. They developed a coarse-grained force field (102) that is applied to membranes since it uses amphipathic assembly forces that match the properties of membranes. Martini has, also, a coarse-grained water model that represents four water molecules in one coarse-grained bead (103). The Martini system seems to represent lipid-protein systems relatively accurately and efficiently (101). It is now implemented within the MD program, Gromacs (104, 105, 106, 107, 108).

4.2 Computational methods mathematics

Molecular dynamics is a computational technique used to model complex systems at the atomic level. It applies the Newtonian equations of motion to an initial system configuration and solves them numerically to produce a time trajectory from which the system's thermodynamic and kinetic properties can be derived. Molecular dynamics rely upon the relationship between force, F, mass, m and acceleration, a, where both acceleration and force are vector values to create the trajectory.

$$\vec{F} = m \times \vec{a}$$

Equation 1

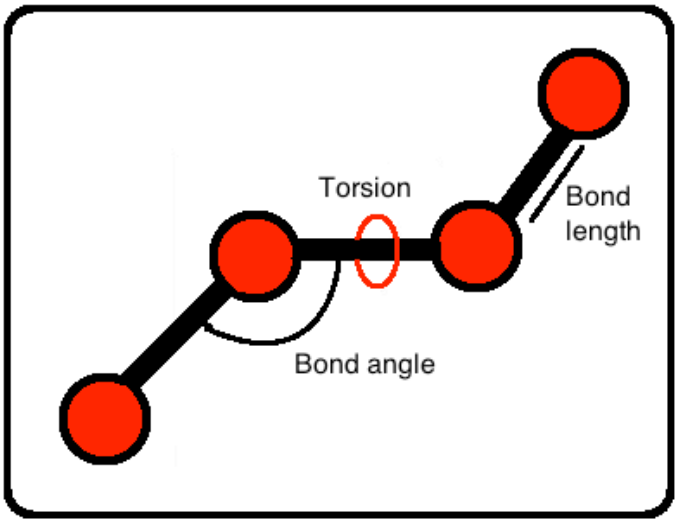

Figure 13 Simplistic representations of the bonded terms defined within a force field.

The force field governs how each particle in the system moves or how much effect it has on the entire system. The force field consists of sets of parameters used to calculate the system's potential energy throughout the molecular dynamic simulation. These parameters for the force field can be derived either from previous experimental work or via a series of quantum mechanical calculations.

Force fields can be divided into two sets of terms:

1. Bonded; this includes bonds, angles and dihedrals.

2. Non-bonded; this includes permanent electrostatics, dispersion and repulsion.

The total energy in a force field can be written as:

$$\mathbf{E_{total} = E_{bonded} + E_{unbonded}}$$

Equation 2

where

$$\mathbf{E_{bonded} = E_{bond} + E_{angle} + E_{dihedral}}$$

Equation 3

$$\mathbf{E_{nonbonded} = E_{electrostatic} + E_{van\ der\ waals}}$$

Equation 4

Each of those terms are quantified numerically by solving the following equations:

$$\sum_{bonds} \frac{1}{2} k_i (l_i - l_{i0})^2 +$$

$$\sum_{angles} \frac{1}{2} k_i (\theta_i - \theta_{i0})^2 +$$

$$\mathbf{V\,(rN)} = \sum_{torsions} \frac{1}{2} k_x [1 + \cos(nx - \sigma)] +$$

$$\sum_{impropers} \frac{1}{2} k_i (\phi_i - \phi_{i0})^2 +$$

$$\sum_{i}^{N} \sum_{j}^{N} \left[4\varepsilon_{ij} \left[\left(\frac{\sigma_{ij}}{r_{ij}} \right)^{12} - \left(\frac{\sigma_{ij}}{r_{ij}} \right)^{6} \right] + \frac{q_i q_j}{4\pi\varepsilon_0 r_{ij}} \right]$$

Equation 5

The sum of all the above equation gives the potential energy, V of a system containing N number of particles, r where:

k is the stiffness constant, l_{i0} is the initial position and $l_i$is the current position.

k is the force constant θ_{i0} , is the initial position and θ_i is the current position.

k_x represents the barrier minima, n is the number of periodic cycles, σ is the angle used.

k is the stiffness constant ϕ_i is the current displacement value, and ϕ_{i0} is the equilibrium position.

Where $\mathcal{E}_{ij}$ is the depth of the energy minima σ_{ij} is the distance of interaction and r_{ij} is the distance between the particles in question.

The last equation represents the addition of non-bonded terms and the permanent electrostatic interactions needed to give total energy to the system.

4.2.1 Bonded interaction potentials

Bonded interactions, including bond length, angles and out of plane bending bonds, can be modelled by simple harmonic potential. Harmonic potential assumes that most two particles, joined by a bond, behave like two balls joined by a spring. The spring, which represents the bond, governs the force constant k where the higher the k-value, the stronger the bond/stiffer the spring and, thus, there will be a smaller amount of movement of the particles.

As shown in Figure 14, as the constant k becomes larger the curve becomes tighter and represents a smaller displacement from the optimum position (O) for the two particles in question. In turn, this reflects the strength of the bond holding the two together.

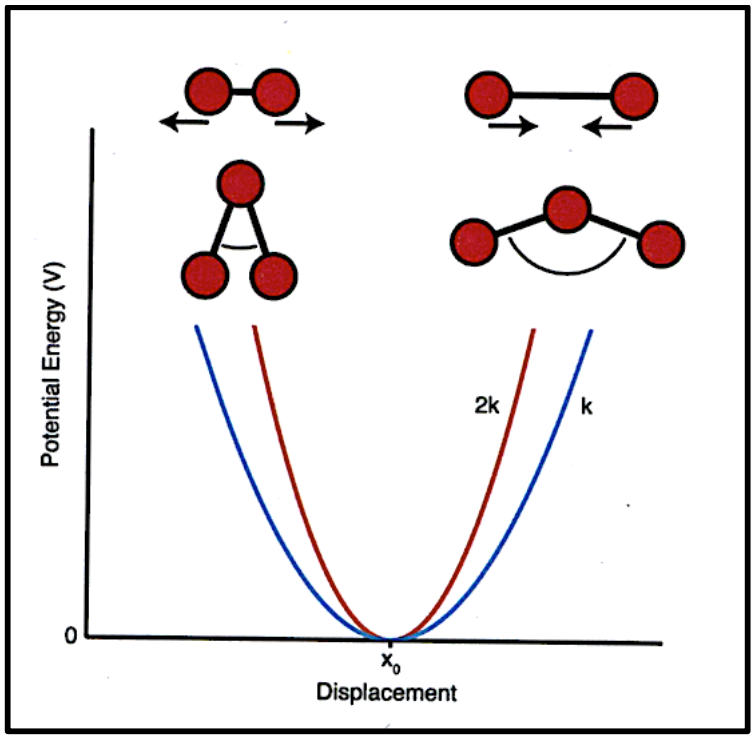

Figure 14 Harmonic Potential used in modelling bonded interactions and improper interactions where *k* represents the force constant and *2k* represents a larger force constant and X_0 is the optimum.

Bonds

The bonded terms are modelled using simple harmonic potential; these are represented by the following equation:

$$\mathbf{V}(x) = \frac{1}{2}\, k(x - x_o)^2$$

Equation 6

Where k is the stiffness constant x_o is the initial position and x is the current position.

Solving this equation provides an accurate value for the potential energy in bond stretching over a short distance from the equilibrium position. However, it does not work well for large displacements because, at large distances, the harmonic approximation breaks down. For long distance estimates, other potential energy functions (for example Morse potential) should be used since they model bond stretching more accurately than harmonic potential. Since, for these experiments, large displacements are not expected to occur throughout the simulations, it would be

acceptable to model using simple harmonic potential without the need to model long-distance movements more accurately.

Angles

As with the bonds, angles are modelled by using a harmonic potential represented in the equation below:

$$\boldsymbol{v(x) = \frac{1}{2} k_i(\theta_i - \theta_{i0})^2}$$

Equation 7

Where k is the force constant, θ_{i0} is the initial position and θ_i is the current position.

Changing the force constant parameter will either broadening or steepening the gradient of the parabola of the harmonic potential.

Torsions (dihedrals)

Since the potential energy surrounding a chemical bond making a 360-degree turn is periodic, torsions are expressed mathematically by using a cosine function (Figure 15), as in the equation below.

$$\boldsymbol{V(x) = \frac{1}{2} k_x[1 + \cos(nx - \sigma)]}$$

Equation 8

Where k_x represents the barrier minima, n is the number of periodic cycles, and the angle, used in the equation, is the one between the first 3 particles of the dihedral and the last 3 particles of the same dihedral.

The torsion energy is modelled by using the cosine periodic function shown in Figure 15 below. In these graphs, the height of each curve is governed by the constant k and the number of periods is governed by the n value in Equation 8 below. The angle σ moves the entire curve along the axis.

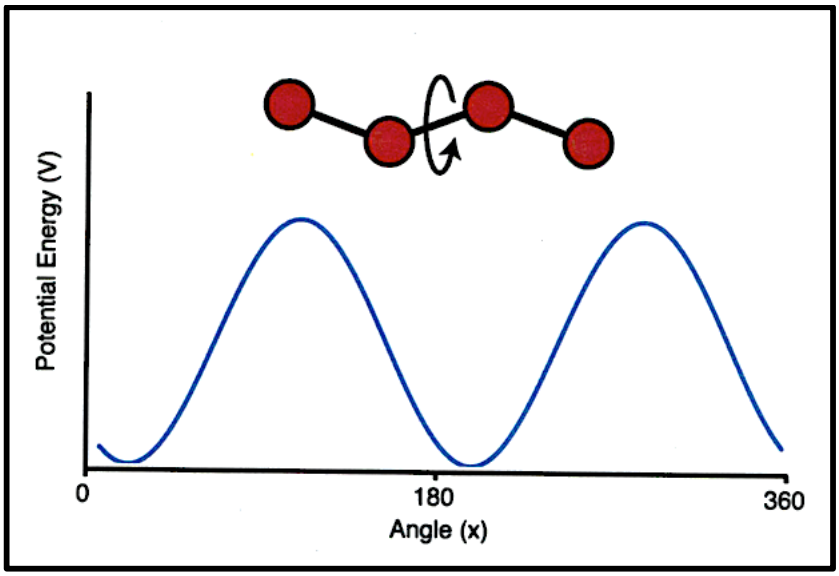

Figure 15 Cosine periodic function used to model rotations about bonds.

Improper

Improper refers to out of plane bending of bonds, and like bonds and angles, these are modelled by using a simple harmonic potential. The potential energy in their movement is calculated by using Equation 9 (shown below) where k is the stiffness constant; ϕ_i is the current displacement value, and ϕ_{i0} is the equilibrium position. As with bonds and angles, large displacements of these bonds are not expected to occur within the simulations required for this research. Consequently, it was concluded the use of harmonic potential should give sufficiently accurate results.

$$\sum_{impropers} \frac{1}{2} k_i (\phi_i - \phi_{i0})^2$$

Equation 9

4.2.2 Non-bonded terms

Non-bonded interactions consist of Van der Waals forces and electrostatic interactions between the particles. The Van der Waals can be represented by using Lennard-Jones potential that is represented by:

$$\boldsymbol{Potential\ energy = 4\mathcal{E}_{ij}\left[\left(\frac{\sigma_{ij}}{r_{ij}}\right)^{12} - \left(\frac{\sigma_{ij}}{r_{ij}}\right)^{6}\right]}$$

Equation 10

Where $\mathcal{E}_{ij}$ is the depth of the energy minima, σ_{ij} is the distance of interaction and r_{ij} is the distance between the particles in question.

As the particles get closer together, the $\left(\frac{\sigma_{ij}}{r_{ij}}\right)^{12}$ dominates the V value of the equation creating a repulsive force between them (Figure 16). At intermediate distances, the term $\left(\frac{\sigma_{ij}}{r_{ij}}\right)^{6}$ (also known as the attraction term) tends to dominate the function indicating there is an attraction between the two particles. At large distances between particles r_{ij} both the attraction and repulsion terms tend towards zero. However, the repulsion term does this faster than the attraction term by forcing the function to asymptote at zero. However, it remains marginally negative at the end.

Leonard jones potential is favoured in computational chemistry because the values for repulsion $\left(\frac{\sigma_{ij}}{r_{ij}}\right)^{12}$ can simply be derived by squaring the value for attraction $\left(\frac{\sigma_{ij}}{r_{ij}}\right)^{6}$.

Figure 16 (below) shows the Leonard Jones potential model for non-bonded interactions.

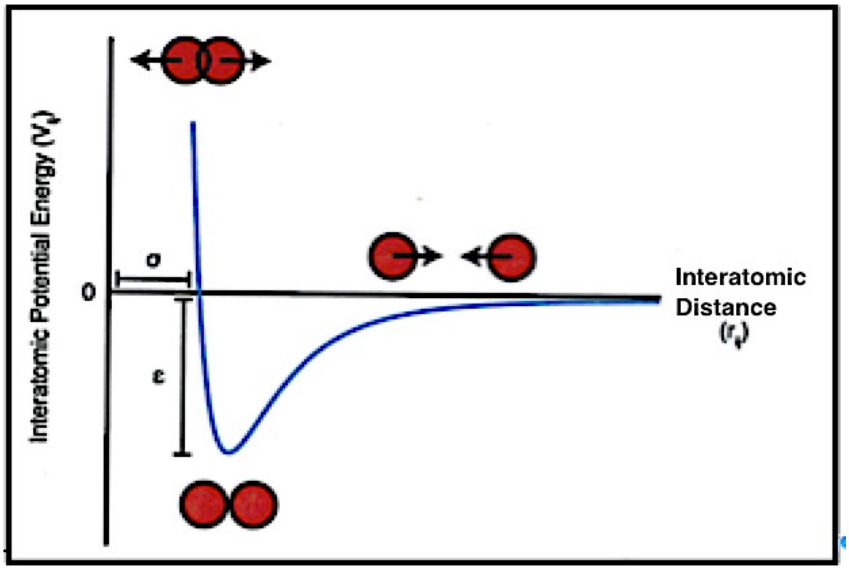

Figure 16 Leonard jones potential to model Van der Waals interaction.

Coulombs law is used when calculating electrostatic potentials.

$$V_{ij}^{qq} = \frac{q_i q_j}{4\pi \mathcal{E}_0 \mathcal{E}_r r_{ij}}$$

Equation 11

Where q is the point charge on particles j or I, $\mathcal{E}_0$ is the electric charge in vacuum, $\mathcal{E}_r$ is the relative electric charge and r_{ij} is the distance between point charges.

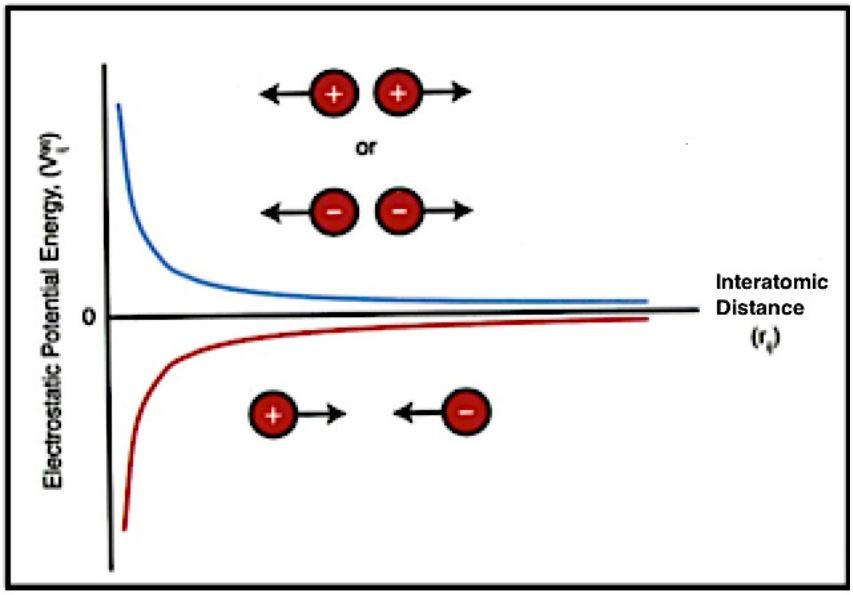

Figure 17 The dependence on intermolecular distance of the potential energy due to permanent electrostatics.

4.2.3 Boundary conditions

Periodic boundary conditions are used in molecular dynamic simulation to prevent interactions with the simulation box edges. Simulating in periodic boundary conditions means that, although the particles of the systems are confined to a box, they are surrounded by an infinite number of replica boxes in all directions. The boundaries between all these cells are non-existent. This means that particles pass freely from one box into the next without affecting the overall number of particles in the original box since an identical particle to the one that exits a box enters it from the opposite replica box. By carrying out molecular simulations in this manner, it is possible to simulate efficiently the interactions of a large volume of biological material and extrapolate conclusions from the results.

4.2.4 Long range interactions

These calculations summarize the interactions between a pair of particles throughout the system and, therefore, they require a lot of computational power. To reduce the amount of computational exertion, a cut-off distance for interactions is imposed. This cut-off distance can be applied without the loss of any accuracy because of the Lennard-jones potentials approaching zero quickly at distances greater than 0.1 nm (as discussed above in Section 4.2.3) and there is often no need to calculate interactions beyond this distance. This means interactions, taking place beyond the cut-off, are not calculated, allowing the computational energy to be focused on relevant interactions to the system. To further increase the computational efficiency, a cut-off distance can limit, also, the electrostatic calculations. However, applying this cut-off can result in a lack of accuracy since the electrostatics tend towards zero slower than the Lennard-Jones potential.

4.2.5 Initial co-ordinates of proteins and membrane:

The initial coordinates for the membrane were created by using the martini insane.py script (109). The script works by forming a grid and filling it up systematically with protein lipids and water. The script can be used to embed proteins into membranes of different compositions. The script was used to create the two types of membrane utilized in the simulations. The first membrane was composed of one part POPC and two parts of each POPG and POPE lipids and another POPC only membrane. This

method was used to create only the membranes and not to incorporate the proteins into the membrane. This was because the thesis' aim was to understand how the proteins interact with the membrane surface and how it penetrated the membrane surface.

The initial structure of Dermaseptin B2 peptide was downloaded from the Protein data bank. From the protein data bank, it was possible to download experimentally verified accurate structure for the peptide Dermaseptin B2 used for this research.

The second peptide, used in this research, was unavailable to download from the protein data bank but, since the sequence of the protein was known, it was possible to build a starting structure using the Modeller program (110). This program uses comparative structure modelling to predict tertiary and quaternary structures of proteins. It does this by using a technique, known as satisfying spatial restraints, in which a set of geometrical criteria is used to predict the location of each atom within a protein structure. It uses known structures of proteins with similar sequences effectively to create a new model for the new peptide. Modeller was used in creating a reasonably reliable yet unverified structure for Dermaseptin DS01 that was used throughout the course of these simulations (110).

4.2.6 Energy minimization

Minimization steps are done to eliminate overlapping of atoms or bad contacts in a system. The energy minimization, used in these simulations, was done by using the steepest descent integrator; this works by moving particles in the direction vector of a negative potential energy (111). This algorithm's first step is set to a default following which the step size is increased gradually to a point where an increase in potential energy is seen. If a step increases the potential energy, the step size is reduced in the following repetition to re-establish the lowest energy potential of the system by using a small step size in all subsequent repetitions. This process is continued until either the set number of steps is reached or the forces have converged to a potential energy that is lower than the maximum tolerated value.

4.2.7 Initial velocity

This is the velocity given to each particle for the reference temperature. The velocity is assigned randomly to the particle from the Maxwell-Boltzmann distribution. This describes particles speeds in idealized gasses where they can move freely inside a container without interacting. Then, this velocity assigned is adjusted to make the total momentum of the system zero.

4.2.8 Integration algorithm

For a large number of particles, the equations cannot be solved analytically. This makes it difficult to predict a configuration that evolves with time for a system. Since the particles demonstrate chaotic behaviour, it makes it difficult to produce a trajectory of the particle motion over time from using the starting position and velocity of particles. Consequently, to reach those trajectories, finite difference integration methods are used to integrate the equations of motion.

This integration algorithm approximates the new position of particles velocity and acceleration by using Taylor series expansion.

4.2.9 Verlet algorithm

This is one of the first algorithms to be developed (112). It uses the position of a particle and its acceleration at time t and its position from time (t – δt) to calculate the particle's new position at time (t + δt) by using a Taylor series expansion for particle positions r at both (t + δt) and (t – δt). This is described in equation 12 shown below.

$$\boldsymbol{r(t+\ \delta t) = 2r(t) - r(t-\delta t) + a(t)\delta t^2}$$

Equation 12

A disadvantage of this algorithm is that the particle velocities are cancelled out by the equations and, therefore, the velocities must be estimated. The verlet algorithm does not self-start, meaning the particle positions at time (t – δt) are unknown and must be predicted so that the process can have a starting point which leaves some room for error (because it relies upon that first approximation of particle positions).

Leapfrog integration algorithm (113) is an alternative to verlet; it has been used in all simulations completed for this thesis. The algorithm works by calculating velocities of particles at ½ time intervals and new positions of particles at full-time intervals. The position and velocity of particles are calculated using equations 13 and 14 respectively shown below:

$$\boldsymbol{r(t+\delta t) = r(t) + \delta t v\left(t + \frac{1}{2}\delta t\right)}$$

Equation 13

$$\boldsymbol{v\left(t + \frac{1}{2}\delta t\right) = v\left(t - \frac{1}{2}\delta t\right) + \delta t a(t)}$$

Equation 14

Although the leapfrog algorithm produces simulation trajectories that are identical to the verlet algorithm, it has the following two main advantages over the verlet algorithm:

- It has an equation dedicated to calculating the velocities of each particle; this adds a welcomed degree of accuracy to the trajectory.
- It does not need the difference between two large floating points numbers to be calculated which, in the verlet algorithm, introduces a large rounding error.

4.2.10 Thermostats

Thermostats are used in the systems to regulate the temperature of the system. Several thermostats were developed over time and all serving a cause.

4.2.10.1 Berendsen thermostat

This couples the particles to the temperature of an external thermal bath (114). The temperature of the bath is set to the desired temperature in the mdp file and then the bath adds or removes kinetic energy to the system so that it remains at that set temperature throughout the simulation.

$$\frac{dT(t)}{dt} = \frac{1}{\tau}\left(T_{bath} - T(t)\right)$$

Equation 15

$$\Delta T = \frac{\delta t}{\tau}\left(T_{bath} - T(t)\right)$$

Equation 16

Where τ is the coupling parameter, T_{bath} is the temperature in the bath and *T(t)* is the set temperature.

Where τ is the coupling tightness to the heat bath. If this value is small, it means the system is coupled strongly and vice versa.

The velocity of the particles is re-calculated every time step by using a factor λ. The velocity of the particles is multiplied by factor λ to try and get the temperature closer to the set temperature.

$$(\lambda^2 - 1)T(t) = \frac{\delta t}{\tau}\left(T_{bath} - T(t)\right)$$

Equation 17

$$\lambda^2 = 1 + \frac{\delta t}{\tau}\left(\frac{T_{bath}}{T(t)} - 1\right)$$

Equation 18

Where λ is the proportionality constant, τ is the coupling parameter, T_{bath} is the temperature in the bath and *T(t)* is the set temperature.

4.2.10.2 Berendsen barostat

The Berendsen Barostat maintains a constant pressure by coupling the system to an external pressure bath with a coupling constant τ (114). This ensures any change in pressure occurs gradually over time. These are calculated using the following equations.

$$\frac{dP(t)}{dt} = \frac{1}{\tau}\left(P_{bath} - P(t)\right)$$

Equation 19

As the simulation progresses, the volume of the box is scaled by a factor of λ which is calculated by equation 20 shown below.

$$\lambda = 1 - k\frac{\delta t}{\tau}(P - P_{bath})$$

Equation 20

In the simulations, completed for this thesis, the coupling was semi-isotropic. This means that the simulation box was scaled in the XY vectors independently of the Z vector. This manner of coupling allows the membrane bilayer to equilibrate itself independently of the solvent around it.

Chapter 5: Simulation Methods

5.1 Molecular Dynamics Simulations

All molecular dynamics simulations were run using the Martini CG 2.0 coarse-grain force field (102) and the Gromacs 4.5.5 software package (www.gromacs.org). The Martini coarse grain model was implemented since Gromacs fully supported it and there was sufficient evidence to support its use for lipid-protein systems (101, 105). Coarse-graining was applied to achieve a higher magnitude of time from the relatively large systems to be simulated compared to all atom simulations. Coarse-graining was also suitable because the case of lipid –peptide interactions being studied here the compromise between detail and timescale was in favour of timescale. This is because long timescales are required to study binding and membrane interactions. In that sense, it was necessary to have the longest timescale possible for the simulations and, accordingly, this justified coarse graining the system. This method combines atoms into larger coarse-grained beads and thus reduces the overall number of particles in the system whilst maintaining the same system size. As fewer calculations now must be done per time-step, longer timescales are accessible for the same amount of computer time compared to atomistic simulations.

The lipid bilayer was built by using the Martini insane.py script (109) designed by the Marrink group. It is intended to place lipids randomly around proteins and, thereby, quickly and simply building a protein-lipid system that does not limit the lipid composition of the membrane. This script was used to make various membranes of different sizes and different compositions. All of which were used for this thesis. The script works by building a grid upon which it places either the protein or lipids and water to create an effortlessly diverse system. The script works by creating two leaflets of a membrane in 2D and surrounding it in a 3D structure of solvent which, in many cases, is water. In this way, the script can incorporate protein very easily into a membrane and, in the same way, it is used to build membranes with varied lipid content and various sizes. For this thesis, Insane.py (109) was used to create two membranes, one containing a mixture of POPC, POPG, POPE in the ratio of 1:2:2 (designed to imitate the inner membrane of Staphylococcus aureus bacterium) (115), and another membrane containing just POPC. The second membrane was created to

be used as a comparison platform for the prediction that the positively charged antimicrobial peptides were attracted to the negatively charged lipids in the membrane. Consequently, the POPC membrane should provide comparative data of what happens when the antimicrobial peptides are put into positively charged membranes. In theory, this can be considered as the basal interaction of membrane and protein and provides a clean slate to compare the results of the bacterial inner membrane to. Although, to the best of the researcher's knowledge, this thesis is the first to take this comparative approach, it seems fair, when testing a theory, that antimicrobial peptides are attracted to negatively charged lipid to place them in a positively charged and to observe how they interact with it.

The protein was coarse-grained by using another martini script, martinize.py (108). This parameterizes an all-atom structure of the protein and produces a coarse-grained version of it. The script uses a standardized bead description to classify and map each cluster of atoms into a coarse-grained bead. It uses the following four bead types: polar; non-polar; apolar; and charged. These are each sub-divided into various groups which total 20 bead types to cover most possible atomic states. In this way, the coarse-grained model, created by this script, is highly reflective of the actual state of the same all-atom model and, therefore, can be trusted.

The Lennard-Jones interactions (in the range of 0.9-1.2 nm), as well as electrostatic interactions (in the range of 0-1.2 nm), were shifted to 0, as recommended by the martini group when using their force field (102).

Non-bonded neighbour list was updated every 10 steps with a cut off of 1.2 nm.

All simulations were done under constant pressure and temperature that were coupled individually by different barostat and thermostat and both were coupled semi-isotropically. The temperature for all lipids and proteins were coupled by using the V-rescale thermostat and was set to the same temperature for every component in the system. The system's temperature was raised systematically throughout the simulations. Since most experimentalists considered the peptide at room temperature, it seemed appropriate to start off simulations at 300 K. Since there was no significant membrane penetration, the temperature was raised slowly to 315 K (which is above the normal body temperature but it takes into consideration fevers which are associated with infections) and, ultimately, settled at 320 K. It did not seem

logical to go above that temperature because the peptide was unlikely to interact with a realistic membrane at a temperature considerably higher than normal body temperature.

The pressure was constant, also, for the whole system and was maintained at 1 bar by using the Berendsen algorithm (114). Coupling type was semi-isotropic with a compressibility of 3×10^{-4} bar^{-1}; this ought to have given the system sufficient room to manoeuvre freely and to assemble into new states.

The time step for the simulations was 10 fs and no restraints were used throughout all simulations.

In all systems, the peptides were placed initially outside and above the membrane.

5.2 Table of simulations

Number of peptides	Time MS	Temperature K	Membrane
Dermaseptin B2			
6	10	300	1:2:2 PC:PG:PE
10	10	300	1:2:2 PC:PG:PE
12	10	300	1:2:2 PC:PG:PE
25	10	300	1:2:2 PC:PG:PE
3	10	315	1:2:2 PC:PG:PE
6	10	315	1:2:2 PC:PG:PE
10	10	315	1:2:2 PC:PG:PE
12	10	315	1:2:2 PC:PG:PE
25	10	315	1:2:2 PC:PG:PE
3	10	320	1:2:2 PC:PG:PE
6	10	320	1:2:2 PC:PG:PE
10	10	320	1:2:2 PC:PG:PE
12	10	320	1:2:2 PC:PG:PE
25	10	320	1:2:2 PC:PG:PE
3	10	320	PC
6	10	320	PC
10	10	320	PC
12	10	320	PC
25	10	320	PC
Dermaseptin DS01			
3	10	320	1:2:2 PC:PG:PE
6	10	320	1:2:2 PC:PG:PE
10	10	320	1:2:2 PC:PG:PE
12	10	320	1:2:2 PC:PG:PE
25	10	320	1:2:2 PC:PG:PE
3	10	320	PC
6	10	320	PC
10	10	320	PC
12	10	320	PC
25	10	320	PC

Table 6 Table summarising the simulations with Dermaseptin B2 and Dermaseptin DS01 carried out for this thesis. In all systems, the peptides start outside and above the membrane.

5.3 Summary of simulations

All simulations ran at 300 K 315 K and 320 K for 10 microseconds at a 10 femtoseconds time step.

Temperature coupling: V-rescale

Pressure coupling: Berendsen.

Membrane composition used was 1:2:2 POPC: POPG: POPE with sodium ions to neutralise any excess negative charge.

.

Chapter 6: Results of simulations

All simulations were done by using the coarse-grained method and GROMACS 4.5.5 (www.gromacs.org) in a Martini 2.0 force field (102). The lipid membranes were built by using the insane.py script (109) and varying numbers of Dermaseptin peptides were added to the system outside of the bilayer. Then, the simulations were run under constant temperature and pressure for 10 ms. This chapter records the results.

In the Dermaseptin-B2 simulations, the peptides clustered very rapidly, often within the first 50 frames (0.5 ms) of the simulation and the cluster became membrane bound. In all the independent trials done at various temperatures and with increasing number of peptides, shallow membrane penetration was observed, mostly by the protein side chains but sometimes the backbone, also, penetrated the membrane.

A common observation with all the simulations was that, wherever the protein cluster attached to the membrane, there was a significantly higher proportion of POPG/POPE lipids as compared to POPC lipids. Figure 18 shows some snapshots from various simulations with different protein concentrations at various points in a simulation depicting the protein's lipid preferences.

No pattern was seen relating to protein clustering and protein-membrane association; both these processes appeared to happen randomly with no specific termini playing a significant role in its occurrence.

6.1 Dermaseptin-B2 in POPC, POPG, POPE membrane

Summary of simulations

These simulations were run in coarse-grained structures by using GROMACS. The Lennard-Jones interactions were shifted smoothly to zero at distances between 0.9 nm and 1.2 nm. The non-bonded neighbour list was updated every 10 steps and all simulations were conducted under constant temperature, pressure, and number of particles. The temperatures of the protein, POPC, POPG, POPE, and solvent, were each coupled separately by using the V-rescale thermostat at temperatures of 310 K, 315 K, and 320 K, with a coupling constant $\tau T = 1$ ps. The system pressure was coupled semi-isotropically by using the Berendsen algorithm at 1 bar with a coupling constant $\tau P = 1$ ps and a compressibility

of 5 x 10^{-6} bar^{-1}. Separate runs of each peptide concentration were run at 300 K, 315 K and 320 K for 10 microseconds at a 10 femtoseconds time step and the results were compared.

The system contained varying number of peptides, a POPC, POPG and POPE membrane in water and sodium and chlorine ions to neutralize any excess negative charge.

6.1.1 Lipid specificity Dermaseptin B2

The snapshots in Figure 18 illustrate how the peptides clustered around the POPG and POPE lipids. In all cases, it appears the peptide clusters are bound in areas of high red and grey beads representing the two lipids.

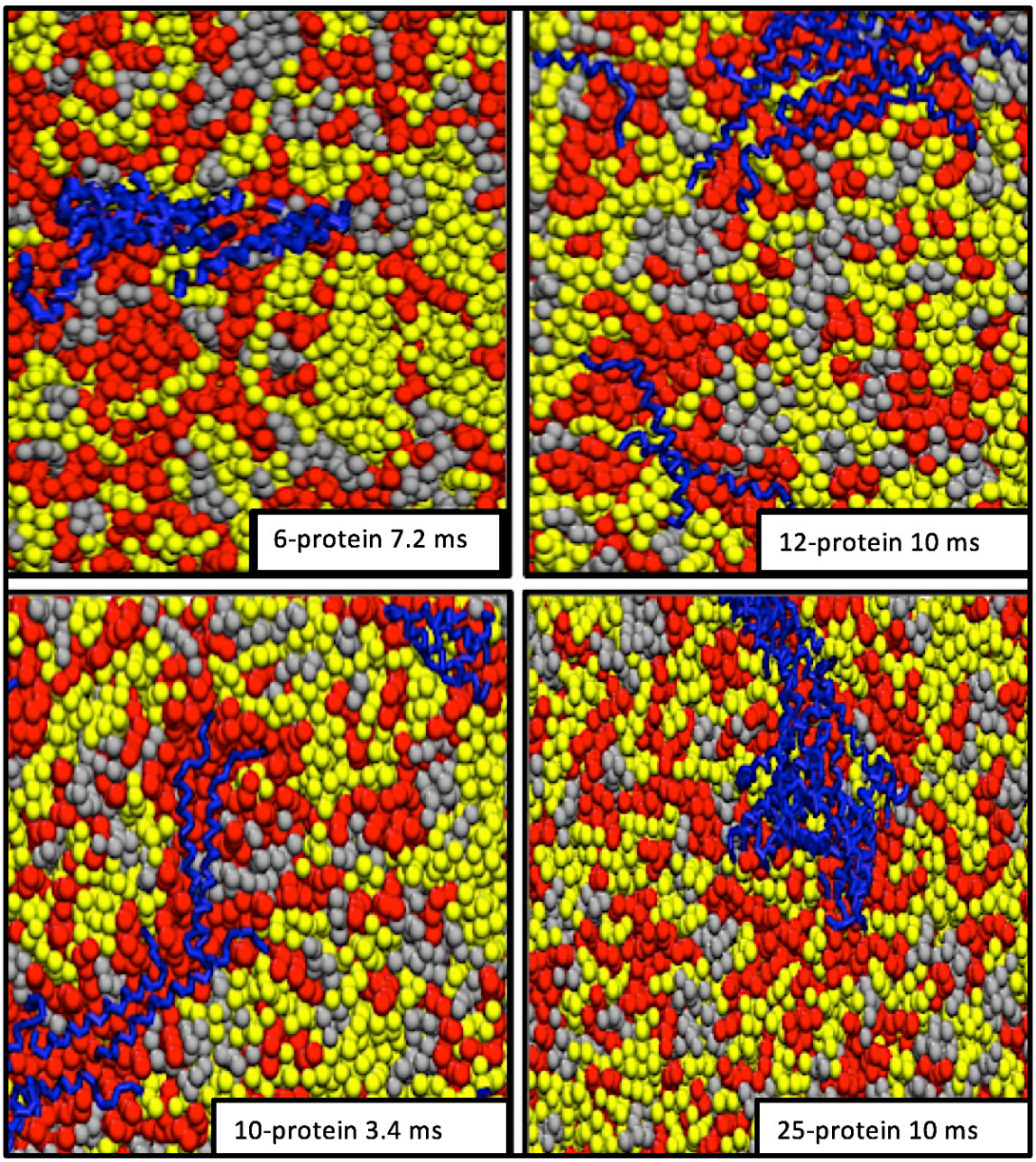

Figure 18 Snapshots showing lipid specificity: Colour scheme: Yellow: POPC Red: POPG Grey: POPE Blue: protein helices. As the pictures show, there are significantly higher proportions of red and grey beads (POPG/POPE) surrounding the protein compared to yellow beads (POPC) suggesting that the proteins prefer a negatively charged environment.

6.1.2 Simulation results

6 protein simulations:

A typical 6-protein simulation scenario would involve a peptide attaching to the membrane within the first microsecond of the simulation and adopting a parallel orientation in relation to the membrane. Then, the rest of the peptides would cluster and that cluster would attach itself to the membrane at the point where the single peptide attached by 5 ms. It is unclear if there is a mechanism that facilitates clustering or binding of a cluster once a single peptide becomes membrane bound. In some simulations, the side chains of the protein can be seen within the membrane bilayer transiently but no full membrane penetration (where the whole protein becomes embedded within the bilayer) was seen in all simulation at all temperatures. This is consistent with the literature.

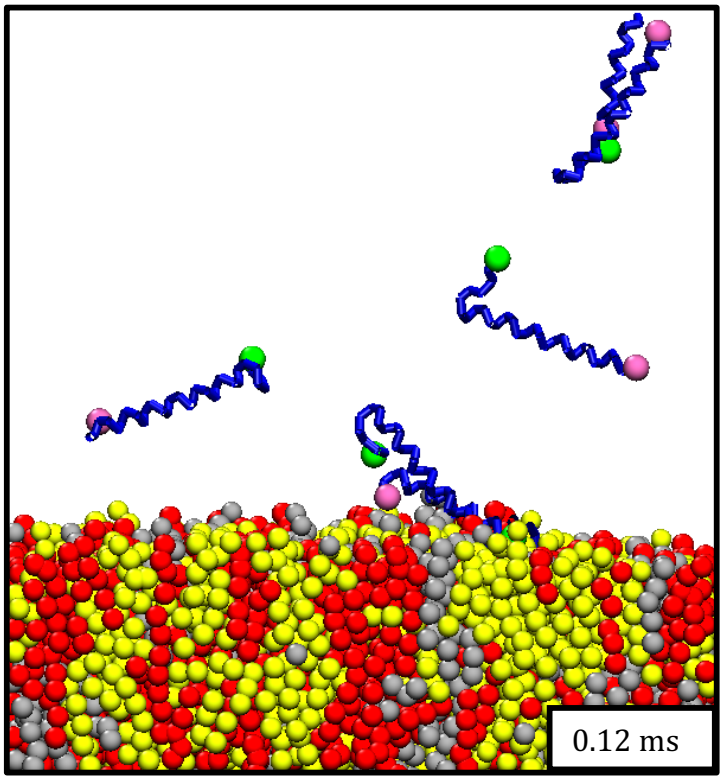

Figure 19 **Colour scheme is: Yellow: POPC Red: POPG Grey: POPE Blue: protein Green: N-terminus of protein and Pink C-termini of protein. This snapshot shows 2 peptides attached to the membrane while a dimer is being formed in the top right corner. As shown by the time, this has occurred very early in the simulation. No specific pattern for clustering or shape to a cluster was seen in these simulations suggesting that the proteins clustered randomly as they approached one another.**

As this simulation went on, the cluster of proteins bound eventually to the membrane surface and the side chains of those proteins can be seen within the membrane bilayer. No specific side chain was noted to always penetrate the membrane surface and the process was very transient. There is, also, some membrane curvature observed. It is unclear if this is relevant either to the antimicrobial function or the mechanism through which it has occurred at this point. There was no mention in the literature about Dermaseptin causing membrane curvature.

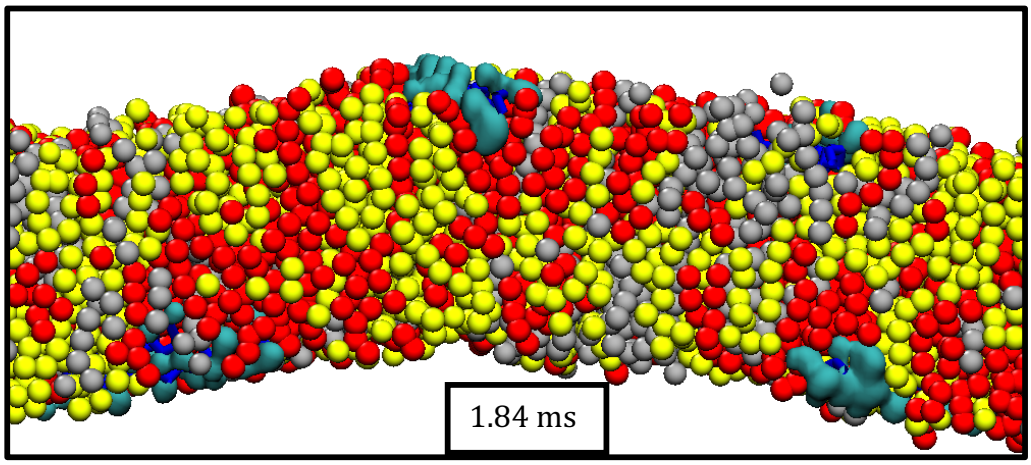

Figure 20 Colour scheme is: Yellow: POPC Red: POPG Grey: POPE Blue: protein and Teal: the protein side chains. As shown in the snapshot, the side chains of the proteins have penetrated the membrane surface partially near the POPG and POPE lipids.

This scenario was observed in all the simulations with 6 proteins. However, there was one simulation where after 8.5 microseconds the protein backbone started to penetrate the membrane surface. As with the protein side chains, the process was also transient as the simulation completed the protein backbone was back on the bilayer surface.

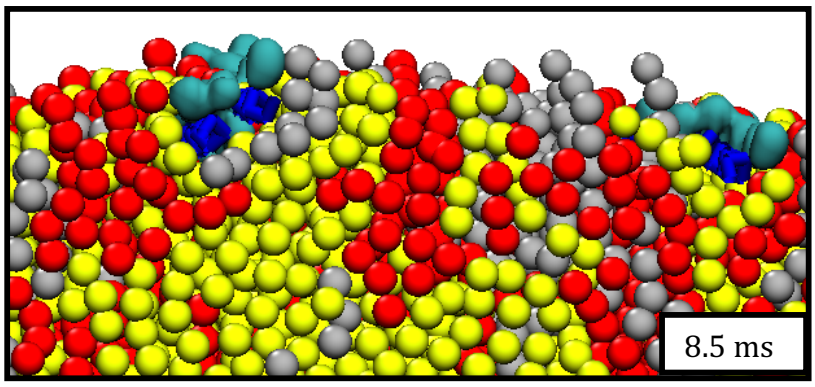

Figure 21 As shown the blue protein helices can be seen deeper into the membrane bilayer. Colour scheme as in figure 20 (above).

10-protein simulations

With these simulations, the findings are as above. One protein became attached while the clustering process was occurring and, once again, the cluster became attached where the first protein attached.

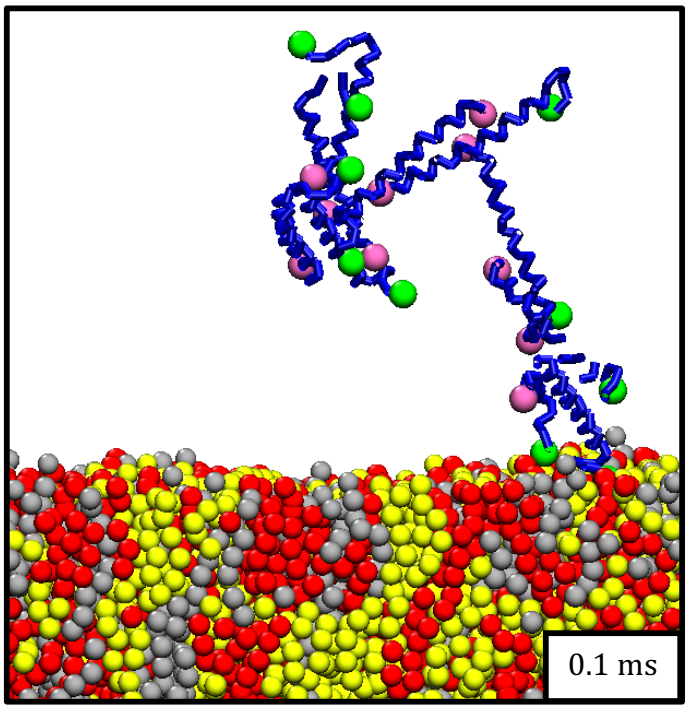

Figure 22 Colour scheme is: Yellow: POPC Red: POPG Grey: POPE Blue: protein Green: N-terminus of protein and Pink C-termini of protein. As shown by the time stamp in this snapshot, both protein clustering and association with membrane occurred within the first 0.1 ms.

Protein clustering was rapid as was membrane protein association. Protein side chains penetrated the membrane briefly and further down the simulation the protein backbone began to do the same. The snapshots in Figure 23 (shown below) highlight this typical pattern of membrane protein association seen throughout the simulations.

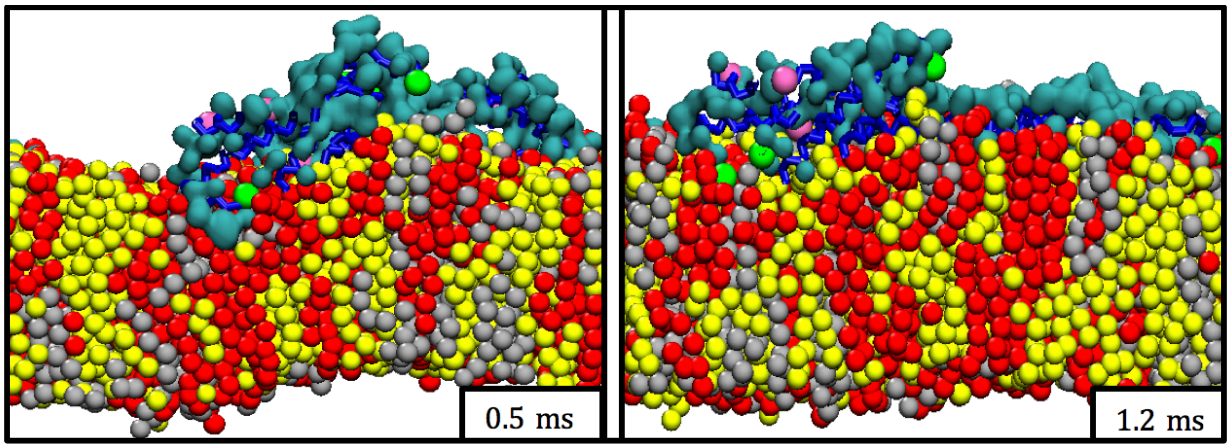

Figure 23 **Colour scheme is: Yellow: POPC Red: POPG Grey: POPE Blue backbone: protein Green: N-terminus of protein Pink C-termini of protein and Teal is the protein side chains. As shown in this snapshot at 0.5 ms, the protein side chains and a small proportion of the backbone can be seen penetrating the membrane surface. There is, also, membrane curvature that by 1.2 ms is re-equilibrated out by the membrane and most of the side chains have been expelled from within the bilayer. One big 10-protein cluster is seen spread out on the membrane surface at the end of the simulation.**

Once again and as with the 6-protein simulations, some membrane curvature is observed in these simulations but, quickly, it re-equilibrates itself out. It is unclear if the membrane curvature is related to the presence of Dermaseptin peptide.

12-protein simulation

The 12-protein simulations were similar to the 6 and 10-protein ones in that protein clustering occurred rapidly and the clusters became attached to the membrane and spent the rest of the simulation time interacting with it. As above, there was some side chain membrane penetration and little membrane curvature that was re-equilibrated by the end of the simulation. An interesting phenomenon occurred with one of the 12 protein trials; it could be seen that, once the proteins attached to the membrane surface, it appeared to stretch out the membrane in the x direction. The snapshots in figure 24 below, taken at 1 ms, shows the proteins clustered together, with time the cluster stretches out and with it the membrane. There was, also, significant membrane disruption seen visually in VMD (116) as the simulation progressed. This involved moments (about 0.5 ms total time) where there was significant particle movement in the system but as with the rest of the simulations, this re-equilibrated quickly. The final snapshot of the simulation taken at 10 ms shows the stretched membrane with the cluster still attached.

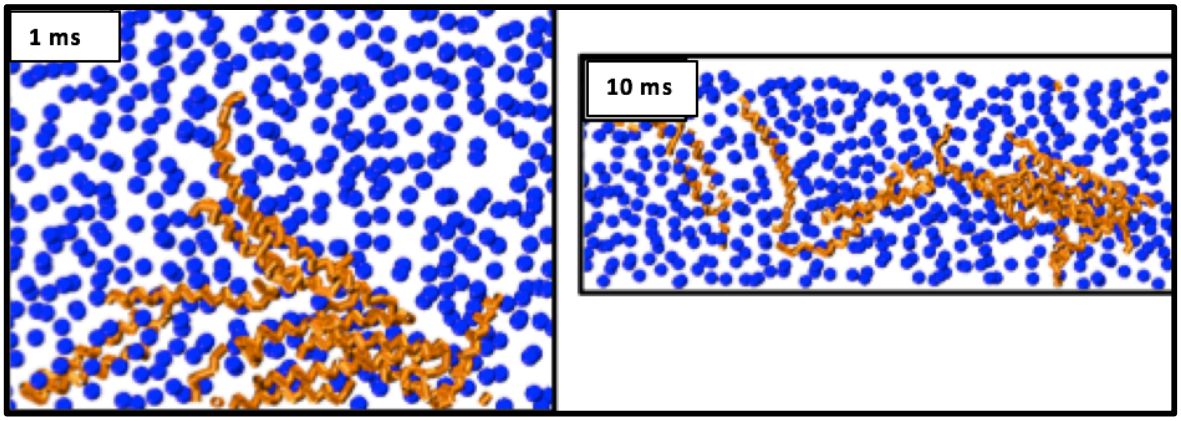

Figure 24 Snapshot from a 12-protein simulation showing a large peptide cluster appearing to stretch the membrane in the x direction. Colour scheme is: Blue, lipid headgroups and Orange, peptide backbone.

It is unclear whether this is either the result of the setup or if this simulation is something that is expected of Dermaseptin. However, it was not seen either in the other two independent trials with 12 protein simulations or any other peptide concentration. Using a locally written script and GROMACS tools, the change in box size throughout the simulation was plotted by using xmgrace (http://plasma-gate.weizmann.ac.il/Grace/) (graph 1).

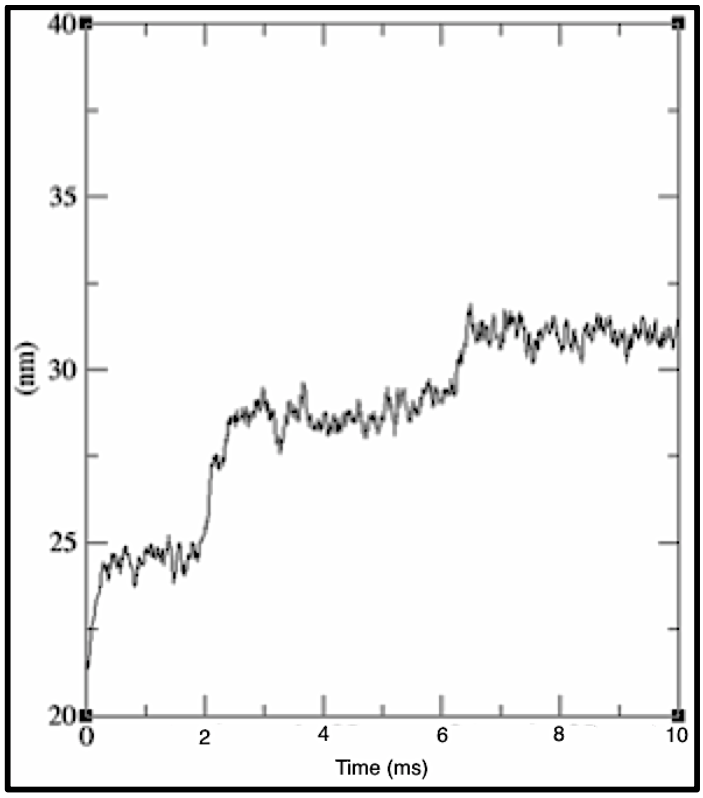

Graph 1 Graph representing increase in simulation box length in the x direction.

Graph 1 shows how the box has changed over the course of the simulation. As shown the box size has increased gradually from around 22 nm to 32 nm by the end of the simulation, increasing by roughly 68 % during the course of the simulation.

25-protein simulation

The 25 protein simulations were done in an attempt to reach the membrane saturation point as Dermaseptin is thought to work through the carpet model (see section 2.2.2) (33). As with the rest of simulations, rapid protein clustering and association was seen but even at this high concentration of peptide no full membrane penetration or destruction was seen. Figures 25 and 26 shows a typical early simulation and end of simulation snapshots.

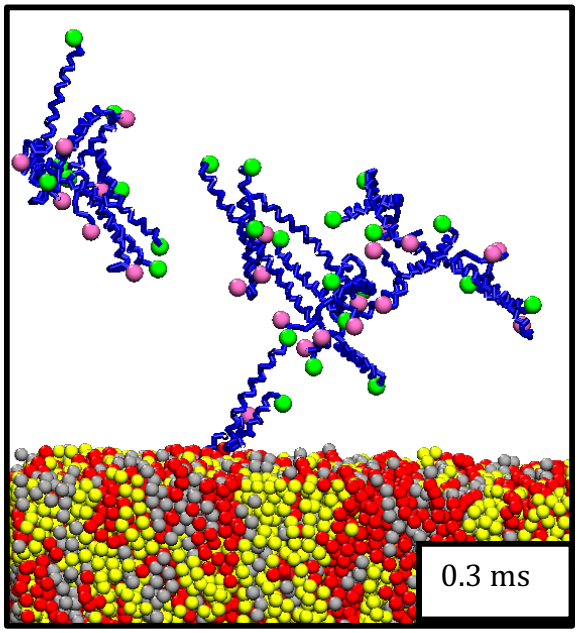

Figure 25 Colour scheme: Yellow: POPC Red: POPG Grey: POPE Blue: protein Green: N-terminus of protein and Pink C-termini of protein.

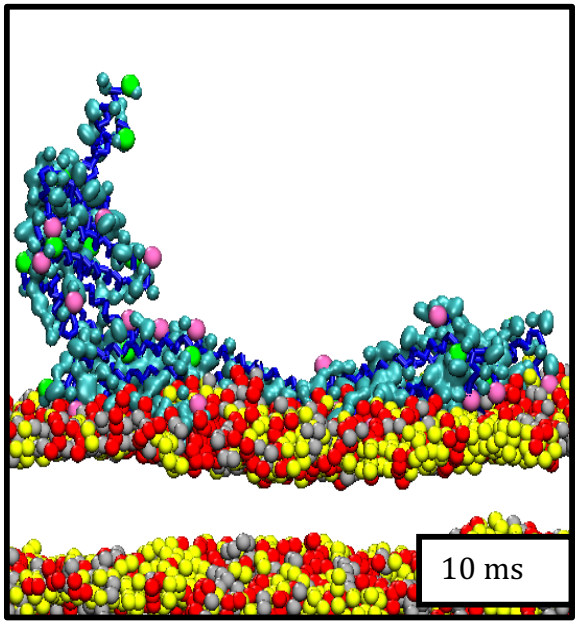

Figure 26 Colour schemes as above and teal representing protein side chains. A snapshot of a typical end frame of a 25-protein simulation.

6.1.3 Moved protein clusters

After running the system for 10 microseconds failed to show full protein penetration (where the entire protein backbone is seen inside the bilayer), the result clusters of protein were moved into the middle of the membrane bilayer. Then, the new system was minimized, re-equilibrated and, while keeping all simulation parameters as above, this new system used as the initial point for a new set of 10 microsecond simulations.

In most cases, the bilayer seemed to force the protein cluster out the membrane but the smaller peptide clusters managed to stay in place. From running these simulations, it was found that the membrane was able to accommodate up to 6 proteins in the middle of it and any bigger clusters were forced out.

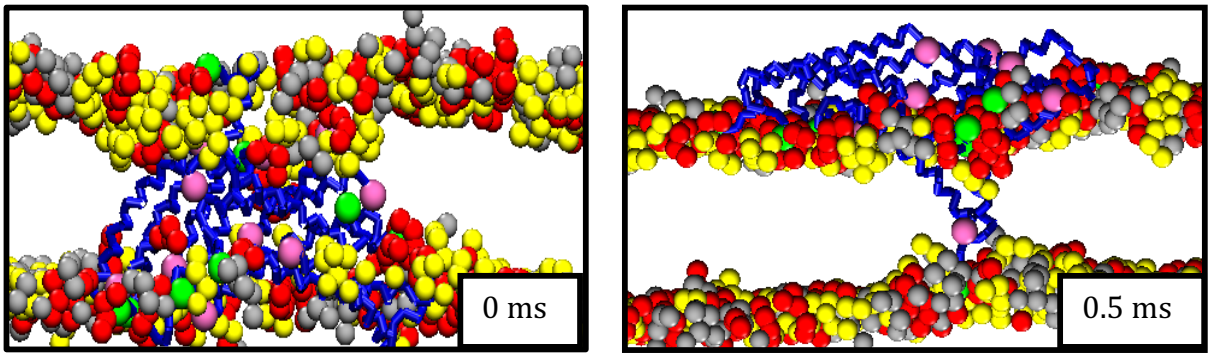

Figure 27 Colour scheme is: Yellow: POPC Red: POPG Grey: POPE Blue: protein Green: N-terminus of protein and Pink C-termini of protein. Snapshots from a 10-protein simulation where the protein cluster were forced into the membrane. The snapshots show how rapidly the peptides were forced out of the membrane; by 0.5 ms all but 2 peptides remain in the membrane.

The two snapshots in Figure 27 were taken from a 10-protein simulation. As seen at the start of the simulation, a 10-protein cluster was in the membrane and half a microsecond later most of the cluster had been expelled from the membrane. The cluster appears to be anchored to the membrane surface by 2 proteins that managed to stay in the middle of the bilayer.

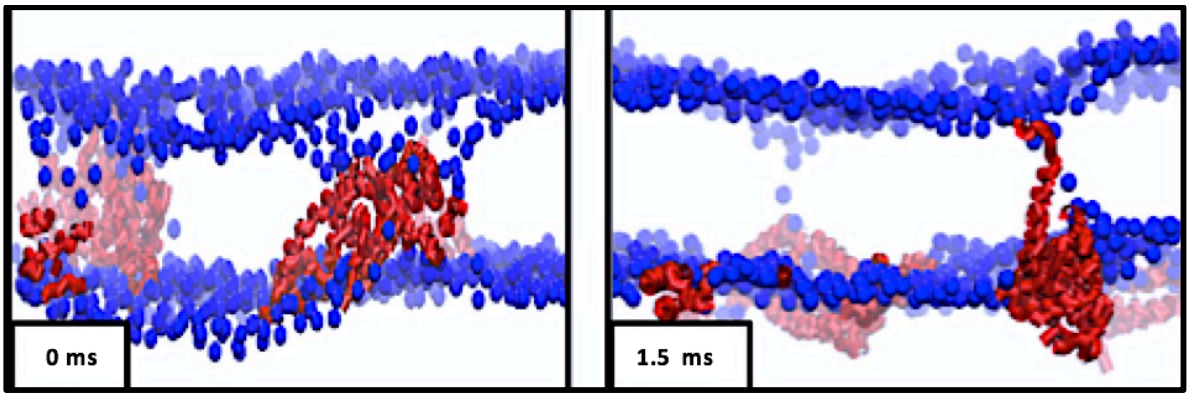

Figure 28 Snapshots taken from a 25-protein simulation where a cluster of peptides was forced into the membrane. The snapshots show the peptides being expelled from the membrane rapidly, with only one peptide remaining in the membrane after 1.5 ms. Colour scheme: blue, lipid headgroups and red, peptide backbone.

Figure 28 shows two snapshots taken from a 25-protein simulation. They show, also, how large clusters are expelled out of the membrane and highlights only that larger clusters stay in the membrane longer. It took the system 1.5 ms to force out most of the 25 proteins as compared to the half a microsecond it took to remove the 10-protein cluster.

3-protein simulation

In these simulations, the three proteins have been put into the middle of the membrane since they were three individual proteins and not a cluster. However, they were unrestrained and able to move freely in the middle of the membrane. By the end of the 10-microsecond simulation, they had formed a cluster that resembled a pore-like structure through the membrane shown in the snapshots in figure 29 below.

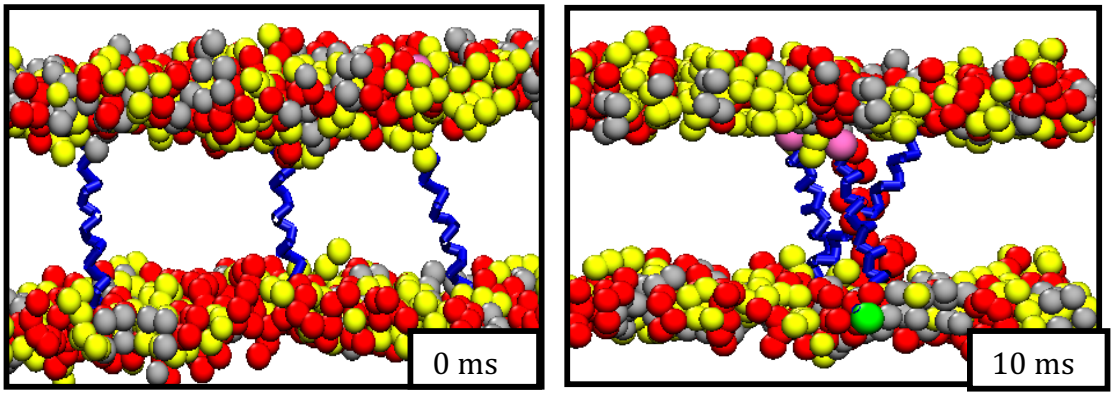

Figure 29 **Colour scheme is: Yellow: POPC Red: POPG Grey: POPE Blue: protein Green: N-terminus of protein and Pink C-termini of protein. The snapshots show that, by the end of a 10 ms simulation, the peptides have formed a cluster that remained within the membrane. Colour scheme: red, lipid headgroups and blue, peptide backbone.**

The snapshot in Figure 30 shows a top view of the 3-protein cluster. As can be seen, it is starting to look like a pore. This particular simulation was extended for another 10 ms hoping to see the pore form and some water passing through it but that had not occurred.

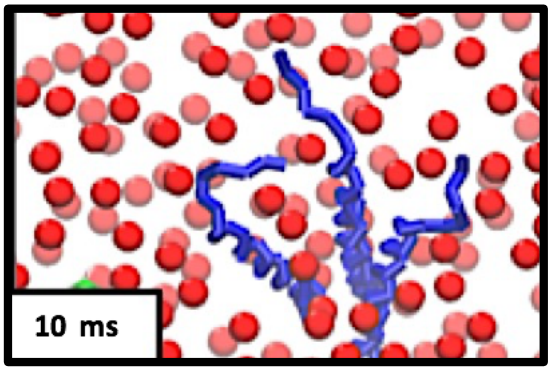

Figure 30 **Snapshots taken from a top view of the 3-protein cluster with the membrane. Colour scheme red, lipid head groups and blue, peptide backbone.**

6-protein simulation

Although it managed to stay in the membrane, the 6-protein cluster caused significant disruption and curvature to the bilayer. The cluster was free to move across the middle of the membrane but, as it moved, there was significant membrane curvature that quickly re-equilibrated once the cluster had moved from the area. The snapshots in Figure 31 below show a disrupted membrane at 3 microseconds and how it managed to equilibrate itself by the end. It appears as if the membrane is about to rupture locally where the cluster of

proteins is located. Therefore, the simulations were extended to see if the membrane split which it did not.

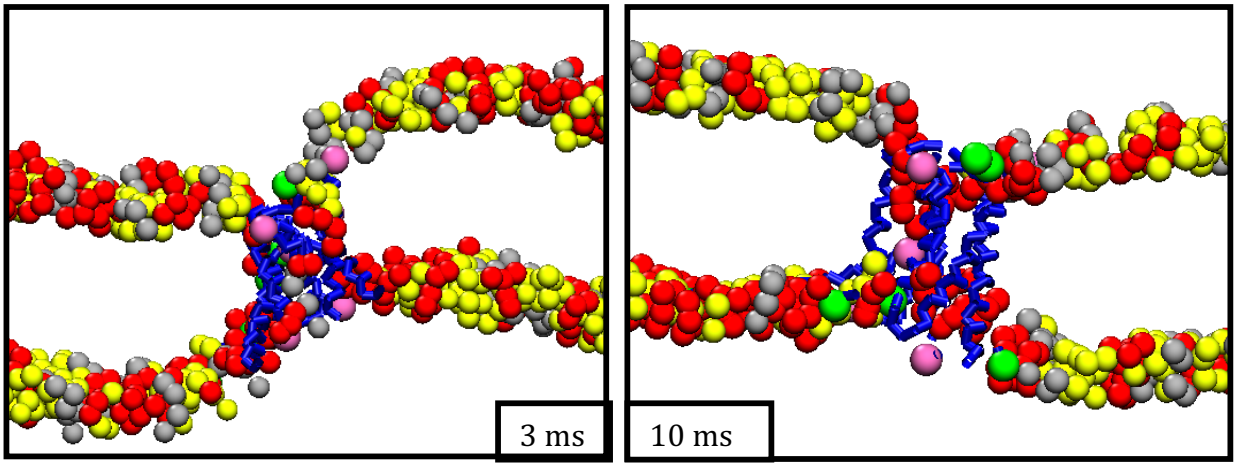

Figure 31 Colour scheme is: Yellow: POPC Red: POPG Grey: POPE Blue: protein Green: N-terminus of protein and Pink C-termini of protein. Snapshots from a 6-protein simulation showing the cluster remained within the membrane and caused significant membrane disruption and curvature.

6.2 Dermaseptin DS01 protein in POPC, POPG, POPE membrane

6.2.1 Lipid specificity

Like Dermaseptin B2, this peptide appears, also, to be attracted to the negatively charged POPG lipid residues. In all the ran simulations and at all peptide concentrations, large clusters of peptides formed in areas of the membrane that were rich in POPG. The snapshots in Figure 32 below are taken from different simulations ran with varying protein concentrations and they show clearly the lipid clustering.

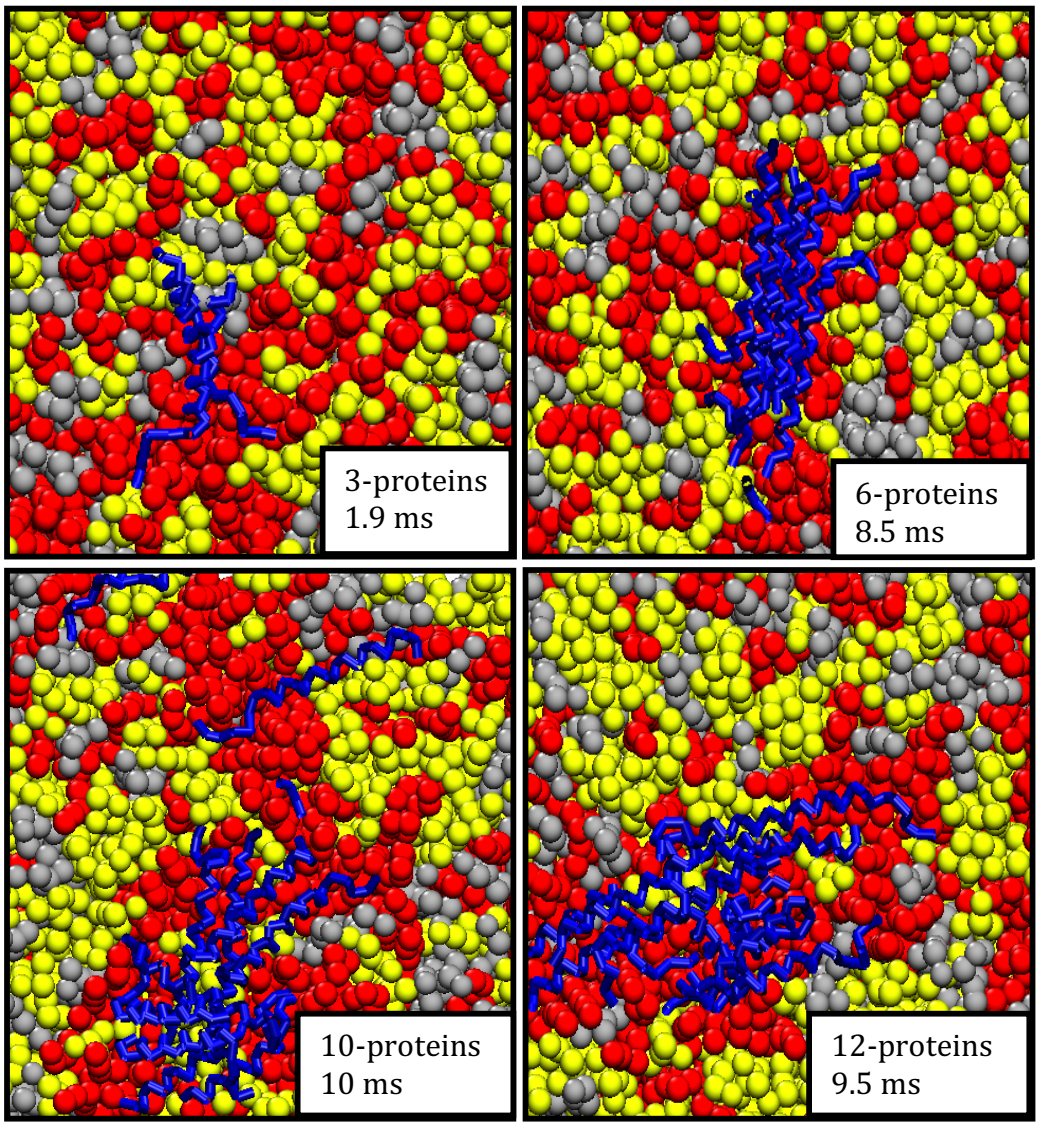

Figure 32 Lipid specificity: colour code is: Yellow: POPC, Red: POPG, Grey: POPE and Blue is the protein backbone. All four snapshots were taken at different times within each of the simulations. As shown, there is a clear pool of red beads surrounding the protein clusters. This suggests that Dermaseptin DS01 is more attracted to the negatively charged lipids.

6.2.2 Simulation results

3 protein simulations

These simulations show that the proteins cluster together very rapidly and become attached to the membrane. There is no effect seen on the membrane; this is presumably because the protein concentration is too low.

6 protein simulations

The simulations often show that the proteins cluster very rapidly at the beginning of the simulation before interacting with the membrane. In all cases, the clusters form and then become attached to the membrane. At first, the cluster is perpendicular to the membrane; however, that soon changes formation and the cluster becomes parallel to the membrane surface. This is seen with the Dermaseptin B2 simulations and, therefore, there appears to be no difference in membrane protein association and cluster formation between the two peptides.

With the 6 protein simulations, membrane disruption is visible where the protein clusters attach. This is not seen with the Dermaseptin B2 peptide and may suggest that this peptide has more membrane surface effect than Dermaseptin B2.

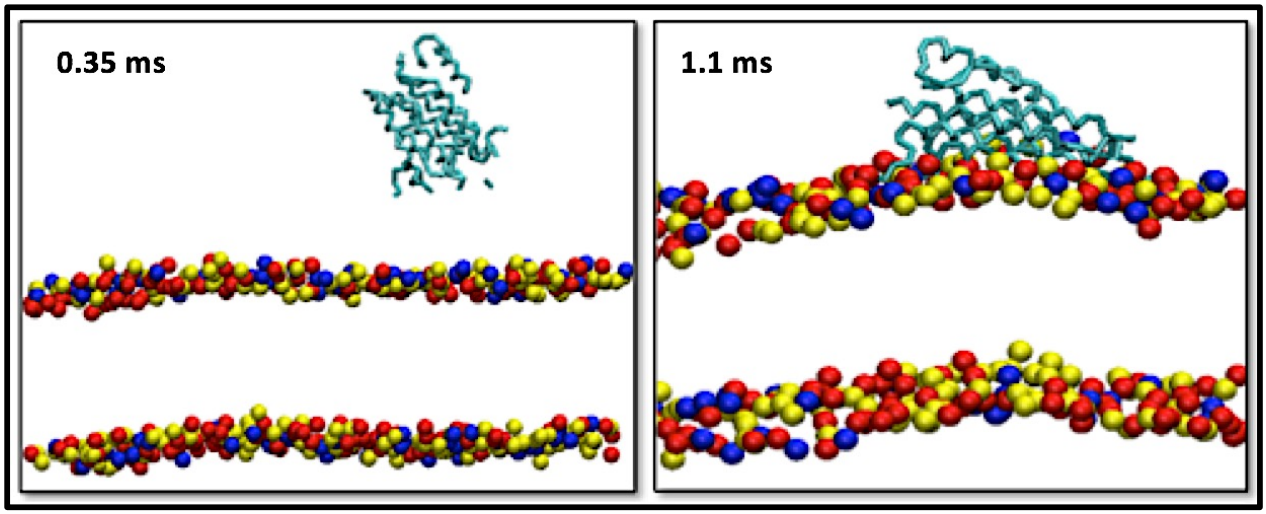

Figure 33 Two snap shots taken from a 6-protein simulation. Colour code is: blue POPC, red POPG, yellow POPE, and cyan protein. The snapshots show a protein cluster forming independently of the membrane and then attaching onto the membrane. The cluster appears to attach parallel to the membrane; this is the same way in which Dermaseptin B2 attaches to the membranes.

10 protein simulations

The 10-protein simulations again show the rapid clustering of proteins and the quick attachment of protein clusters to the membrane. As with the 6-protein simulation, there is, also, significant membrane disruption where the protein clusters attach to the lipid headgroup. However, within a short time, they re-equilibrate themselves out. As expected, the clustering of proteins is very rapid and clusters attach to the membrane in a perpendicular form before settling parallel to the membrane for the rest of the simulation. The cluster was unrestrained and was free to move within the membrane surface causing disruption along its path; this was quickly re-equilibrated.

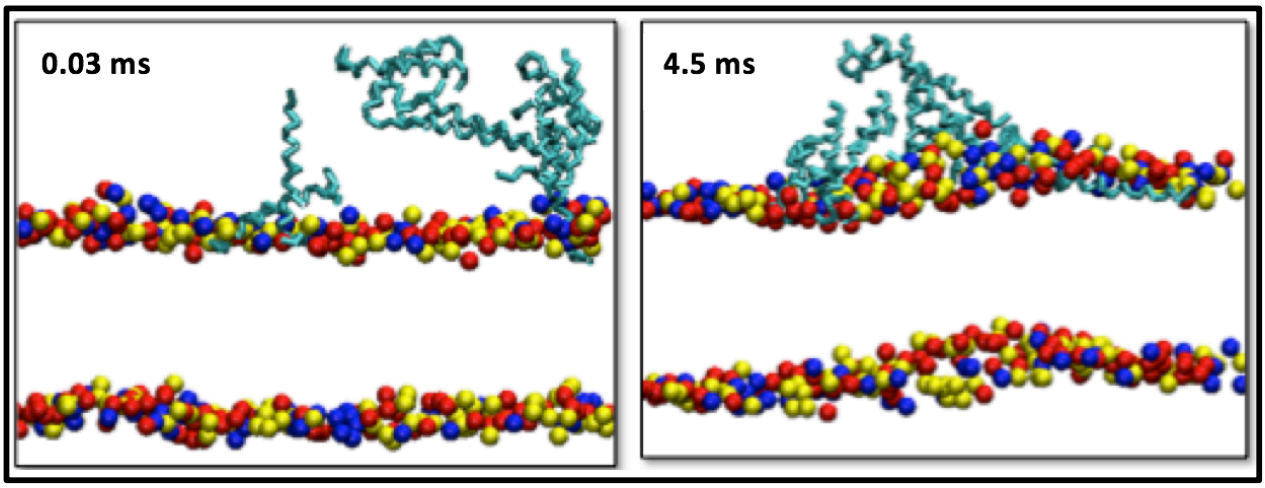

Figure 34 Two snapshots taken form a 10-protein simulation. Colour code is: blue POPC, red POPG, yellow POPE, and cyan protein. These snapshots show that clusters of protein at the membrane surface attract and join with each other to form a bigger cluster at the membrane surface. It shows, also, the familiar pattern of clusters first interacting with the membrane in a perpendicular state before changing and adopting the parallel state often seen at the end of simulations.

12-protein simulations

The 12-protein simulations start off as a typical simulation but, towards the end of the simulation, there appears to be some membrane penetration. This is the first of all the simulations done to show some membrane penetration where, as with Dermaseptin B2, even a 6-protein cluster manages to gain some little transient membrane penetration. This could mean that Dermaseptin B2 is more membrane active than Dermaseptin DS01. The snapshots in figure 35 below illustrate the above findings.

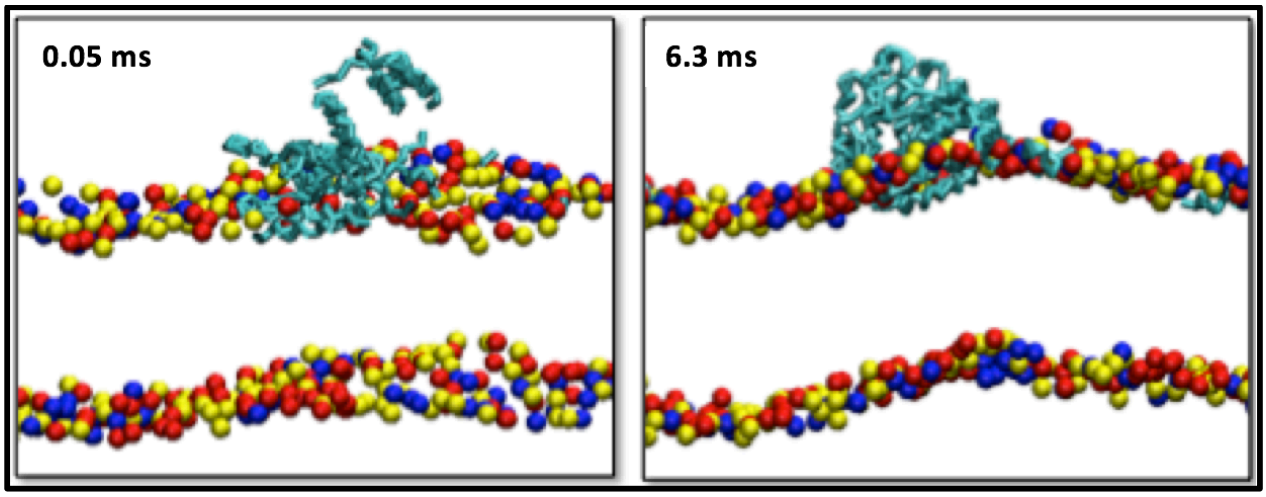

Figure 35 **Snapshots taken from 12 protein simulations. Colour code is: blue POPC, red POPG, yellow POPE and cyan are protein. The first snapshot shows a 12-protein cluster attached to the membrane surface. The second snapshot shows the cluster starting to penetrate the membrane. There appears to be at least one protein within the membrane surface.**

6.3 Dermaseptin B2 in POPC only membrane

Summary of simulations

These simulations, like the mixed lipid membrane ones, were run in coarse-grained structures. The Lennard-Jones interactions were shifted smoothly to zero at distances between 0.9 nm and 1.2 nm. The non-bonded neighbour list was updated every 10 steps and all simulations were conducted under constant temperature, pressure, and particle number. The temperatures of the protein, POPC, and solvent were each coupled separately by using the V-rescale thermostat at 320 K, with a coupling constant τT = 1 ps. The system pressure was coupled semi-isotropically by using the Berendsen algorithm at 1 bar with a coupling constant τP = 1 ps and a compressibility of 5 x 10^{-6} bar^{-1}. All simulations were run at 320 K for 10 microseconds at a 10 femtoseconds time step.

The system contained a varying number of peptides (3-25 peptides), a POPC only membrane in water and sodium ions to neutralize any excess negative charge.

6.3.1 Results of simulations

6.3.1.1 Dermaseptin B2

It is apparent that, at the end of a 10-microsecond simulation, the protein clustering is unaffected by the type of membrane used. In all cases, proteins clustered very rapidly but membrane association took considerably longer to happen. This confirms the lipid preference suggested in the results chapter.

Although it took longer, when eventually the cluster did attach to the membrane no particular termini of the protein were involved in membrane association and clusters tended to associate and dissociate with the membrane throughout the simulations. In most cases, by the end of the simulation, they settled on the membrane. Some membrane penetration is visible in some simulations but only a small part of the protein does so and with minimum membrane disruption. The POPC membrane showed more stability in the presence of the peptides as compared to the mixed lipid membrane.

There is one noticeable change in membrane binding in that it seems the proteins accumulated on top of each other and covered a minimal surface area on the membrane surface. They appear to prefer attaching to each other rather than attaching to the membrane.

Although, where the proteins do contact, minimal membrane contact is observed, some membrane disruption is apparent. However, this resolves itself quickly and the membrane is back at its equilibrated state. This observation is not seen with the mixed lipid membranes and, consequently, it can be concluded that POPC only membrane is less susceptible to disruption by the peptide and can maintain their stability by quick re-equilibrations.

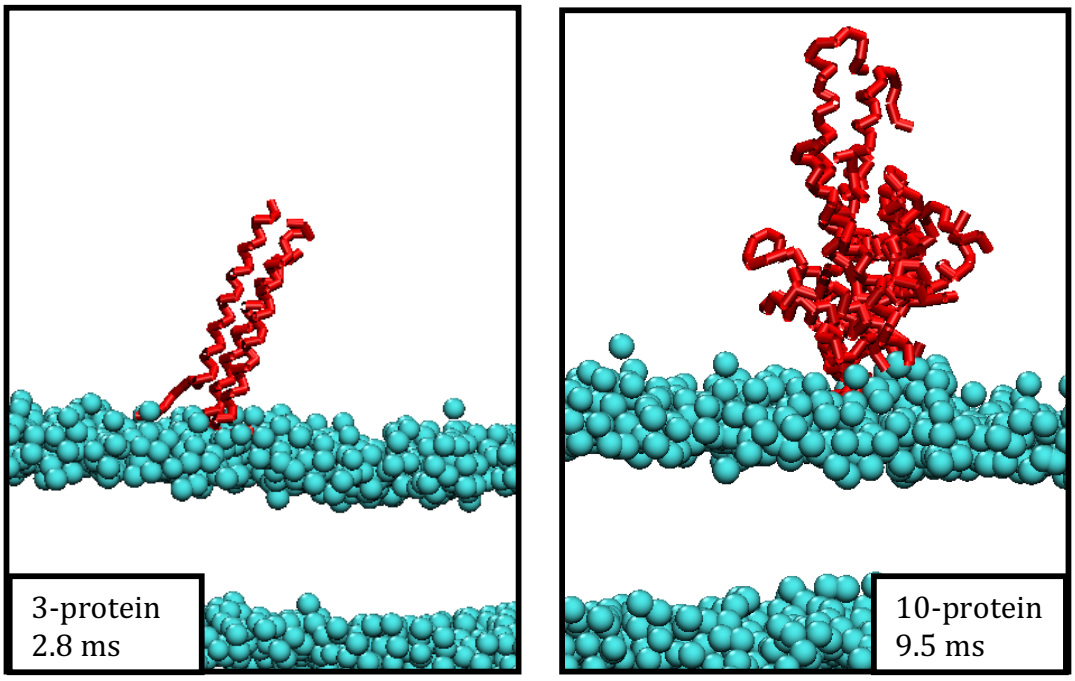

Figure 36 Snapshots taken from various simulations of Dermaseptin with POPC only membrane. It seems the peptides accumulated in relatively large clusters, interacting mainly amongst themselves rather than with the membrane. Although minimum membrane contact was seen, when the clusters attached to the membrane they caused some disruption that was resolved quickly. Colour scheme is: Cyan, lipid head groups and Red: peptide backbone.

6.3.1.2 Dermaseptin DS01 in POPC membrane

Here the peptide is run in the same conditions as the original Dermaseptin B2 to see if there are any differences in potency or membrane penetration.

As with the Dermaseptin B2 simulations, Dermaseptin DS01 did not show much affinity for POPC. In many cases membrane protein association took a while to occur and association with the mixed lipid membrane was significantly quicker. When membrane association occurred, it was usually via a few peptides binding to the membrane and the rest of the peptides in that simulation would cluster with them. The POPC membranes appear to be stable upon interaction with the DS01 peptide clusters compared with Dermaseptin B2, as when the cluster does become membrane bound they did not cause much membrane disturbance. There was some membrane penetration seen in some simulations, but this was intermittent, and only a small proportion of the protein backbone was viewed penetrating the membrane surface. It is unclear how many residues penetrated as this was not looked at since the process was very transient. Membrane cluster association also appeared to be periodic with the membrane-bound clusters detaching and attaching to the membrane.

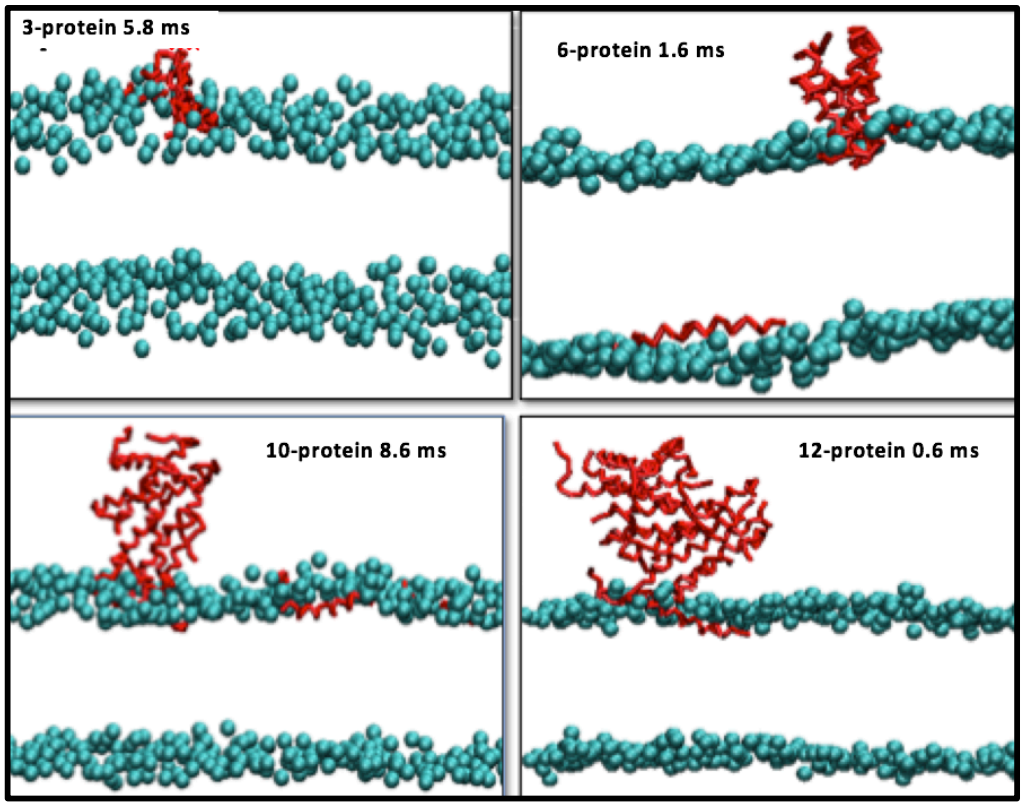

Figure 37 Snapshots of various protein concentrations in a POPC membrane. As shown, all but the 3-protein simulations show some degree of membrane penetration.

Chapter 7: Simulation analysis

7.1 Lipid contact analysis

Visually, it was easy to see that both Dermaseptin B2 and Dermaseptin DS01 showed a clear preference for POPG and POPE lipids. In order to quantify this lipid contact, analysis was carried out on all the protein simulations. This chapter plots the results visually and graphically. The lipid contact analysis (where contact is defined as $r \leq 0.6$ nm) was done by using a locally written script.

Dermaseptin B2

While reviewing the simulation frames of Dermaseptin B2, no particular side chain, group or termini is seen to mediate or play a significant role in protein clustering or membrane binding. There was also no specific clustering patterns noticed nor precise termini associated itself with the membrane more than the other.

Dermaseptin B2 lipid contact graphs

This part of the analysis considered the amount of contact each lipid within the membrane bilayer made with the proteins. This was done by using a locally written tickle script (.tcl) in combination with VMD (116) where the amount of contact with each lipid was recorded in a data file. Then, the data file was converted into an excel file and manipulated in Microsoft Excel to produce line graphs plotting the number of contacts against time. The results for all lipids were plotted together to make easier comparisons.

All graphs show significant preference towards POPG lipids while, as expected, POPC received the lowest number of contacts. This supports the literature findings that Dermaseptin-B2 is attracted to the negative charge of anionic lipids such as POPG.

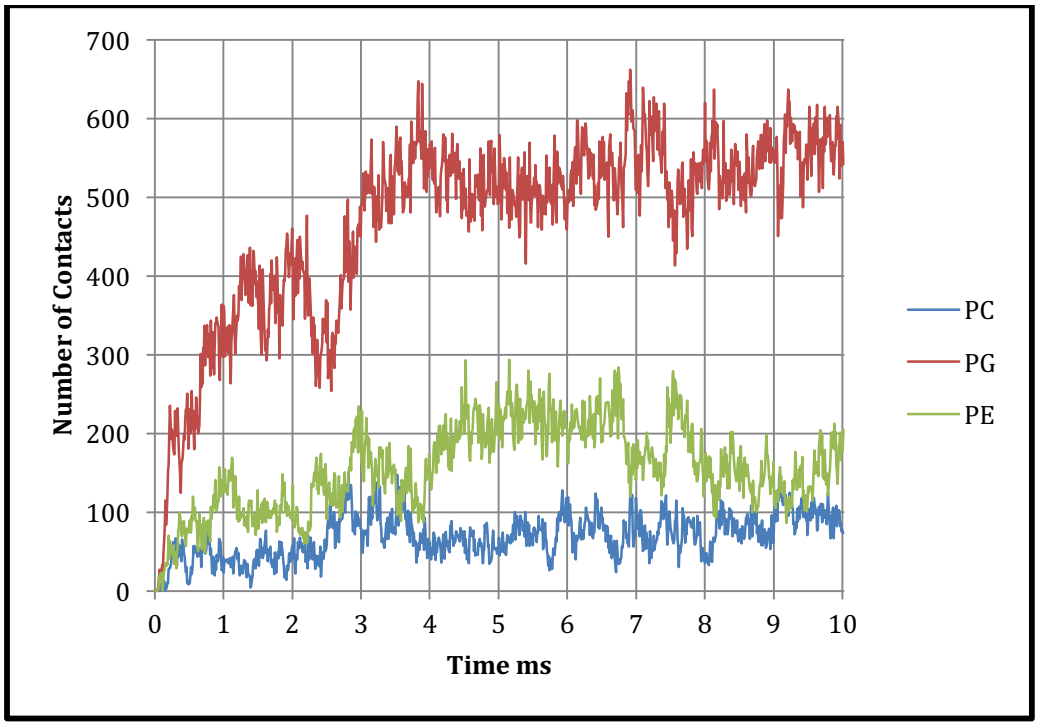

Graph 2 **Lipid contact graph for a 6-protein simulation with POPC/POPG/POPE membrane. The data for the graph considered contacts between the whole of the protein and the whole of the lipid bilayer.**

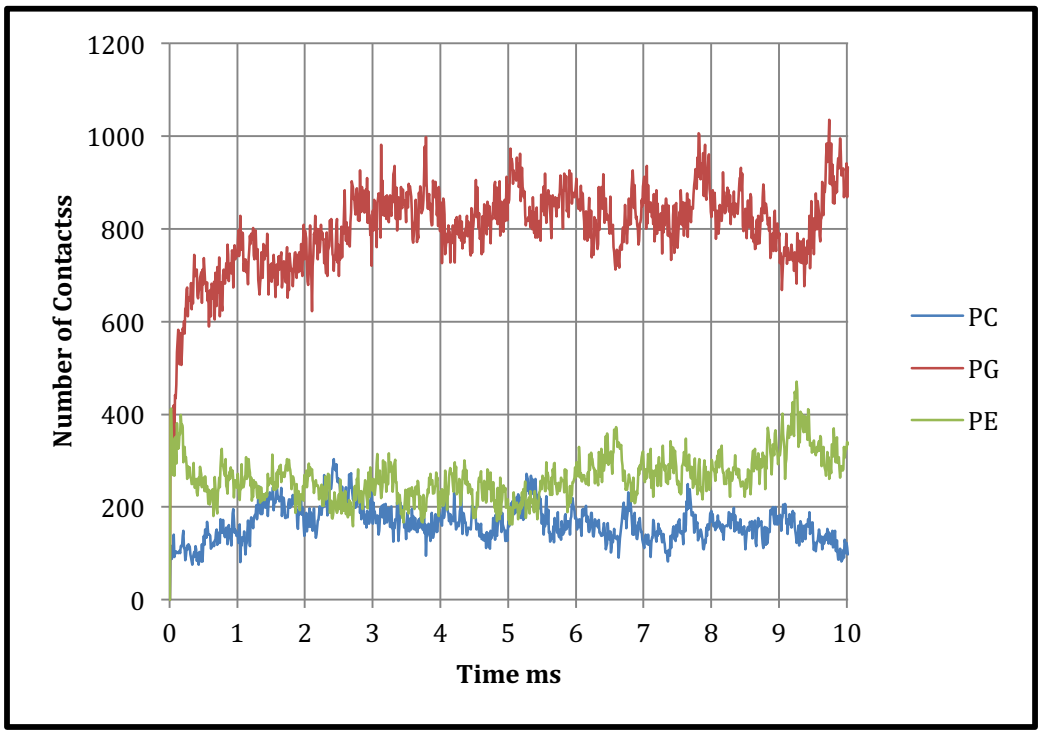

Graph 3 **Lipid contact graph for a 12-protein simulation with POPC/POPG/POPE membrane. The data for the graph considered contacts between the whole of the protein and the whole of the lipid bilayer.**

As both charts show, there are a significantly higher number of contacts with the POPG lipid even though it was used at the same ratio as POPE. This suggests a marked preference for Dermaseptin B2 for POPG compared to POPE or POPC.

Dermaseptin DS01 lipid contact graphs

The same lipid specificity graphs were plotted for the Dermaseptin DS01 simulations. These peptides showed the same pattern of lipid preferences as Dermaseptin B2. In the simulations, POPG received a significantly higher (in some cases more than double) number of protein contacts than all the other lipids. Once again, POPC received the least number of contacts.

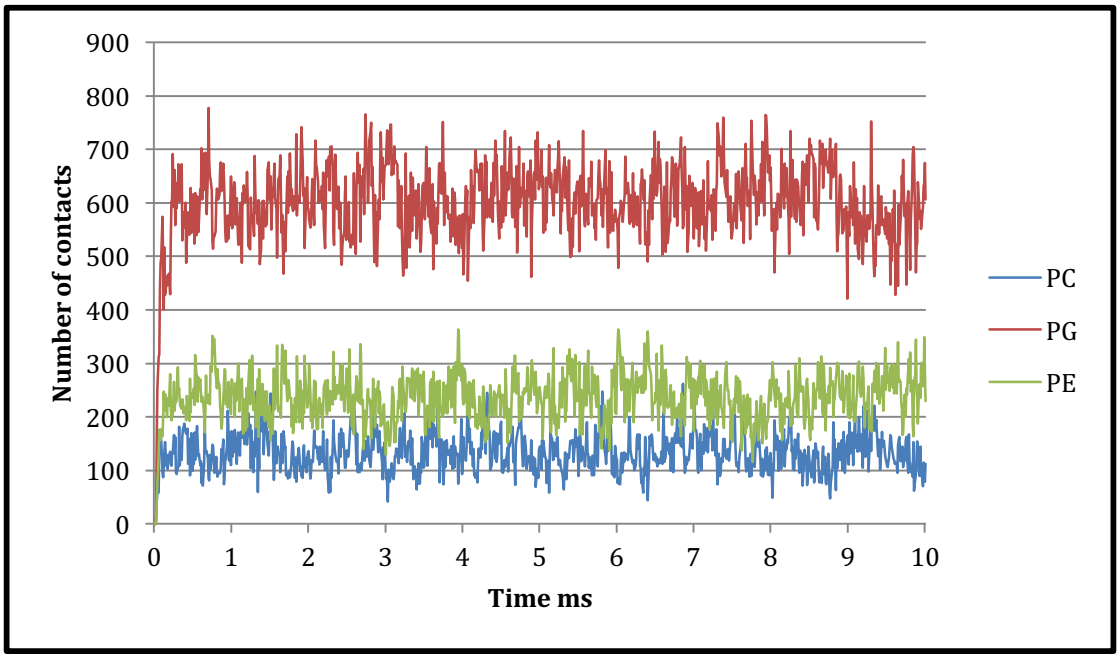

Graph 4 **Lipid contact graph for a 6-protein simulation. The data for the graph considered contacts between the whole of the protein and the whole of the lipid bilayer.**

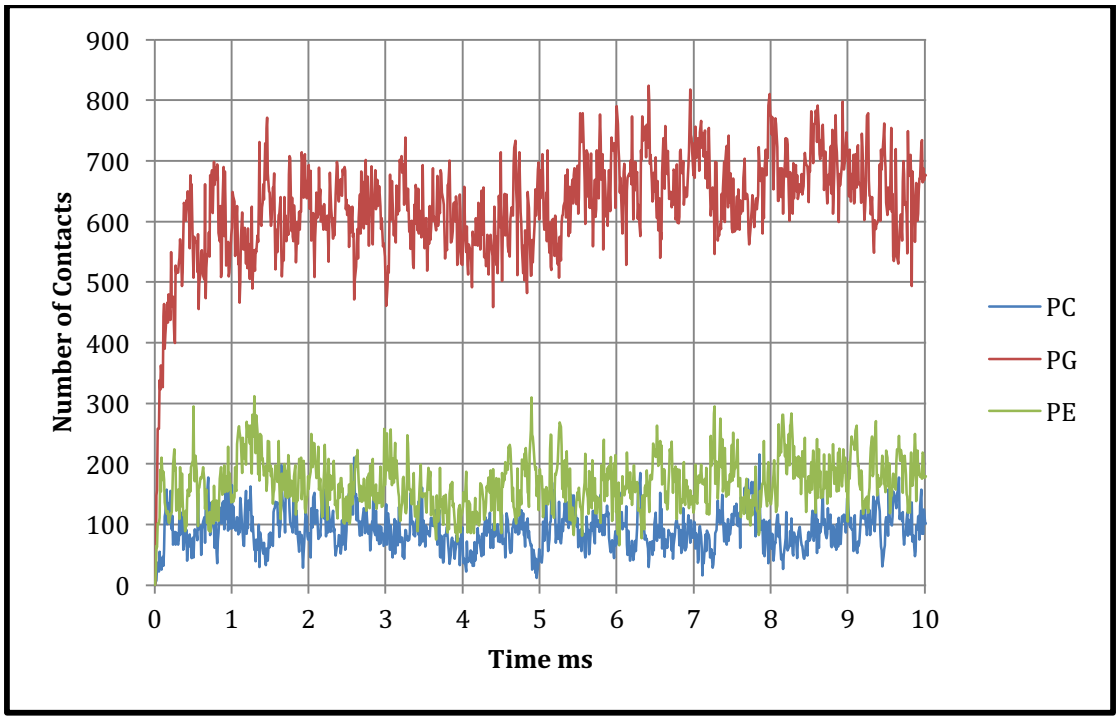

Graph 5 **Lipid contact graph for a 12-protein simulation. The data for the graph considered contacts between the whole of the protein and the whole of the lipid bilayer.**

7.2 Density plots

The density plots track and changes in density of each of the components within the system in the given simulation time. These were done, also, by using a locally written script. The scripts were used to plot the densities of POPC, POPG, POPE and the protein separately and, then, these three graphs were plotted in combination using xmgrace (http://plasma-gate.weizmann.ac.il/Grace/).

The resulting plot presents an idea of how the densities of each component of the system change with one another. In turn, this can provide information of lipid preferences.

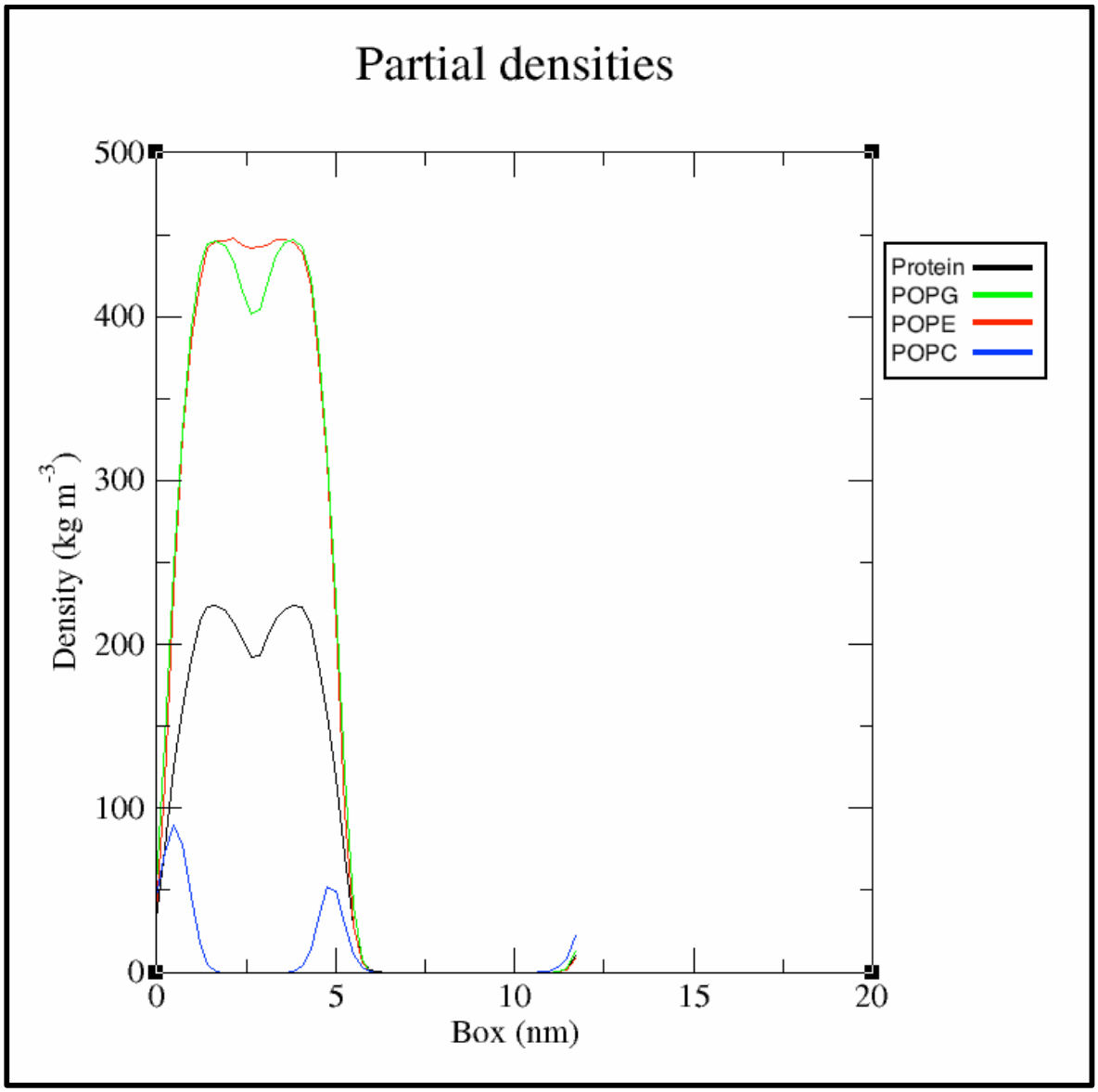

Graph 6 **Partial densities plot for a 3-protein simulation. Colour code, blue POPC, black protein, green POPG and red POPE.**

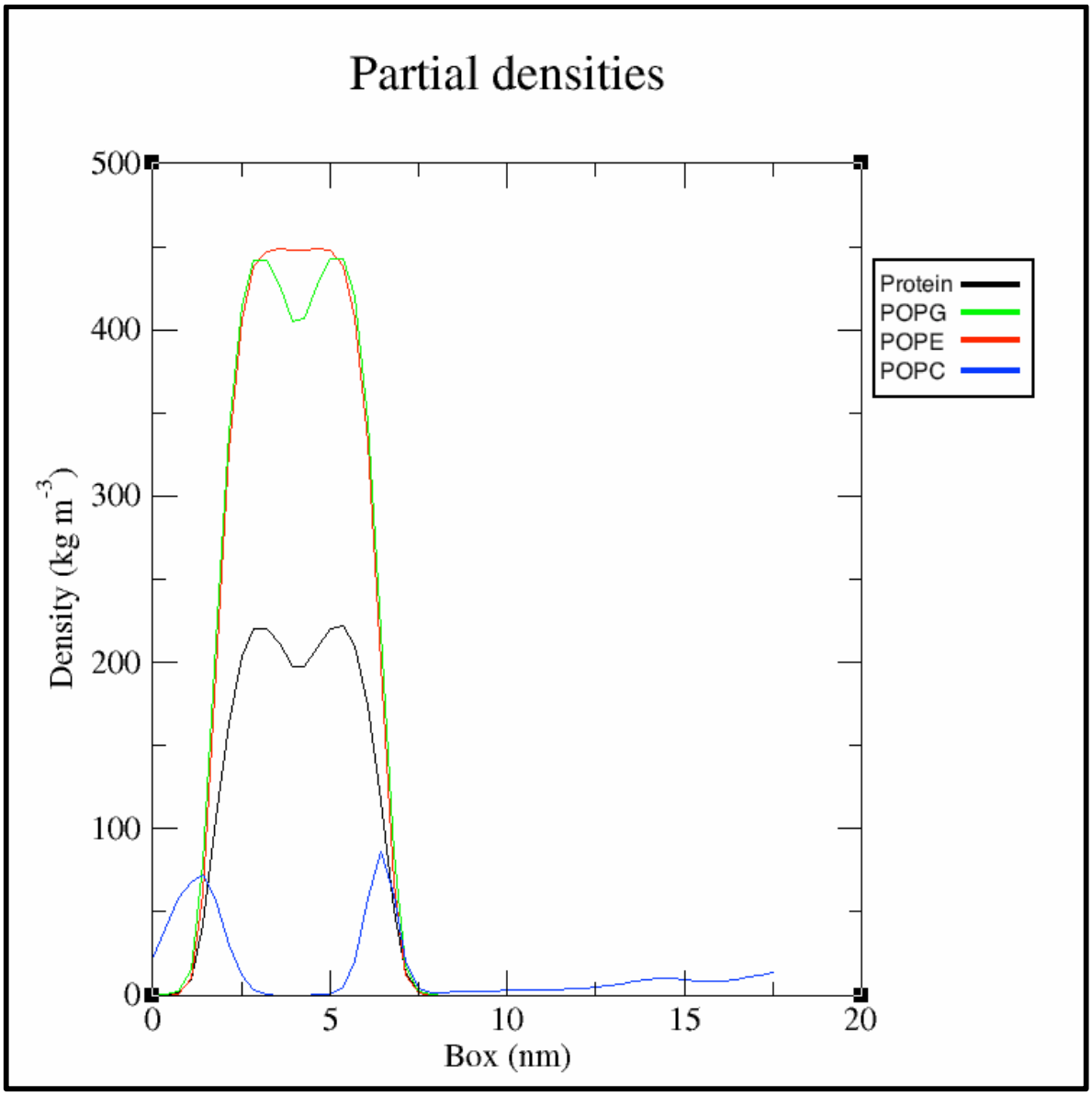

Graph 7 **Partial densities plot for a 6-protein simulation. Colour code, blue POPC, black protein, green POPG and red POPE.**

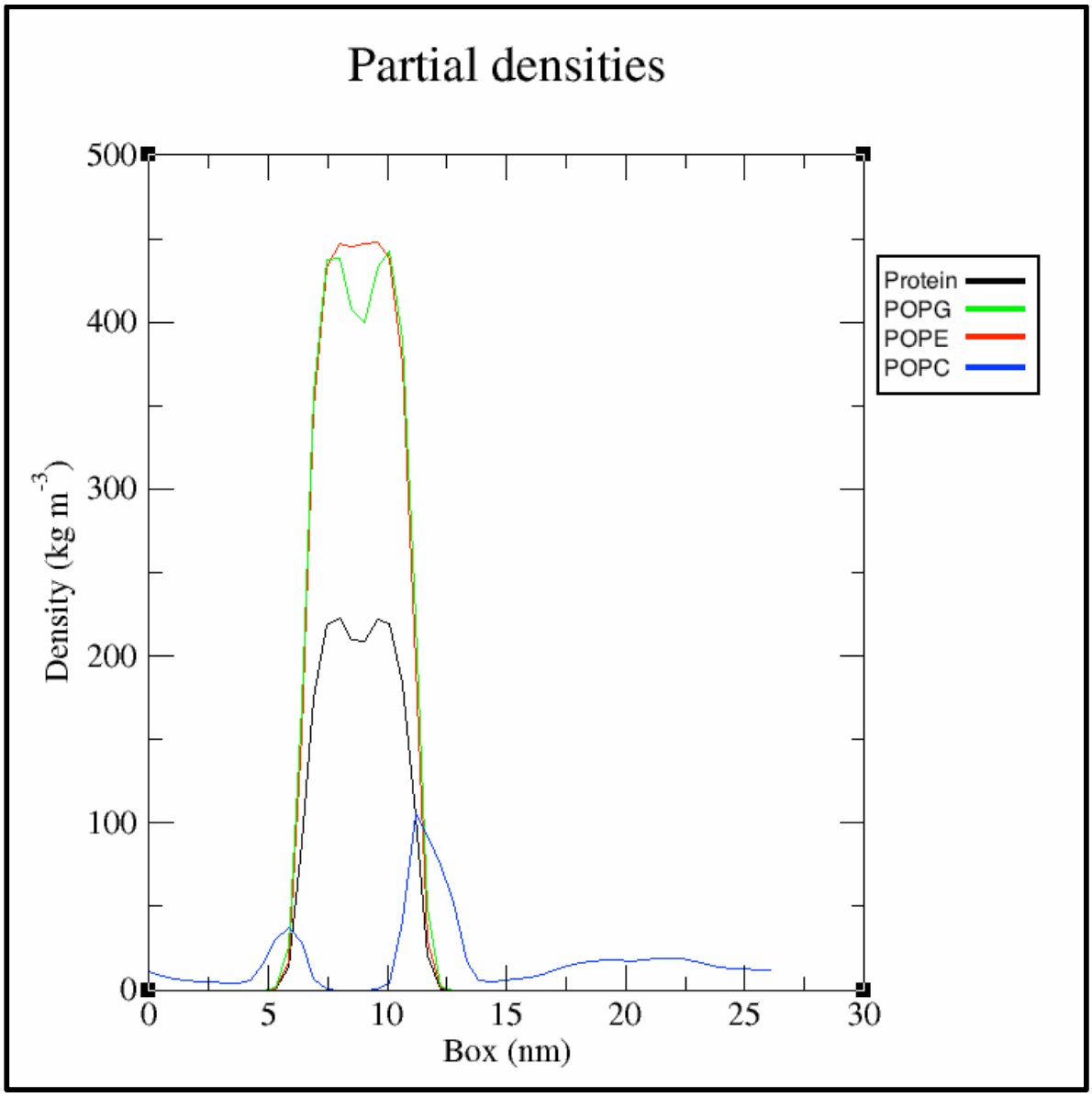

Graph 8 **Partial densities plot for a 10-protein simulation. Colour code, blue POPC, black protein, green POPG and red POPE.**

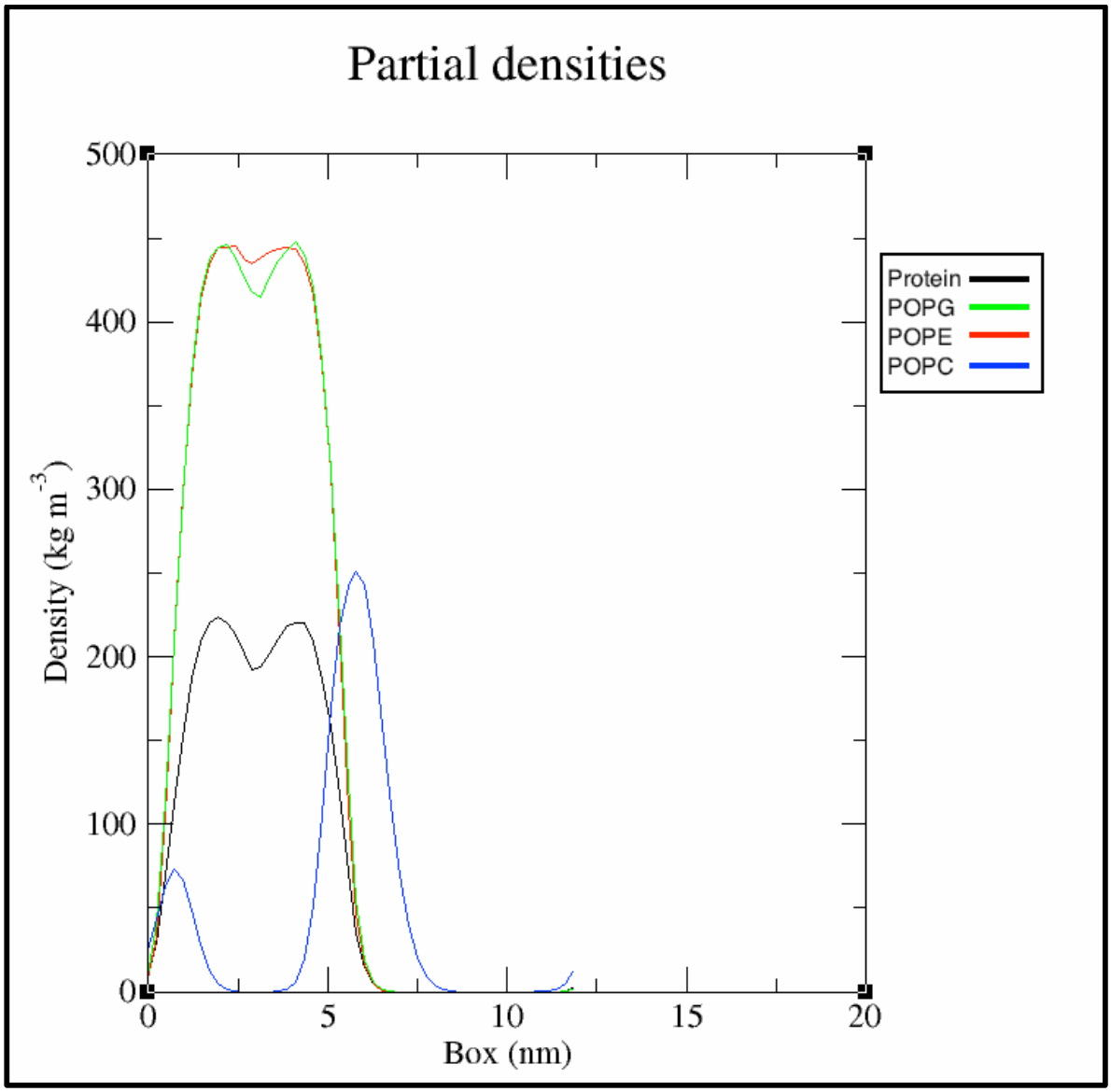

Graph 9 Partial densities plot for a 12-protein simulation. Colour code, blue POPC, black protein, green POPG and red POPE.

The graphs seem to exhibit a similar pattern and all show that, as the partial density of POPG/POPE rises, so does the partial density of the protein. This suggests that the densities of these two system components are related. Indeed, this is shown by the lipid clustering snapshots and lipid specificity graphs. The increasing and decreasing patterns of partial density share a much closer relationship with the POPG lipid. In particular, this suggests that it is the one most preferred for association by the peptides.

Dermaseptin DS01

The following plots represent a simulation with 3,6,10 and 12 protein peptide simulations of Dermaseptin DS01. As expected, these show very similar results since they come from the same family of peptides.

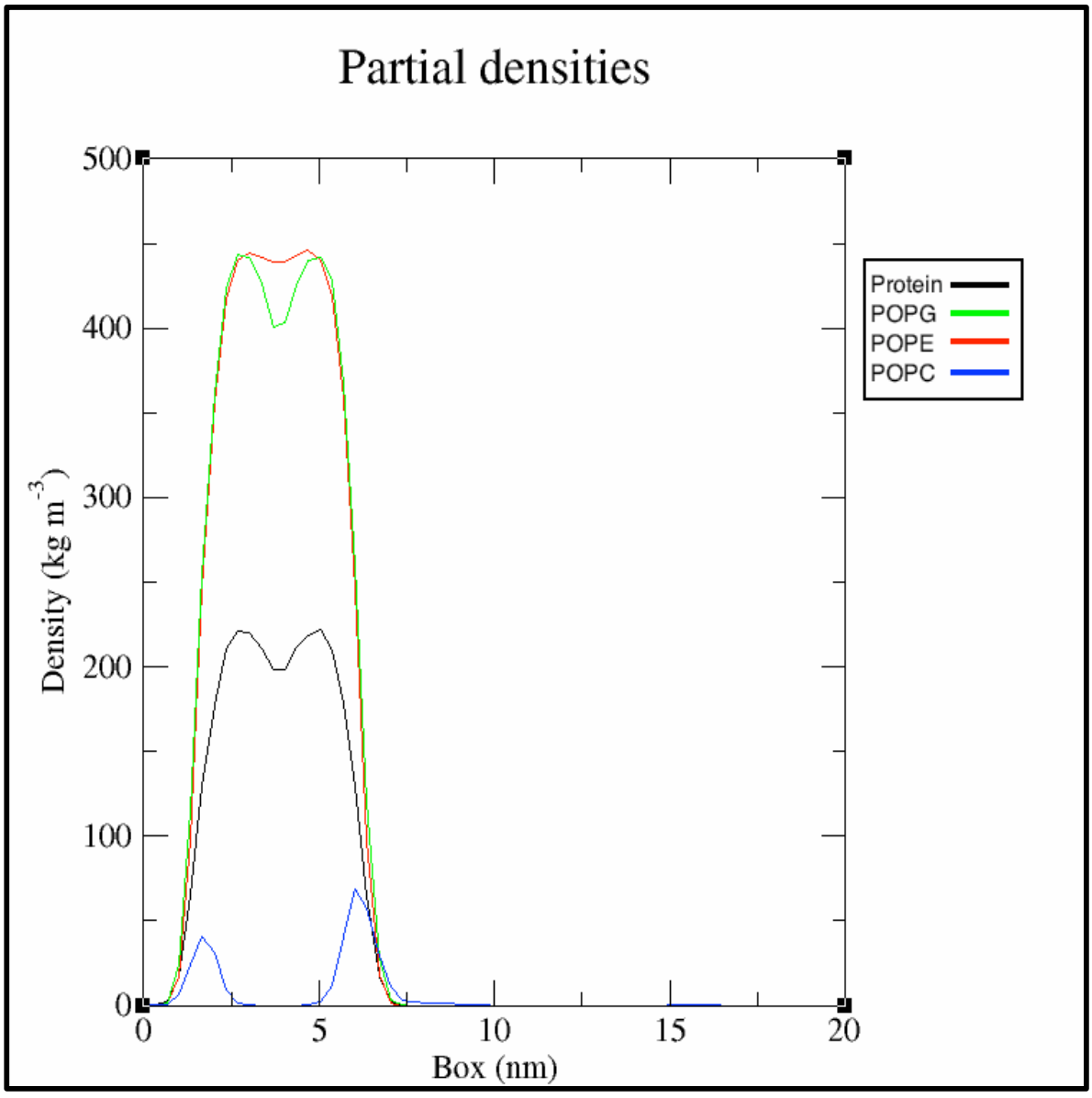

Graph 10 Partial densities plot for a 3-protein simulation. Colour code, blue POPC, black protein, green POPG and red POPE.

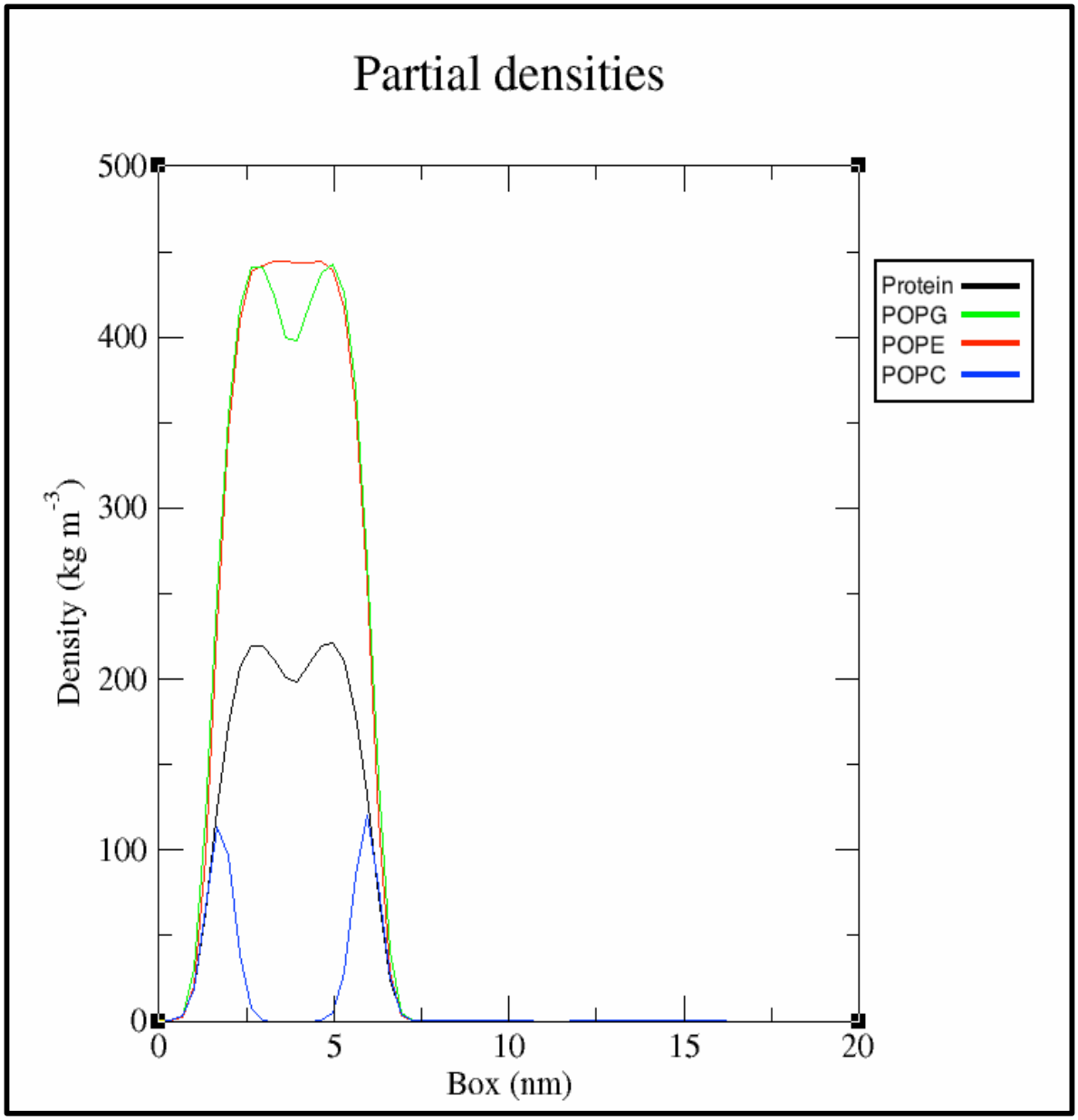

Graph 11 Partial densities plot for a 6-protein simulation. Colour code, blue POPC, black protein, green POPG and red POPE.

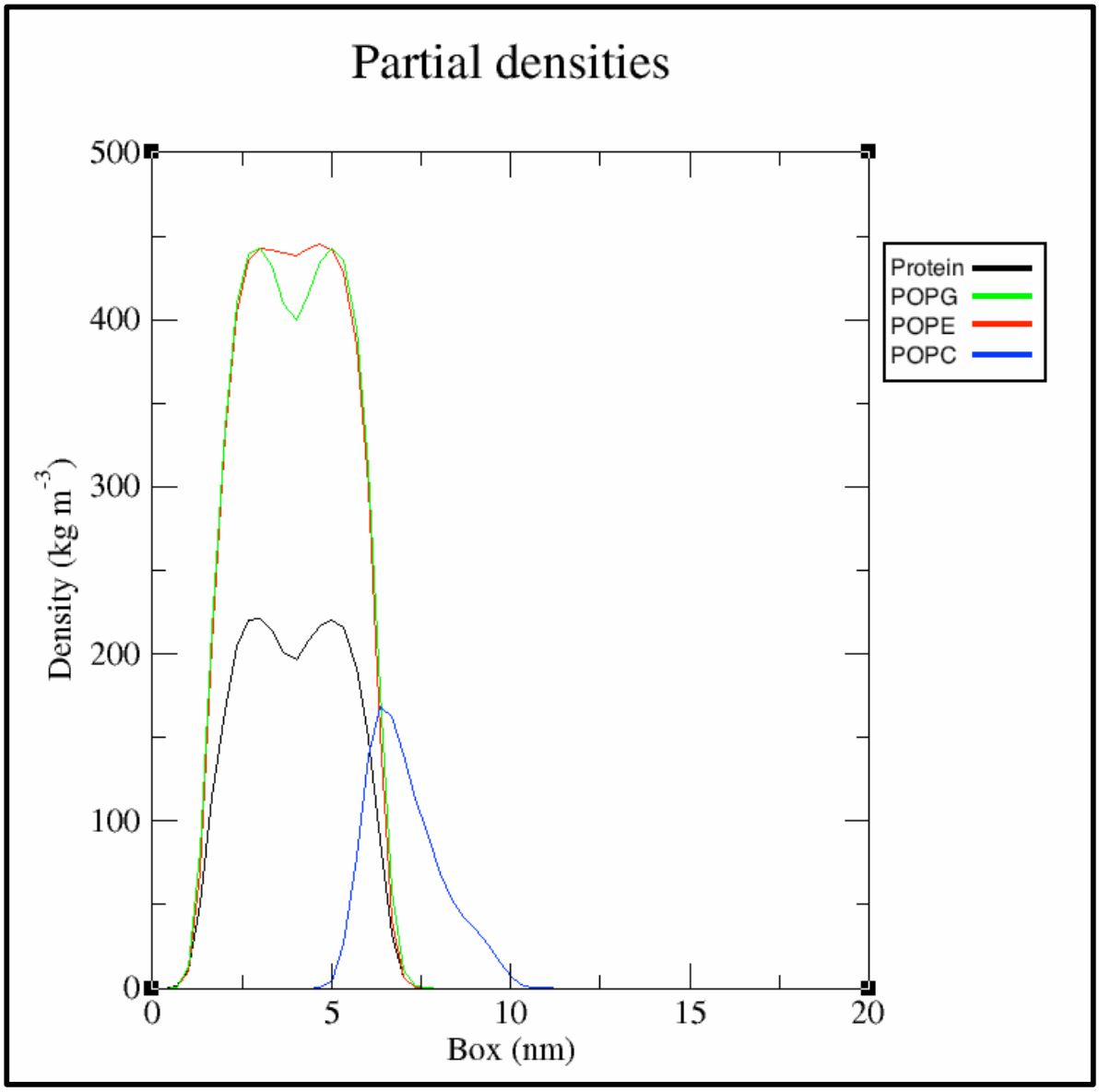

Graph 12 **Partial densities plot for a 10-protein simulation. Colour code, blue POPC, black protein, green POPG and red POPE.**

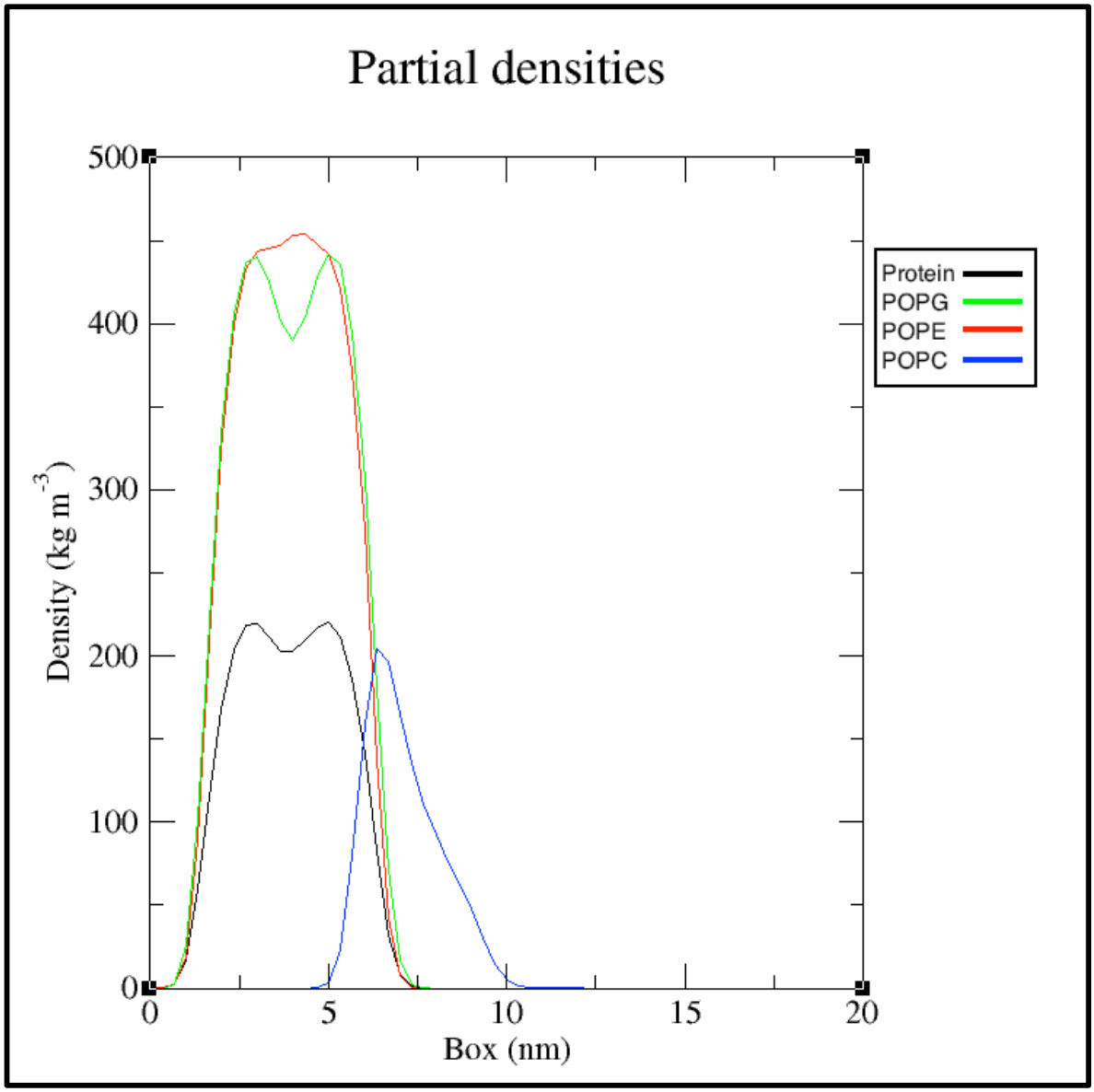

Graph 13 Partial densities plot for a 12-protein simulation. Colour code, blue POPC, black protein, green POPG and red POPE.

7.3 Membrane distance analysis

This part of the analysis considered how the distance between the two leaflets of the membrane changed throughout the course of the simulations. Membrane distance analysis was done to investigate membrane disruption and to see if the peptides exerted any pressure at the membrane surface. This was done by using the g-dist tool in GROMACS to measure the distance between the headgroups of the top membrane leaflet and the headgroups of the bottom membrane leaflet (approximately the highest and lowest points of the membrane).

Dermaseptin B2 in a mixed lipid membrane.

Graph 14 shows a 3-protein simulation. As shown, the membrane is relatively stable throughout the first three-quarters of the simulation following which there is seen to be some disruption to the membrane disruption. In this simulation, it is observed that the clusters of protein attach to the membrane relatively late into the simulation and that this accounts for the stability seen at the beginning of the simulation. Following the brief period of disruption to the membrane, the membrane re-equilibrates itself and adjusts to the presence of the protein cluster on its surface.

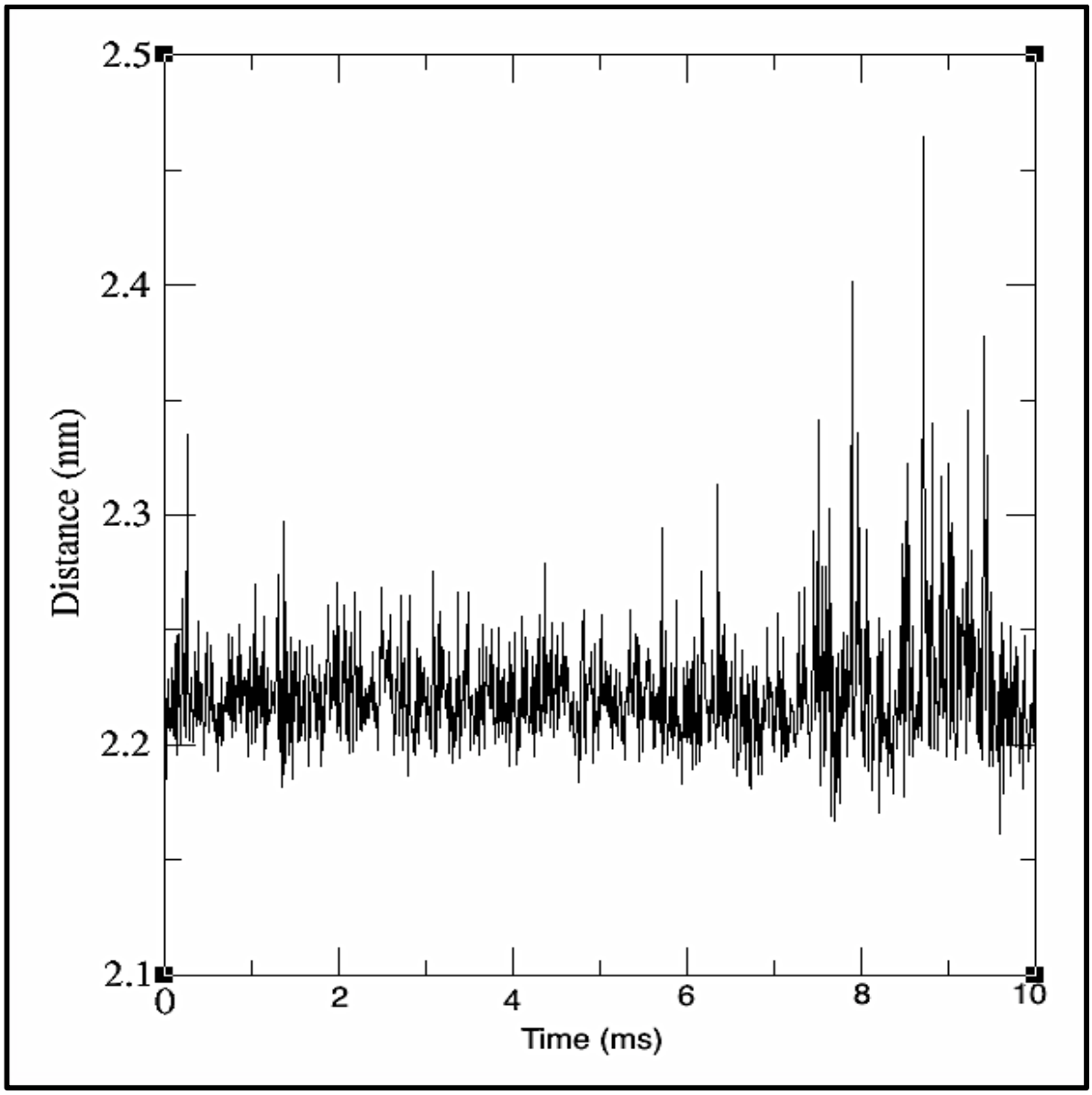

Graph 14 Graph from 3-protein simulation. As seen the distance has declined steadily at the start of the simulation before settling towards the end of the simulation.

The 10-protein simulation shows disruption throughout the simulation. There seems to be periods of membrane disruption followed by an equilibrating period before another disruption-equilibration cycle begins. It appears the distance between the two leaflets of the membrane is becoming smaller. This could be due to the pressure of the 10-protein cluster that is now resting on the surface.

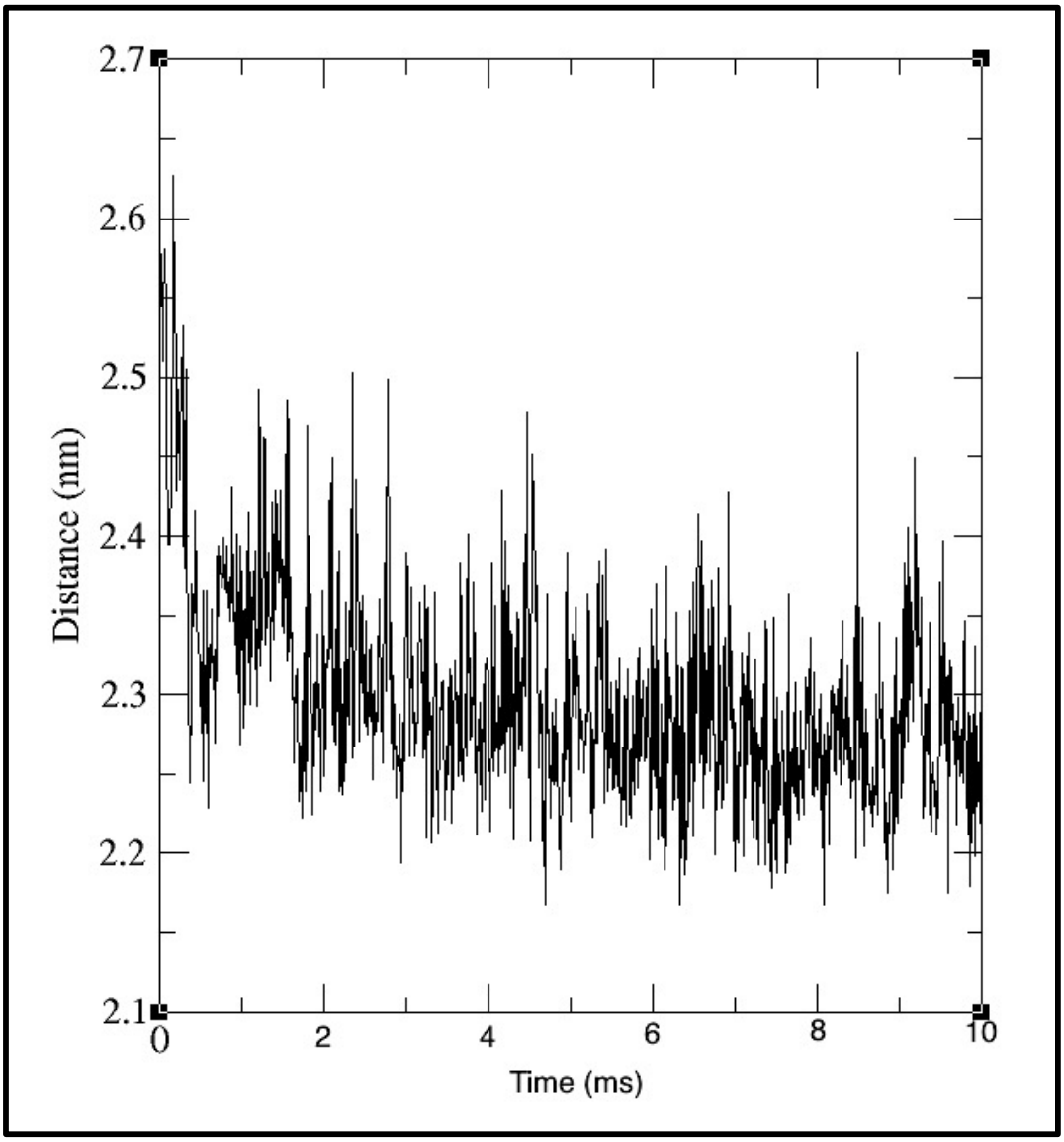

Graph 15 **Graph is plotting the distance between the two leaflets of the membrane throughout a 10-protein simulation. As seen, the distance seems to decline steadily and begins to settles towards the end of the simulation.**

Dermaseptin B2 in POPC membrane:

The amount of disruption is noticeably higher in all POPC membranes. The membrane appears to re-equilibrate itself very rapidly to adjust to significant changes in distances.

Graph 16, which plots the results for a 6-protein system, shows that the distance between the leaflets of the membrane increased at first before starting to decrease slightly. As with the mixed membrane simulation, this could be down to the pressure exerted on the membrane by the protein cluster on its surface.

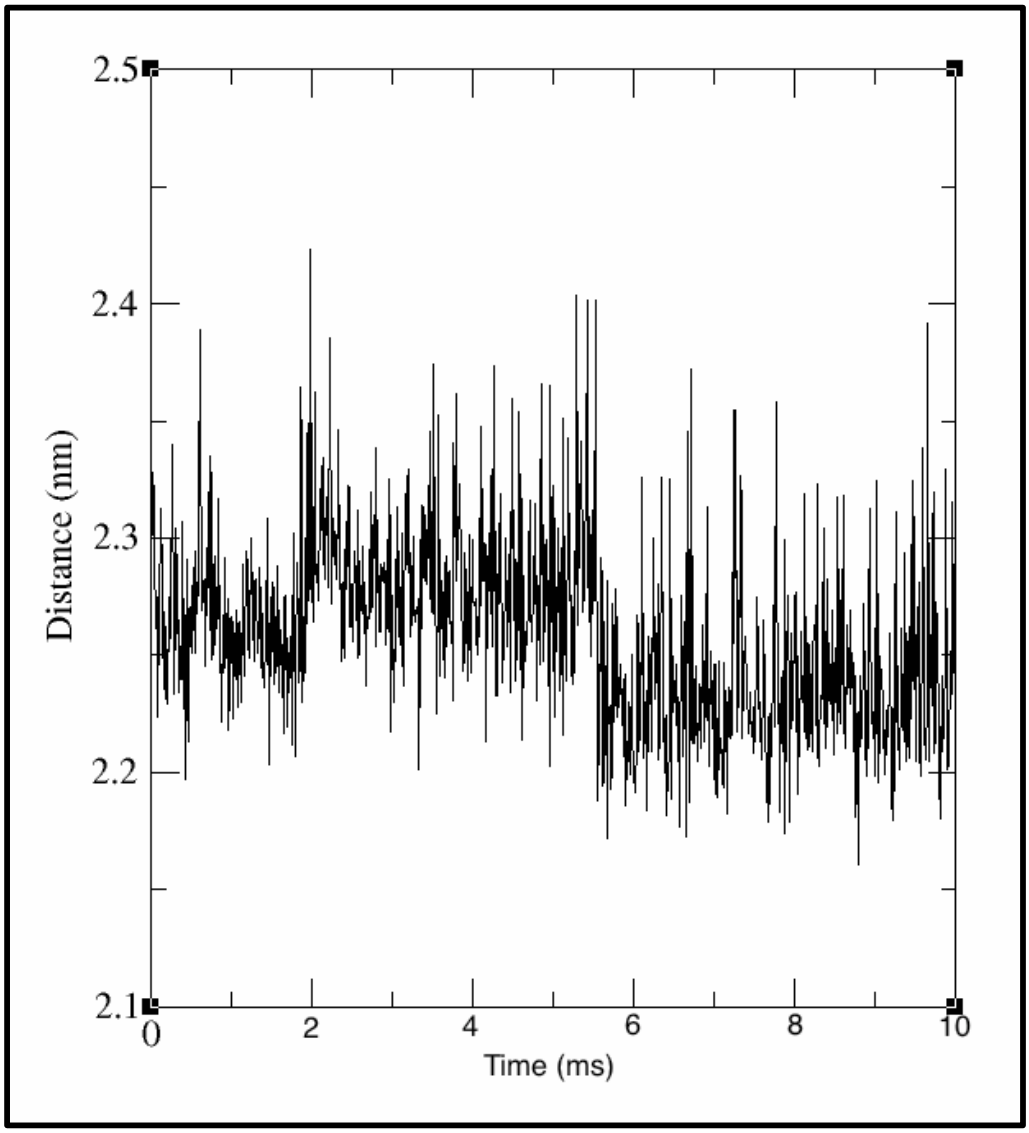

Graph 16 Graph is plotting the distance between two leaflets of a POPC membrane throughout a 6-protein simulation. As shown, there was significantly more disruption in this membrane compared to the mixed lipid membranes.

Graph 17 plots the distance between the POPC membrane leaflets in a 10-protein simulation. The same overall pattern seems to be shown whereby there is a small but steady overall decline in distance. However, there were times when the membrane distance increased before starting to decrease again. When looking at the simulation, it appears that the point, at which the membrane distance began to increase, was the point when the protein cluster became dissociated from the membrane surface. Also, when eventually, it re-associates with the membrane, the distance starts to reduce once again.

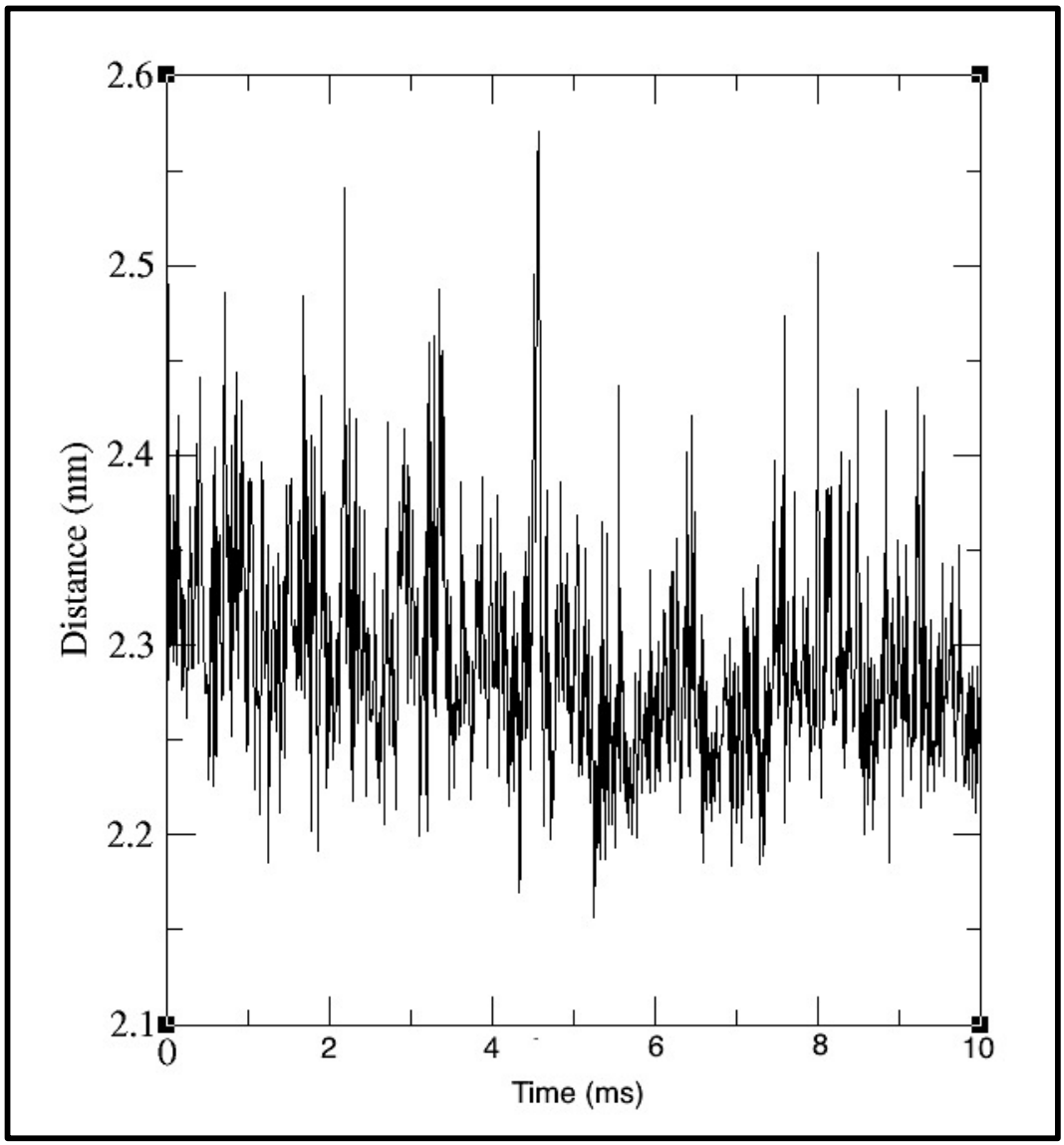

Graph 17 **Graph is plotting the distance between two leaflets of a POPC membrane throughout a 10-protein simulation. As shown, there was significantly more disruption in this membrane compared to the mixed lipid membranes.**

Dermaseptin DS01 in mixed lipid membrane

The following graphs plot the distance analysis for Dermaseptin DS01 in a POPC/POPG/POPE membrane. Graph 18 represents a 6-protein simulation and Graph 19 represents a 10-protein simulation.

Both graphs seem to be unaffected and the membrane distance appears to be constant throughout the simulations. This could be because the Dermaseptin DS01 is slightly lighter in weight, when compared to Dermaseptin B2, and this means that it does not exert as much pressure on the membrane surface.

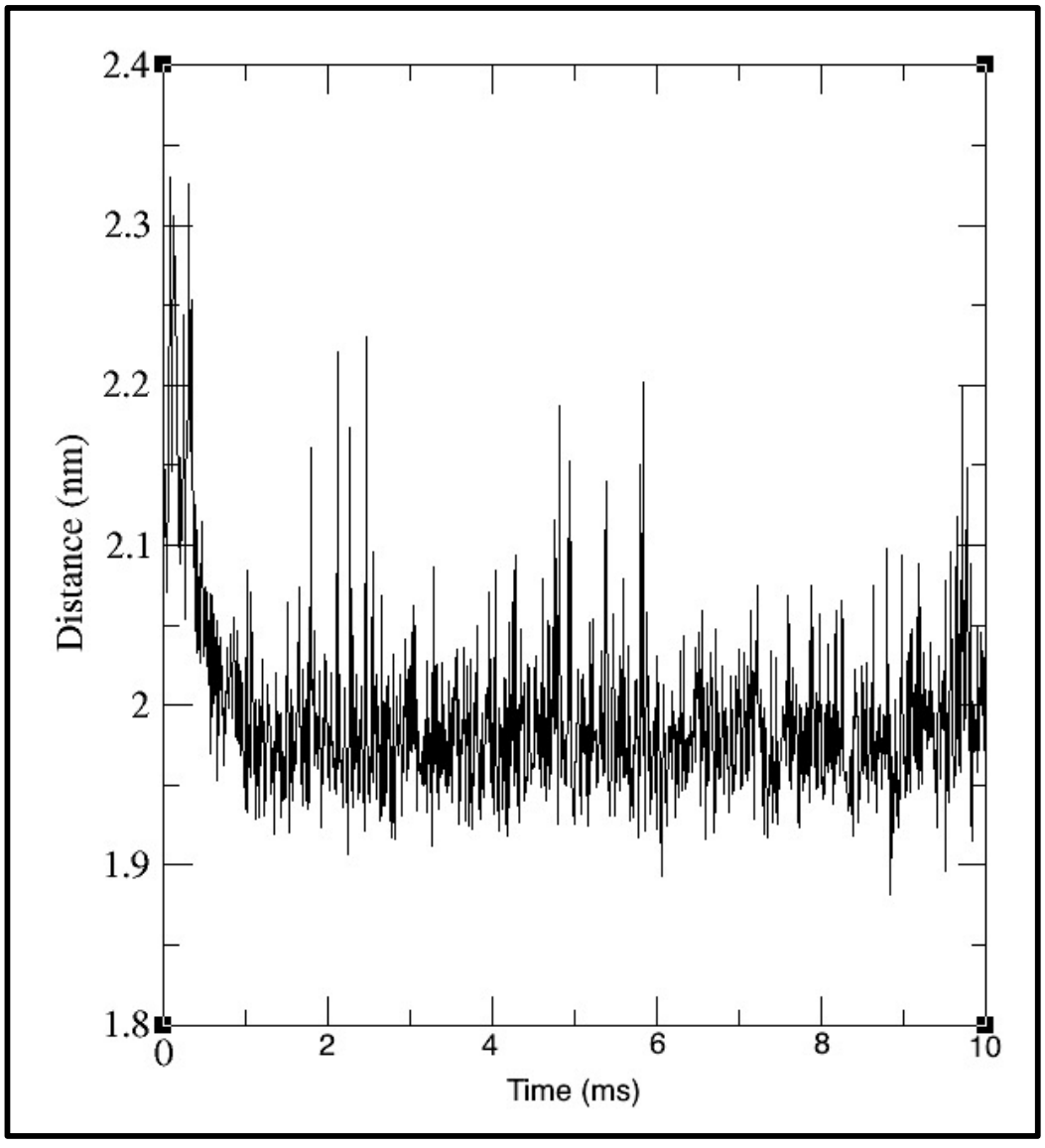

Graph 18 Graph is plotting the distance between two leaflets of the membrane throughout a 6-protein simulation. As seen, following an initial disruption, the distance has remained constant indicating minimal membrane disruption.

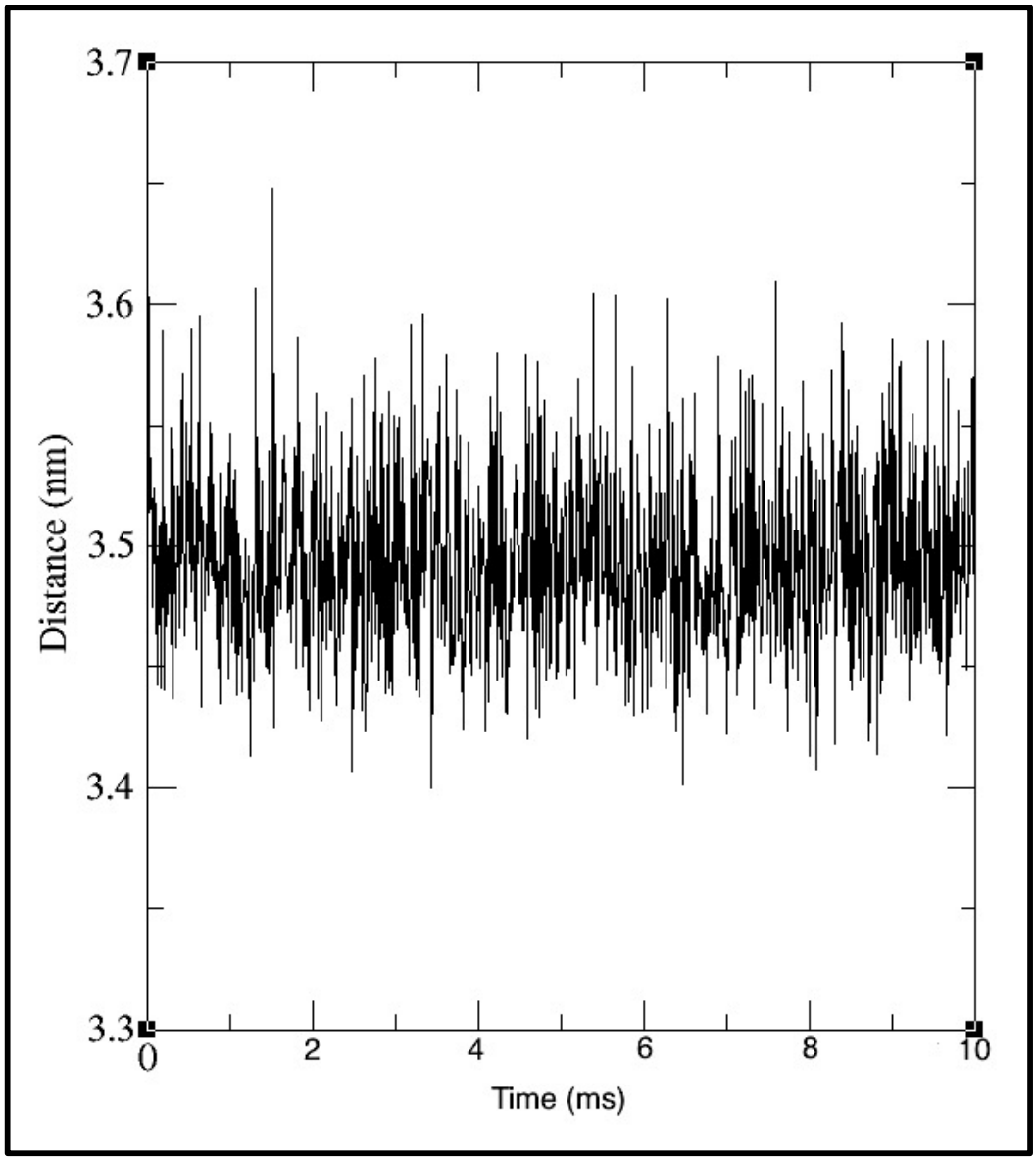

Graph 19 **Graph is plotting the distance between two leaflets of the membrane throughout the 10-protein simulation. As seen, the distance has remained constant indicating minimal membrane disruption.**

Dermaseptin DS01 in POPC membrane.

Graph 20 below represents a membrane distance plot for Dermaseptin DS01 proteins in a POPC only membrane.

It is noticeable immediately that there is considerable membrane disruption here when compared to the mixed membrane simulations.

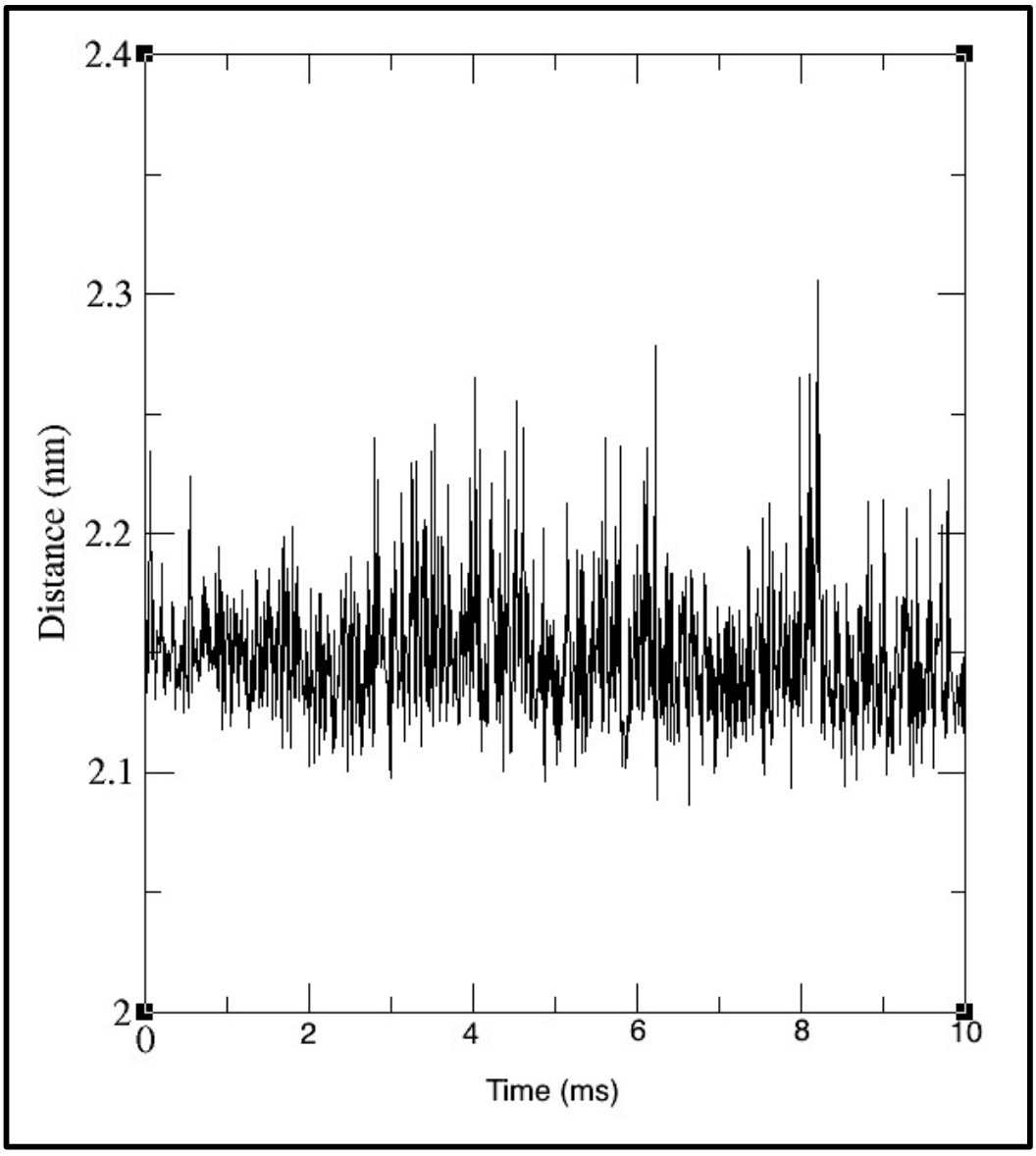

Graph 20 Graph is plotting the distance between the two leaflets of the membrane in a 6-protein simulation. As seen, there is significant fluctuation in distance at the beginning of the simulation that seems to settle towards the end.

Graph 20 shows the distance between membrane's leaflets in a 6-protein simulation. It seems to show the same pattern of membrane disruption and re-equilibration in the end. The distance does seem to remain relatively constant at around 2.15 nm and 2.2 nm.

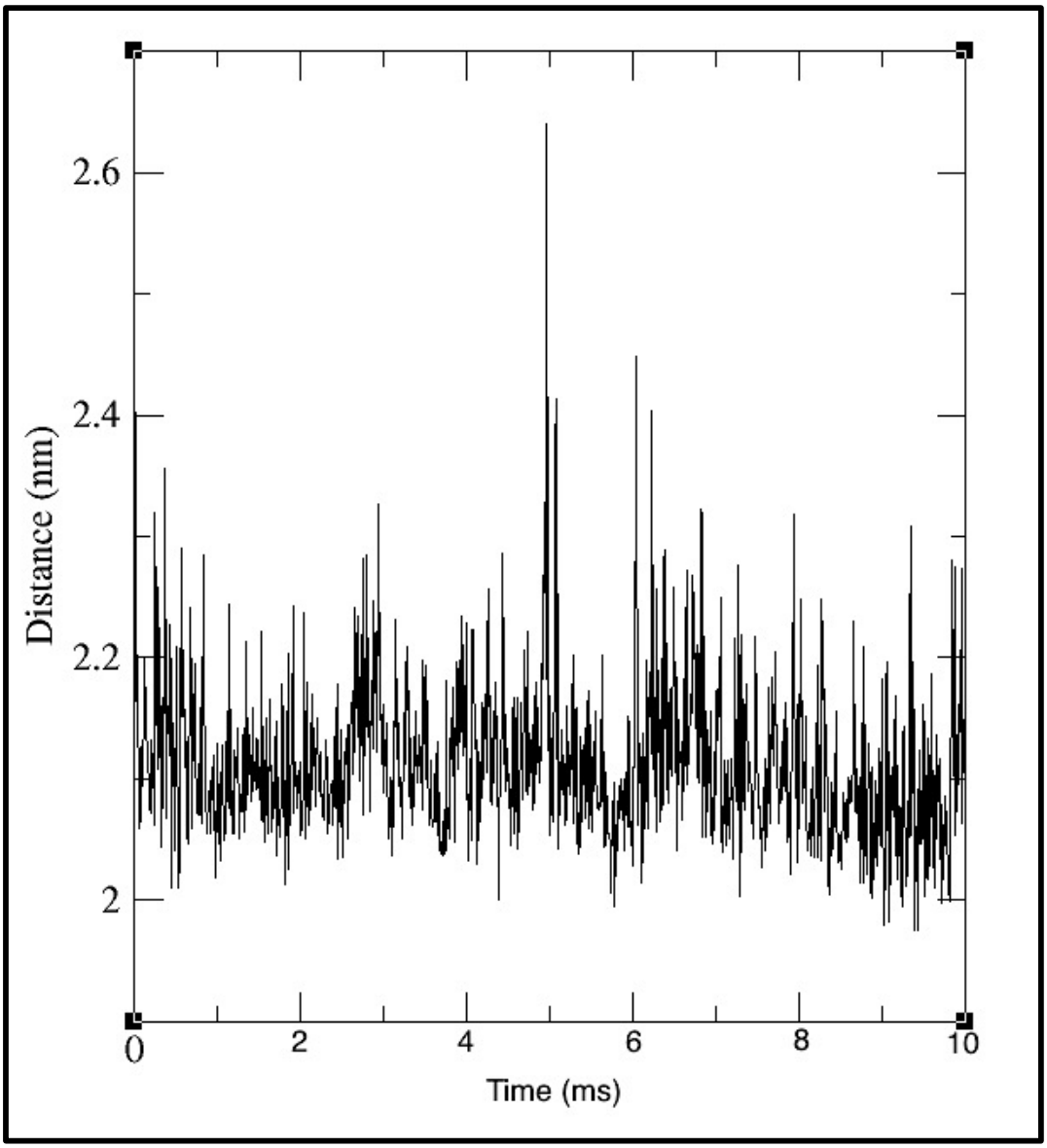

Graph 21 Graph plotting the distance between the two leaflets of the membrane in a10-protein simulation, there is significant fluctuation in distance at the beginning of the simulation that seems to settle towards the end.

Graph 21 shows the membrane distance in a 10-protein simulation. It appears the membrane distance reduced from around 2.2 nm on average to 2.05nm where it could re-equilibrate and establish stability.

As with the previous simulations, it is predicted that this fall in membrane distance could be due to the clusters binding and settling on the membrane surface exerting some pressure and pushing the two leaflets of the membrane closer together.

7.4 Cluster analysis

In this part of the analysis, the size of the clusters was analysed through the course of the simulations. The cluster analysis was done by using the g-aggregate tool created by Barnoud (117) for coarse-grained systems. The g-aggregate identifies the parts of the system that aggregate and computes the size of the aggregate for each frame in the trajectory. For these Graphs, any two peptides that are less than 0.13 nm apart are in a cluster. The tool considers clustering throughout the simulation and produces a graph showing how the cluster size changed with time.

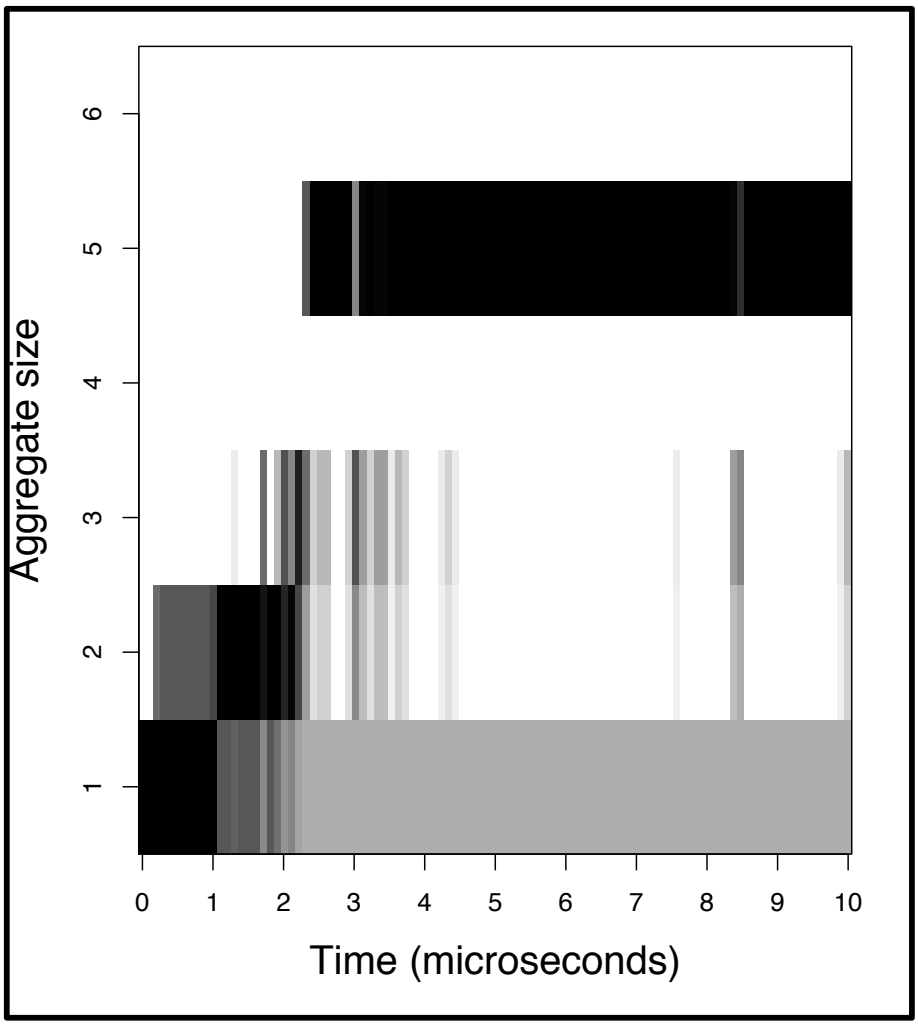

Figure 38 Clustering graph for a 6-protein simulation in POPG/POPE/POPC membrane.

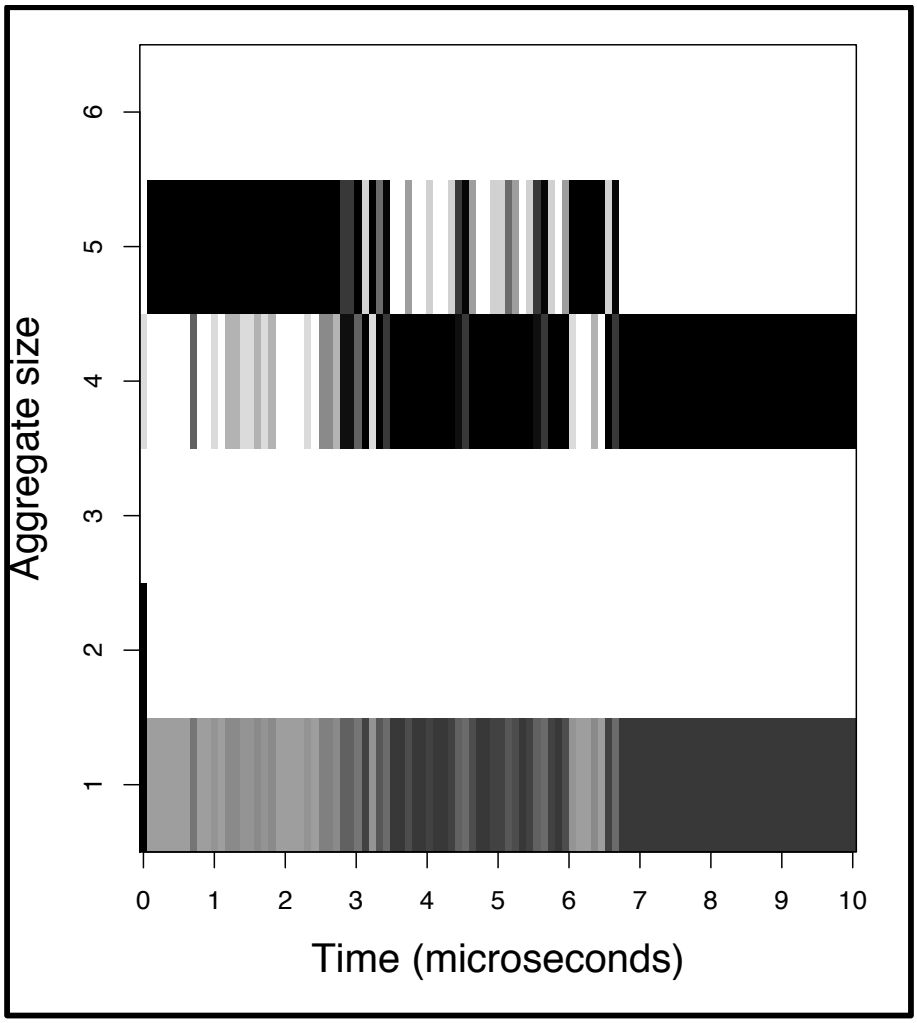

Figure 39 Clustering graph for a 6-protein simulation in POPC only membrane.

Figures 38 and 39 (above) show the clustering patterns in 6-protein simulations in a mixed lipid membrane and a POPC only membrane. As seen in Figure 39, it seems that, in the presence of POPC only membrane, the proteins preferred to cluster amongst themselves for a much higher proportion of the simulation (for most of the simulation the peptides were in clusters of 4 or 5 peptides). Very early in the simulation, a large 5-protein cluster started to form; in the POPC/POPG/POPE membrane, this can be seen only after the first 3 microseconds of the simulation. This shows that, in the presence of POPG/POPE/POPC, the peptides cluster together slower which could be because the peptides are more attracted to the lipids in the membrane than each other.

Figures 40 and 41 are of a 10-protein simulation and they reflect a similar pattern as above but it's easier to see how the membrane affects the clustering pattern of the peptides.

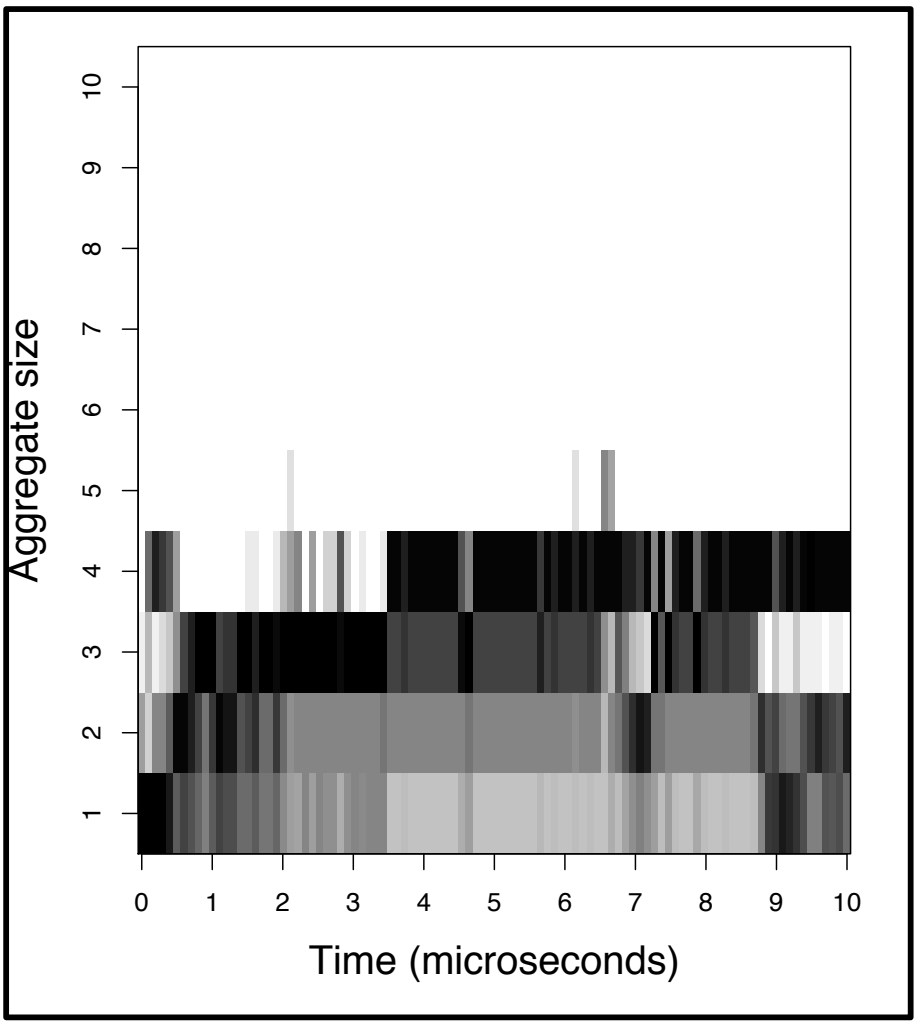

Figure 40 Cluster analysis graphs of 10 proteins in a POPC/POPG/POPE membrane.

In the presence of POPC/POPG/POPE membrane, the peptides formed many smaller clusters that became membrane bound often at different points of the membrane. Some

clusters became larger in size as they were attached to the membrane while others broke into smaller clusters and each attached to the membrane. This shows that the Dermaseptin peptides have a higher affinity for POPG and POPE lipids as compared to POPC. This result is supported by the analysis in this thesis and literature.

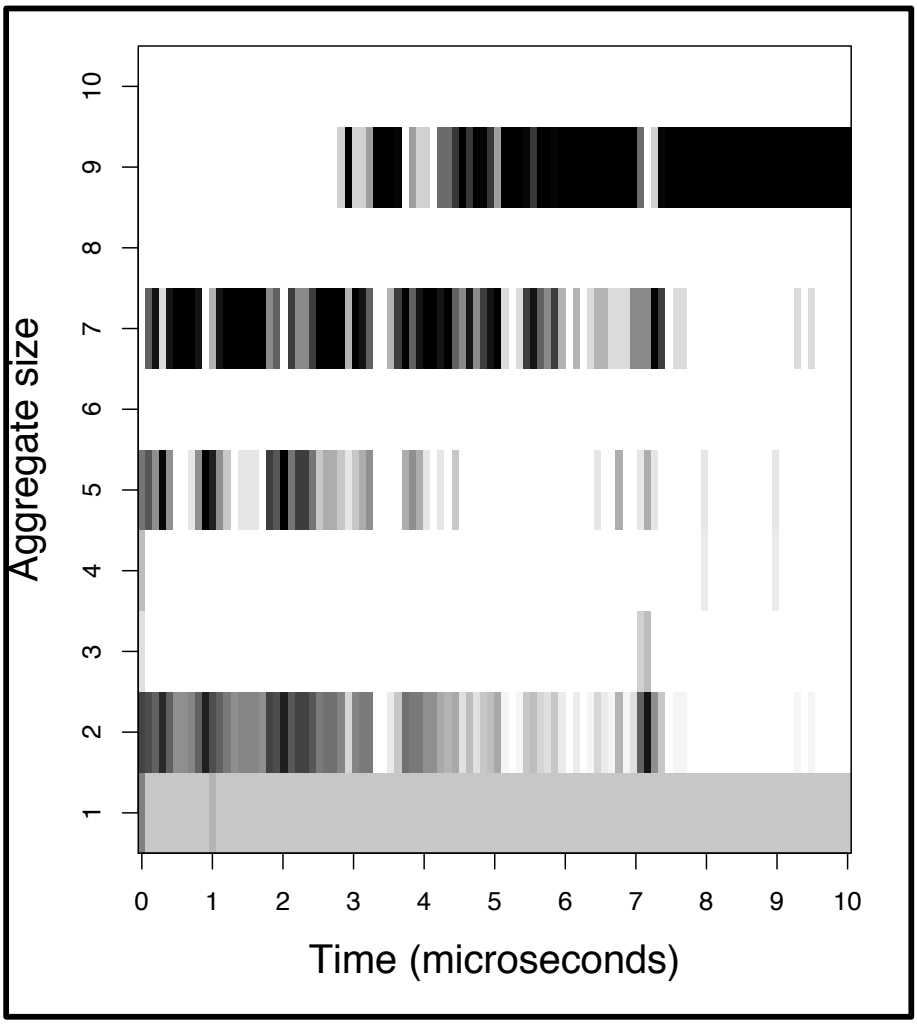

Figure 41 Cluster analysis graph for a 10 proteins simulation in a POPC only membrane.

As shown here, for most of the simulation time, the peptides were in clusters of 7 and 9 peptides. During the simulation, once one peptide became attached to the membrane the rest of the peptides bound to it forming a big cluster on top of that peptide rather than the membrane. This result supports the lower affinity of the peptides for POPC lipids.

In most of the simulations, carried out for this thesis, larger peptide clusters were present in the POPC only membrane as compared to the mixed lipid membrane.

Cluster analysis for Dermaseptin DS01

The same tool was used for the Dermaseptin DS01 simulations. The results were similar in that, with the POPC membrane, the proteins spent a significant proportion of the simulation in a large cluster of 5 peptides while, in the mixed lipid membrane, the cluster sizes were smaller and varied for most of the time.

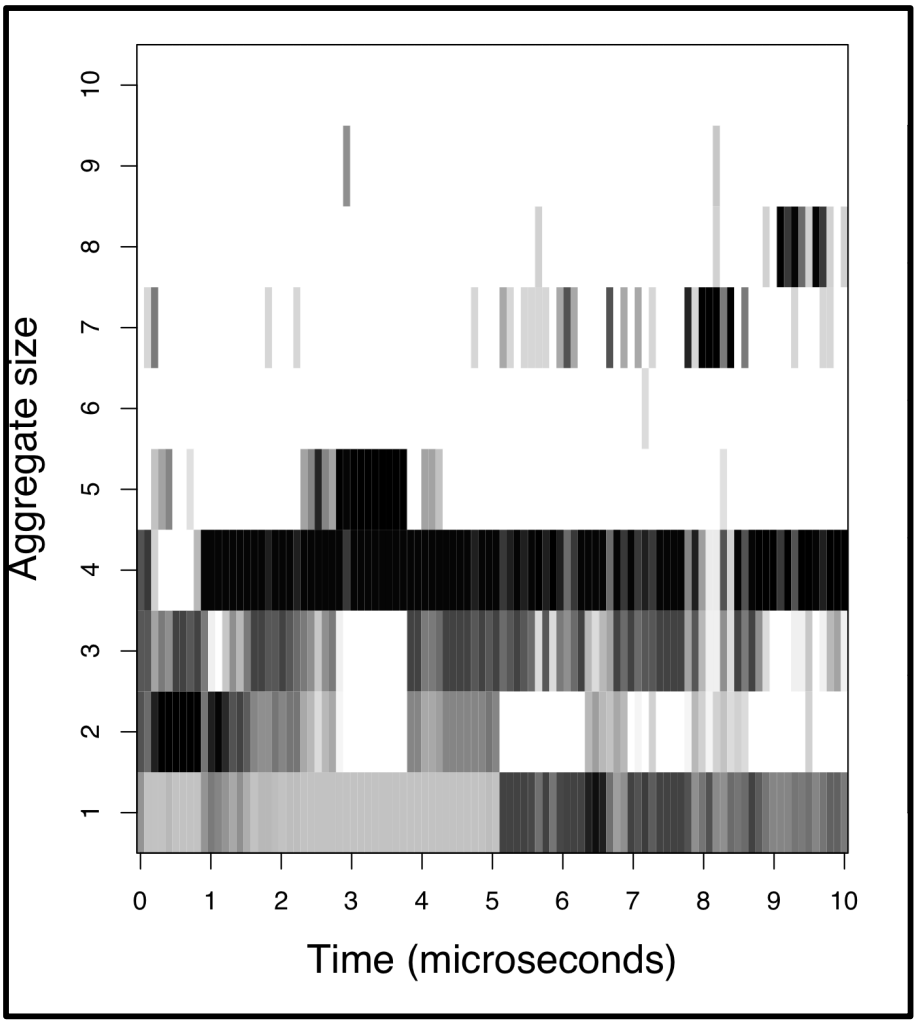

Figure 42 Cluster analysis graph for a 10-protein simulation in POPC/POPG/POPE membrane.

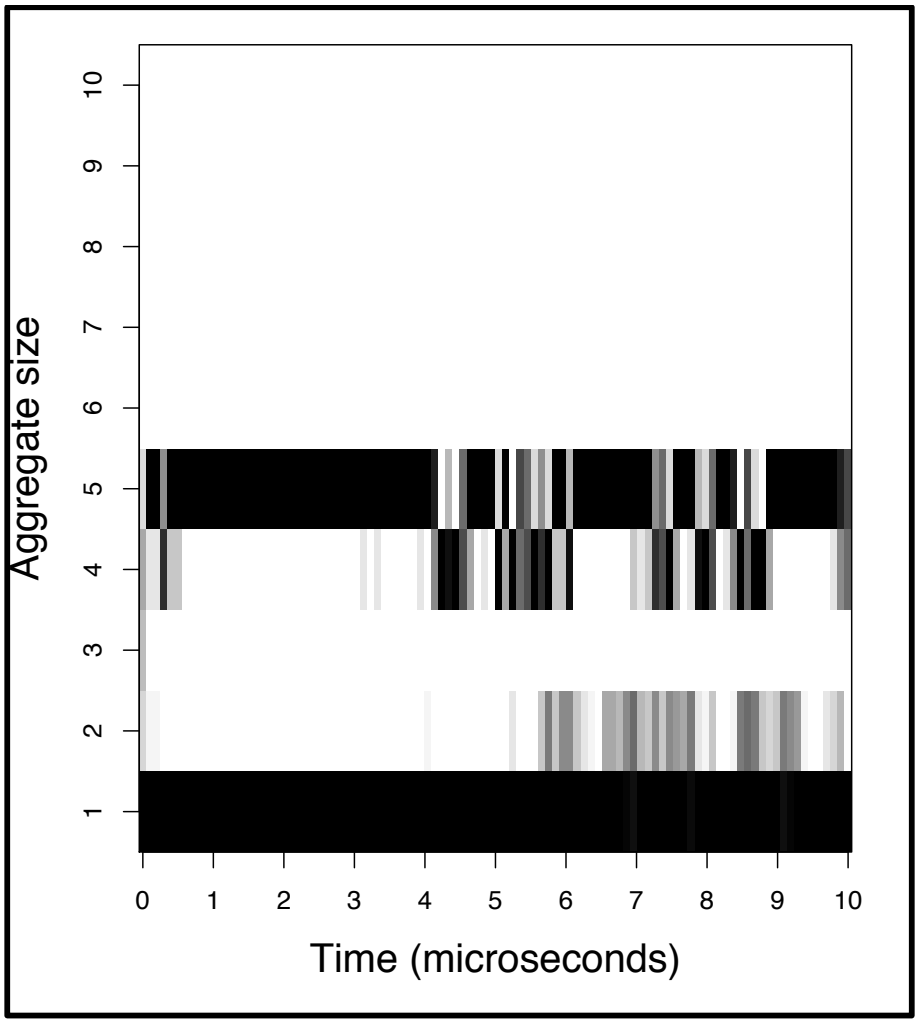

Figure 43 Cluster analysis graphs for a 10-protein simulation in a POPC only membrane.

Chapter 8: Discussion

For this thesis, MD simulations were carried out representing Dermaseptin B2 and Dermaseptin DS01 in two membranes; one was made up of POPC/POPG/POPE and the other membrane was made of POPC. All simulations were carried out using the martini coarse-grained technique in a flat lipid bilayer. This was done to find out how these peptides influenced the membrane structure and to understand how they went about either penetrating the membrane or forming trans-membrane pores.

The aim of the study was to understand the mechanism of action associated with antimicrobial peptides used in killing invading microbial colonies and to figure out why they did not seem to attack mammalian cell membranes. All simulations were done by using the coarse-grained method because it was important to simulate the longest possible time to obtain any meaningful results. All results were compared to experimental results for validation. The results from these simulations should be interpreted in this light.

There are no significant differences between the two peptides when considering the interaction of polar residues in the mixed lipid membrane. The simulations demonstrate explicitly that hydrophobic interactions drive the strong association of both Dermaseptin peptides with membranes and, particularly, the negatively charged lipids. This is an observation documented widely in the literature not only for Dermaseptin but, also, for various other helical antimicrobial peptides. One observation identified from the literature, is that these simulations are unable to verify that the peptides tend to adopt the helical structure in the presence of membranes with anionic lipids. In the simulations, both Dermaseptin peptides started off in a helical structure because this thesis aimed to explore how they formed pores and, therefore, the simulations began with the membrane active structure for the peptides.

When simulated with the POPC only membrane, both peptides maintained their helical structure even though, per the literature, this ought not to have been the case. However, it is there because of the system set up. This specificity in the adoption of the helical structure is key to these peptides' potency towards bacterial membranes while posing no harm to mammalian cell membranes. The stabilisation of the helical

structure of Dermaseptin in the presence of negatively charged lipid headgroups (such as POPG) allows for the membrane association of these peptides and the initiation of the carpet model driven membrane pore formation. The adoption of Reduced helical structure in the presence of zwitterionic membranes allows for lesser membrane association with the membrane and, thereby, to a lower extent, disruption of the membrane. Indeed, in the simulations, significantly lower amounts of peptide-membrane association were observed where, in most cases, a large cluster of peptides was associated/ anchored to a membrane surface by a single peptide.

In all cases of the mixed lipid membranes, minimal membrane penetration was observed. This result agrees with literature where it was found that the loosely helical structure of the protein prevented a protein cluster from becoming deeply embedded in a membrane, preferring to anchor the peptide cluster to the surface of the membrane. Even when clusters of proteins were forced and restrained into the membrane, they moved quickly out of the membrane and became anchored to the surface of the membrane by a few peptides.

Given its interface-parallel orientation in lipid bilayers, it is thought that Dermaseptin brings about antimicrobial activity via the carpet model. All simulations agreed with prediction where all simulations, both in mixed and pure POPC membranes, membrane protein association was parallel. In turn, this means that there is no terminus of these proteins that are fundamental either to antimicrobial activity or membrane association. Indeed, this was the case. In the lipid contact analysis, there were no termini that attracted attention to the amount of contact that it maintained with the membrane.

Although there are vast amounts of experimental data surrounding Dermaseptin and its functionality, very few computational studies investigated these peptides. These simulations aimed to find out how these peptides formed membrane pores that led to cell lysis. With the available computational resources, it was possible to simulate 10 microseconds of interaction between peptide and membrane. In that timescale, it was possible to see membrane attachment, lipid specificity and the shallow membrane penetration of Dermaseptin peptides. However, no membrane pores were observed. This result could have been because the concentration of simulated peptides was not high enough to cause significant disruption to the membrane leading to the formation of pores. Alternatively, it could have been simply that longer simulation times were

required to see the pores. The simulations confirm various experimental observations regarding Dermaseptin (including the lipid specificity, shallow membrane penetration and protein clustering) which, on in its own terms, validates the parameters used to carry out these simulations.

Chapter 9: Conclusion

In conclusion, Dermaseptin seems to be a viable option for the treatment of infections. The peptides appear to have specificity towards anionic lipids abundantly present in microorganism membranes. Dermaseptin is a cationic peptide and, therefore, it is attracted to the negatively charged membranes of the microbial kingdom. This gives the peptide the desired specificity needed in an antibiotic. This preferential binding onto anionic lipid can be seen in the simulations and were shown in the form of various snapshots throughout this thesis' results and analysis chapters. Literature found that only Dermaseptin assumed the helical structure in the presence of anionic lipids. This could not be demonstrated in the simulation since the peptide started out with a helical structure that was maintained in the presence of both POPC lipids and mixed lipid membranes.

The simulations, carried out in this thesis, supported the findings in the literature. Consistent with the literature's findings, all Dermaseptin peptides clustered rapidly and penetrated the membranes transiently in a shallow manner. No pores were formed in the simulations carried out and this could have been due to the short simulated time.

Although this thesis could not provide further information regarding the mechanism of action of these peptides (such as either specific side chains or termini that are fundamental to antimicrobial activity or any more information regarding protein-membrane binding), it did support much of the information in literature and, thereby, solidified the discussed theories.

From the research done for this thesis and the review of the literature, it seems that Dermaseptin is a promising peptide that can have therapeutic benefit in the efforts to find a new class of antibiotics.

Chapter 10: Simulating HCV protein in membranes

10.1 Introduction

HCV NS4B is a 27kDa hydrophobic protein. It has three domains; the carboxy and amino of which being cytoplasmic and the central region that inserts into the endoplasmic reticulum membrane. Studies have suggested that the N-terminus of the protein is involved with multimer formation whereas the C-terminus can be involved in membrane association (1). The protein's function is predicted to be the formation of intracellular membranous webs that the virus uses as grounds on which to replicate. It was found that the amphipathic alpha helix on the protein's N-terminus was pivotal to its association to the membrane. Disruptions by way of mutations in the alpha helix had a huge effect on the protein's ability to associate with a membrane. Therefore, it abolished viral replication making it an ideal drug target in the fight against the virus (2). Further inspection of the NS4B found that it was associating itself with lipid rafts (cholesterol and sphingolipid fragments of a cell membrane resistant to solubilisation). This suggests that the hepatitis virus is amongst a growing group of viruses that uses these lipid rafts to replicate before taking over and infecting the host cell (3). Electronic microscope investigation showed that the NS4B formed membranous webs in the form of vesicles that appeared to be derived from the cells endoplasmic reticulum (4).

In terms of the membrane's lipid specificity, studies found that positive residues on the protein's C-Terminus bound to negative lipid head groups in order to gain access into the cell (5). It appears that generally NS4B is attracted to negatively charged lipids and that it shows some specificity towards some lipids, phosphatitylinositol 4 phosphate (PI4P) being of particular importance for the HCV life cycle (5). The presence of anionic lipids (negatively charged lipids) is important to the binding and dissociation of the alpha helices that, in turn, facilitates the re-structure of the membrane. This is particularly true for the phosphatidyglycerol where PNMR results show that an increased concentration of this lipid facilitates alpha helix dissociation and membrane re-structure (2).

There is a lot of information about where the NS4B prefers to attach and what it seems to mediate in terms of structural change. Therefore, I carried out some

molecular dynamic simulations in an attempt to understand how the binding occurred and to visualize the changes that it made to the membrane. From the simulation place HCV peptide helix in a POPC/POPG membrane with a ratio of POPC: POPG of 2:1, I expected to see that the alpha helix bound to the POPG residue to bring about a membrane conformational change. In order to compare the association with negatively charged lipids, I ran, also, simulations with PIP2: POPC membranes in the same 2:1 ratio. I selected PIP2 due to its structural similarity to PI4P and lack of data and structure on PI4P.

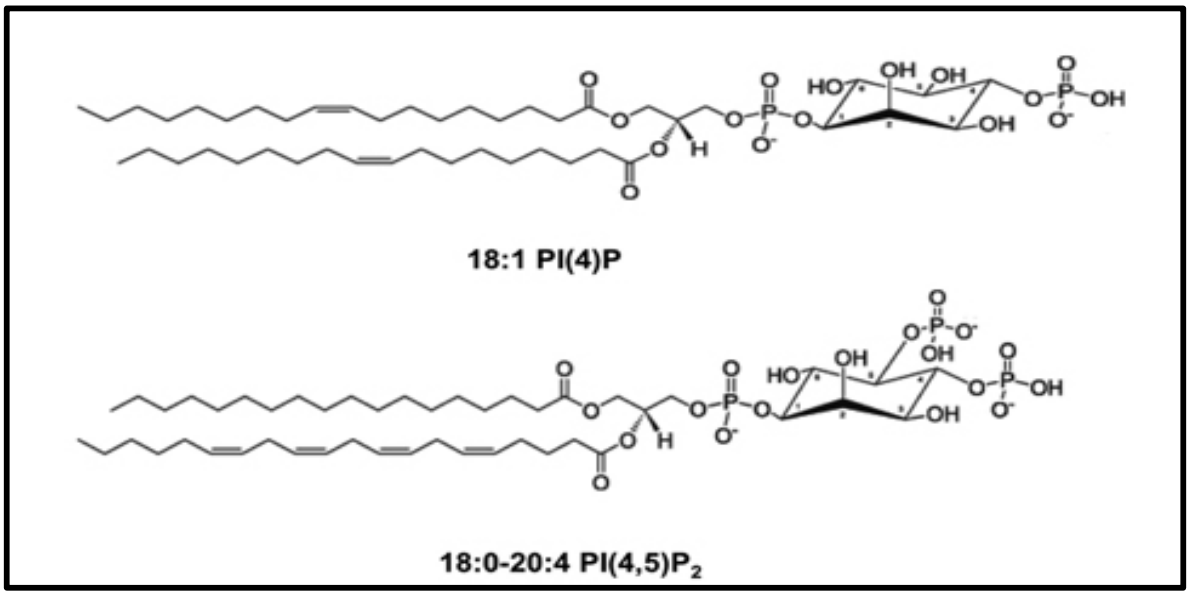

Figure 44 Structures of PIP2 and PI4P lipids Picture modified from (6).

10.2 Methods of simulations

All simulations were done using the coarse-grain method. Coarse graining was used since it represented the system using fewer degrees of freedom. In turn, this allowed for longer simulation time scales in shorter real time and provided more data to be analyzed. The simulations were performed using GROMACS 4.5.5 (www.gromacs.org) in a Martini 2.0 force field. The parameters for the PIP2 lipids were as described in (6). As described in (7, 8, 9), all simulations involved self-assembly of a lipid bilayer from a random configuration of lipids, ions and water. Next, varying numbers of peptides, 3, 5 or 10 (PDB code: 2JXF) were added to the system outside of the membrane in the bulk water region. Implementing an elastic network model retained

the integrity of the HCV helix. Details of the simulations systems are given in Table 7 below.

Simulations (3 independent runs of each)	Number of peptides	Membrane composition	Length of each simulation	Multimers formed
PG_HCV3	3	3:1 POPC:POPG	50 ns	2
PG_HCV5	5	3:1 POPC:POPG	50 ns	2, 3, 5
PG_HCV10	10	3:1 POPC:POPG	50 ns	2, 3, 4, 6
PIP2_HCV3	3	2:1 POPC:PIP2	50 ns	2, 3
PIP2_HCV5	5	2:1 POPC:PIP2	50 ns	2, 3, 4
PIP2_HCV10	10	2:1 POPC:PIP2	50 ns	3, 4, 5, 8
PC_HCV	3	100% POPC	50 ns	2, 3
PC_HCV	5	100% POPC	50 ns	3, 5

Table 7 Summary of simulations.

Lipid transition phase temperature:

The lipid transition temperature is the temperature at which the lipid bilayer adopts a solid gel state from the original fluid state of a membrane. For the lipids, used in these simulations, these were:

POPC: 271.15 K
POPG: 271.5 K
PIP2: 271 K

10.2.1 Details of simulation:

For all the coarse-grained simulations, Lennard-Jones interactions were shifted smoothly to zero between 0.9 nm and 1.2 nm, and electrostatics were shifted smoothly to zero between 0 and 1.2 nm, with a relative dielectric constant of 20 used for explicit screening. The non-bonded neighbour list was updated every 10 steps. All simulations were performed at constant temperature, pressure, and number of particles. The temperatures of the protein, POPC, POPG, PIP2, and solvent were each coupled separately by using the Berendsen algorithm (10) at 300 K, with a coupling constant τT = 1 ps. The Berendsen coupling system was chosen for both temperature and pressure since it did not allow the system to diverge out of the set pressure and temperature for long. Thus, it ensured accurate results. The system pressure was coupled anisotropically by using the Berendsen algorithm at 1 bar with a coupling constant τP = 1 ps and a compressibility of 5×10^{-6} bar^{-1}. The time step for integration was 10 fs. Analyses of the CG simulations were performed by using GROMACS tools and locally written code and visualization used VMD (11). The system was neutralised by using sodium ions and minimized and equilibrated for improved integration into the system. By using martini insane.py script a symmetrical membrane bi-layer, containing 492 lipids in the ratio of 2:1 POPC: POPG and another using PIP2: POPC, were generated. Then, these membranes were used in all the simulations (500ns each) with 3, 5, and 10 HCV proteins to see how the protein interacted with the membrane while looking for any lipid specificity. Three independent repetitions were made for each of the simulations in order to verify any findings.

The system minimization and equilibration steps were 10 ns long. Minimization and equilibration steps were done after every step in the simulation process; i.e. after adding the membrane to a water box, addition of neutralising ions and at the point of adding the various proteins to the mix. This ensured that the system was well accommodated to everything in the mix and that any results from the simulations could be relied upon.

The end of the simulation run generated 500 frames for analysis. Those were used to find information about: how the helices clustered together; how they interacted with the membrane; and whether they showed any lipid specificity.

Throughout the simulations, it was observed that the HCV proteins tended to cluster together before binding onto the membrane. It is unclear whether clustering is related to membrane curvature but it does seem to happen randomly. There was neither specific pattern to clustering nor a specific end shape to the cluster. The proteins appeared to associate with each other randomly as they crossed each other's paths. Throughout the simulation cluster size was calculated at the base of the cluster at the first point it associated itself with the membrane using VMD. These sizes varied from 1.8 to about 6.0 nm and all had completely different shapes.

A common observation, seen throughout the simulation, was that all the membranes showed some curvature by the end of the simulation. The curvature appeared, also, to be protein concentration related, i.e. the higher the concentrations of protein present the faster the first point of curvature was reached. There is, also, a higher degree of curvature with more proteins. It is unclear whether or not this is due to clusters forming faster. Nevertheless, these results show, also, that membrane curvature is dependent not only on protein concentration but, also, that it is reliant on the presence of POPG or PIP2 (or perhaps any negatively charged lipid?). This was shown by the lack of curvature in the POPC only membrane even though the protein cluster formation had occurred and the cluster had associated itself with the membrane. These finding agree with the reviewed literature when planning the simulations although the mechanism, through which membrane curvature happens, remains unclear. All observed cluster sizes are recorded in Table 8 below.

	Repetition 1		Repetition 2		Repetition 3	
	Cluster formation time (NS)	Cluster size (nm)	Cluster formation time (NS)	Cluster size (nm)	Cluster formation time (NS)	Cluster size (nm)
3 protein PG	33	2.35	80	3.95	27	1.82
5 protein PG	36	2.45	42	5.49	21	2.71
10 protein PG	24	2.12	33	5.86	27	2.37
3 protein PIP	21	2.3	34	1.5	23	2.4
5 protein PIP	3	2.0	9	2.4	3	2.9
10 protein PIP	3	3.7	1.5	4.1	4.2	4.7

Table 8 Summary of protein clustering.

10.3 Results of POPG simulation:

In all simulations, the HCV peptides moved freely out of the water in the simulation box towards the lipid bilayer where they were seen interacting with the surface of the membrane but not penetrating the bilayer. A description of a typical scenario where 10 peptides were left to interact with the model membrane made up of POPC: POPG in a ratio of 2:1 respectively. 3 nanoseconds into the simulation 1 of those peptides became membrane associated quickly adopting an orientation parallel to the membrane surface. It appears as though this single peptide membrane association facilitated the binding of clusters onto the membrane. Then, the peptides began to cluster forming a tetramer, trimer and dimer after 4 ns of simulation time. The tetramer was first to attach itself to the membrane at around 7 ns with 15 ns later the

dimer attaching to it forming a membrane-associated hexamer by 22 ns of simulation time (Figure 31). The trimer formed also became membrane associated after around 12 ns so all peptides in the simulation became membrane bound at 24 ns.

The clusters were formed randomly with no orientation or termini being particularly involved in the process. Lipid-protein interactions were analyzed (where interaction is defined as $r \leq 0.6$ nm) and, despite the majority of lipids in the membrane being POPC, they showed a clear preference for POPG lipids over POPC lipids. Taking the point where all ten peptides were surface associated, approximately 450-500 of the lipid protein contacts were made (counting all the lipid and protein particles) with POPG lipids. There were between 400-420 contacts made with POPC lipids despite the higher proportion of POPC in the membrane compared to POPG. The difference in contacts was more prominent when only the dimer became membrane associated. At that point, around 50 contacts were made with POPG lipids and around 10 were made with POPC.

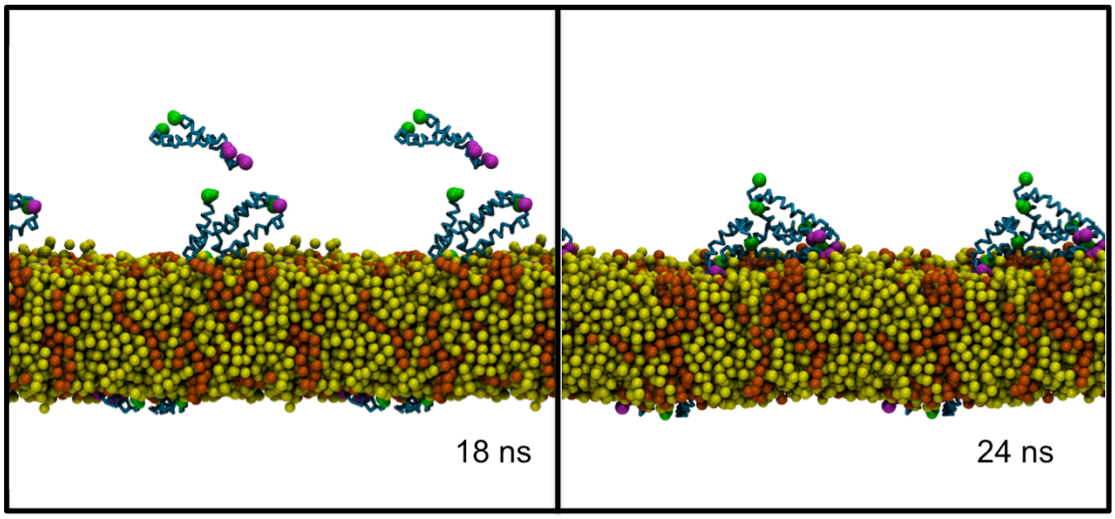

Figure 45 **Two snapshots were extracted from a 50 ns simulation of 10 x HCV peptides in a 3:1 POPC:POPG lipid bilayer (two periodic images are shown). The colour scheme is as follows: POPC lipids are yellow, POPG lipids are orange, peptides are cyan, the N -terminus backbone bead is purple and the C-terminus backbone bead is green. The tetramer is already membrane-associated after 18ns and, after 24 ns the dimer has become attached to the tetramer, it forms a surface-associated hexamer.**

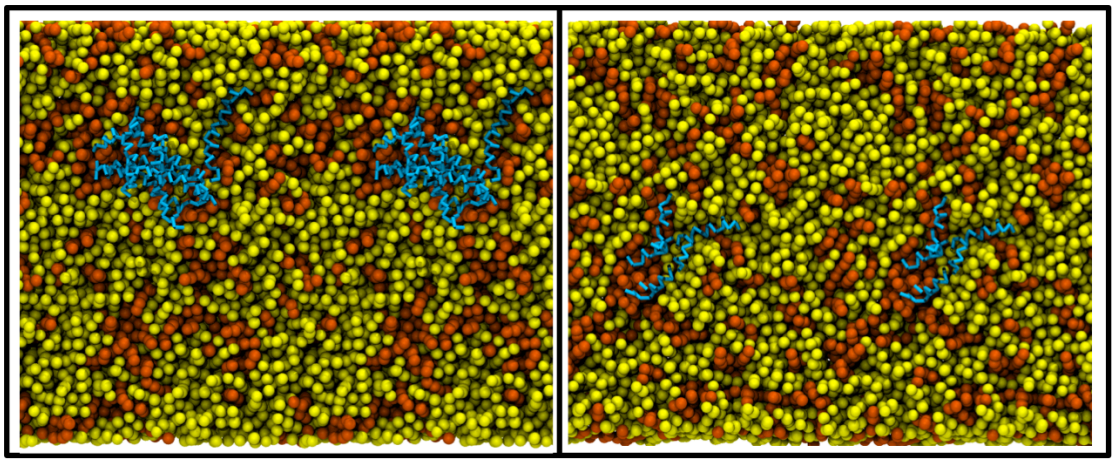

Figure 46 **Two snapshots were extracted from the same simulation as in Figure 47. Looking down at the surface of the membrane, it is possible to see the clustering of POPG lipids around the tetramer (left) and the trimer which is associated with the other leaflet (right). Two periodic images are shown and the colour scheme is the same as in Figure 31.**

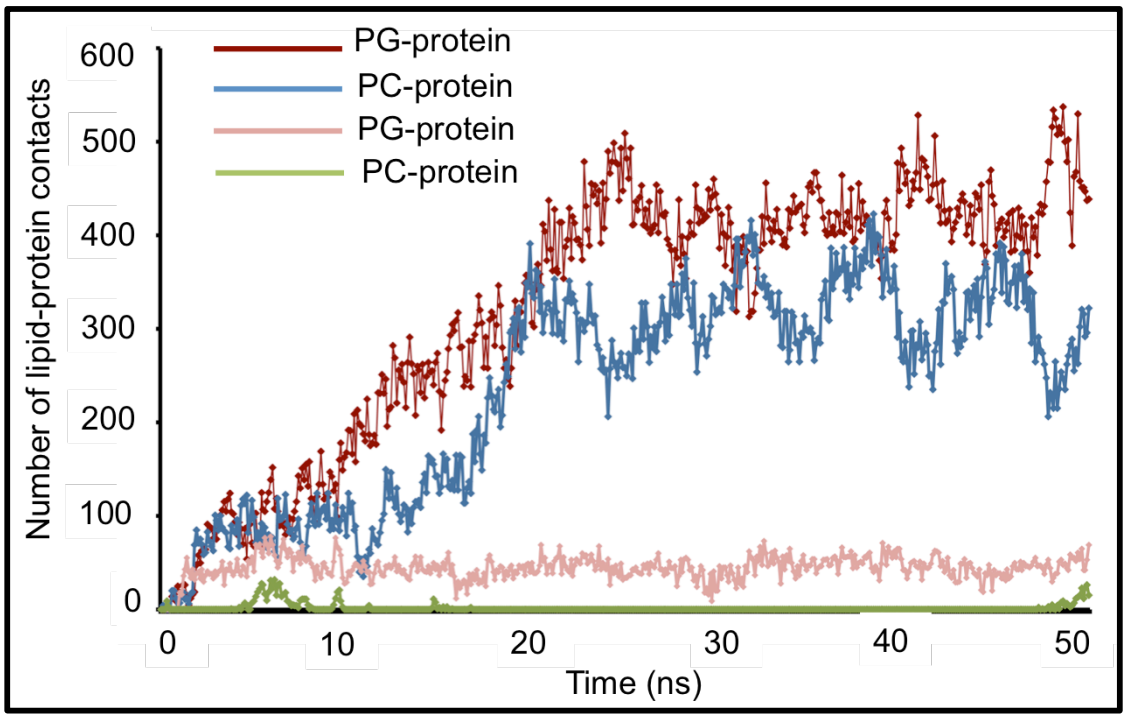

Graph 22 **Lipid-protein contacts are shown over 2 simulations. The magenta and blue curves correspond to all ten peptides being membrane associated and the pink and green curves correspond to only two peptides being membrane associated.**

10.4 Results of PIP2 Simulations

In much the same way that is observed with the PG simulations, membrane association was observed always but never membrane penetration. Membranes tended to cluster very early in the simulations, in most cases clustering occurring within the first 5 nanoseconds. In the high concentrations (10 proteins) simulations it was common to see one protein quickly becoming membrane associated and attracting other proteins to cluster around it. In this way, large clusters of 5 proteins or more became very quickly membrane associated. The largest cluster, seen within the simulations, contained 10 proteins and was 4.7 nm wide at its base. Typically, once a cluster became membrane associated, it did not dissociate and remained that way throughout the rest of the simulation. In most cases, membrane association was rapid, occurring within the first 10 nanoseconds. The exception was the 3 protein simulations where association took place within the first 20 nanoseconds. This could be down to the big simulation space and, therefore, the probability of the protein, coming in contact with the bilayer, was smaller than in the higher concentration simulations.

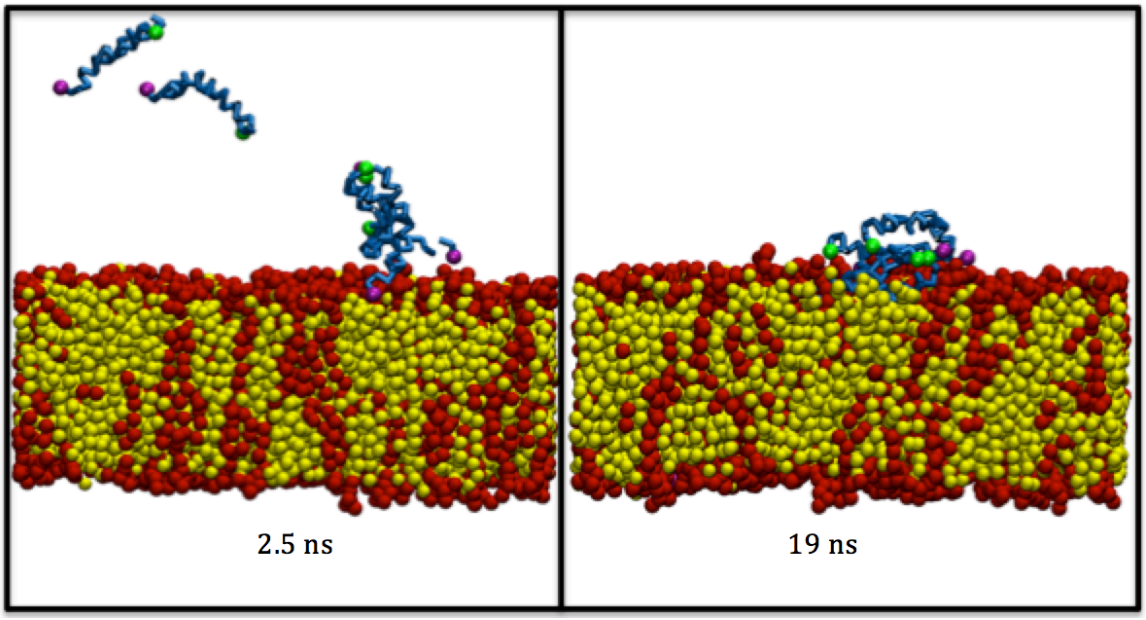

Figure 47 Two snapshots were taken from a 50 ns simulation of 5 x HCV peptides in a 2:1 POPC: PIP2 lipid bilayer (two periodic images are shown). The colour scheme is as follows: Red: PIP2 Yellow: POPC Cyan: protein Green bead: N-termini Purple bead: C-termini. The image shows a membrane bound tetramer at 2.5 ns and after 19 ns the floating dimer has attached onto the tetramer forming a 5-protein membrane associated cluster.

As with the POPG simulations, peptide clustering was rapid and random with no observable pattern. Membrane association appeared, also, to be random. However, the literature suggested that the protein's C-termini was responsible for membrane association. The first picture of Figure 50 (above) is a snapshot taken from a 5-protein simulation showing a trimer associating with the membrane surface. As the simulation progressed, the remaining two proteins in the box were attracted to and became attached to the trimer forming a 5-protein cluster that was membrane associated. The snapshots highlight, also, how protein clustering is found usually in areas of high PIP2 density. Figure 51 (below) shows snapshots taken from a 10-protein simulation. The first picture shows a few proteins becoming membrane associated. The second picture highlights how membrane associated peptides attract the free peptides towards themselves to form membrane bound clusters. This is a representation of a typical 10-protein simulation scenario where, in most cases, one protein becoming membrane attached results in the formation of a large membrane bound protein cluster.

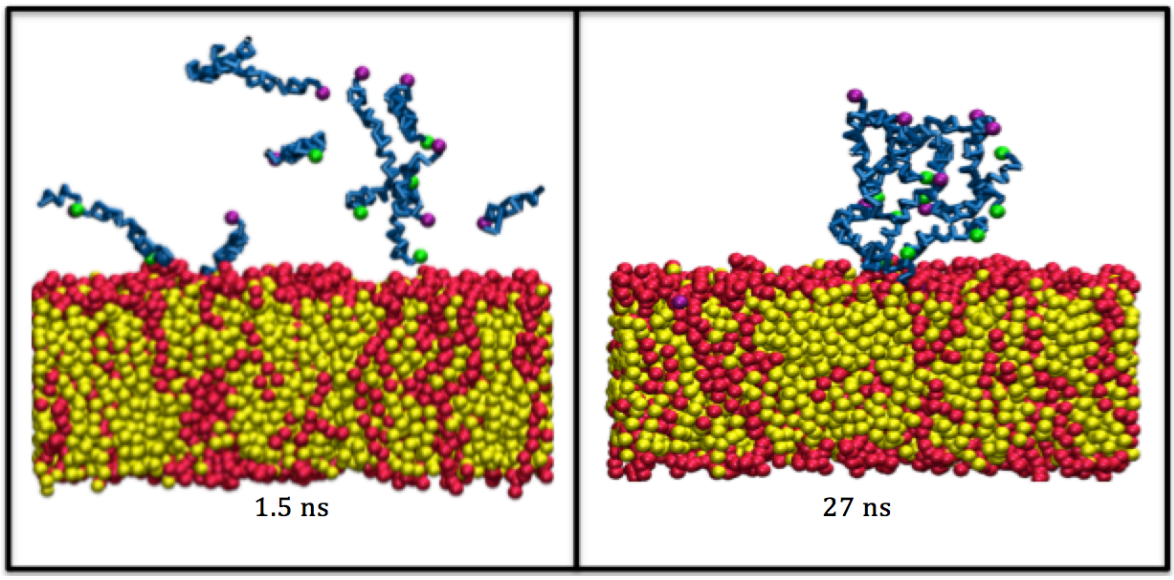

Figure 48 Two snap shots were taken from a 50 ns simulation of 10 x HCV peptides in a 2:1 POPC: PIP2 lipid bilayer. Colour scheme is as above. The image indicates a typical simulation where one peptide attaches to the membrane and facilitates the other peptides attachment.

Looking at the simulation from the top, it is easy to see the clustering of PIP2 lipids around the protein and where the proteins attached themselves to the membrane. Figure 52 (below) shows a snapshot taken at 27 ns from a 10-protein simulation. As shown, there is a high density of red beads (representing PIP2 lipids) surrounding the protein (Cyan tubes) cluster.

The second snapshot is taken from a 5-protein simulation at 19 ns. In the same way as the 10-protein snapshot, there is a clear aggregation of PIP2 lipids around the protein cluster.

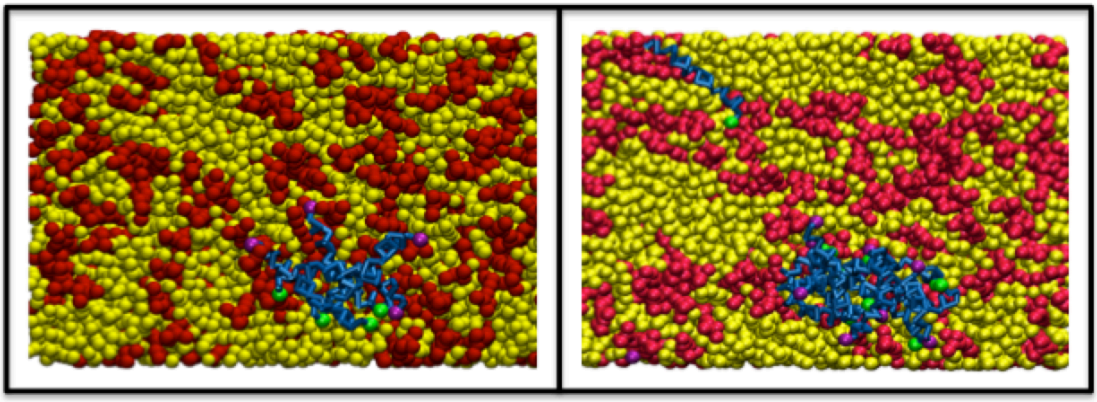

Figure 49 **Two snapshots taken from a 5-protein simulation (left) and a 10-protein simulation (right) viewed from the top. The colour scheme is as above. The snapshots highlight the high PIP2 density surrounding each protein cluster.**

To confirm the visual observation of negatively charged lipids around the protein cluster density graphs were plotted using the GROMACS tool G-density results of which can be found below in graphs 23 and 24.

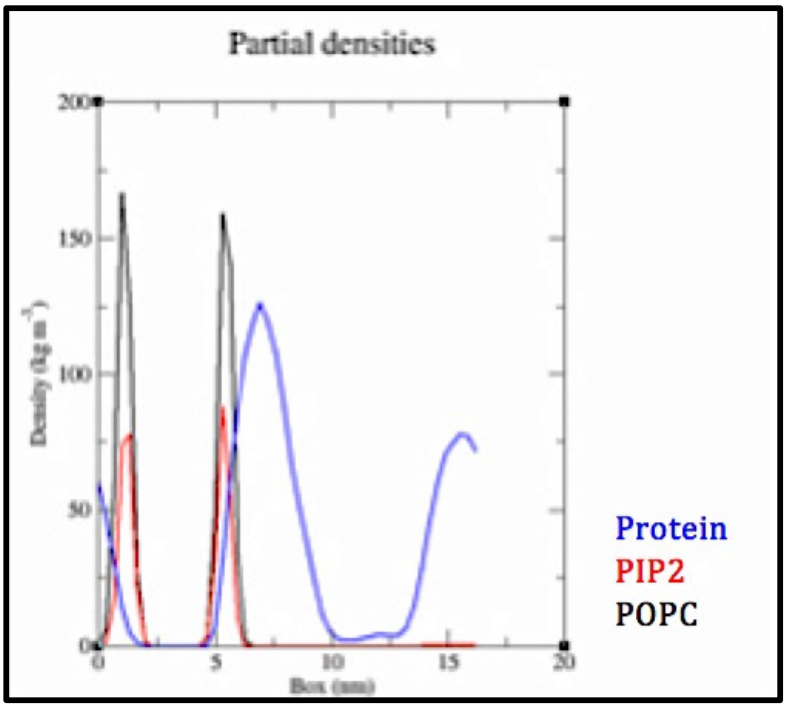

Graph 23 **Density plot as shown from a 5-peptide simulation. The blue line represents the protein and the red line corresponds to PIP2. As shown, there is a relationship between the two lines since, as the PIP2 density increases, so does the protein.**

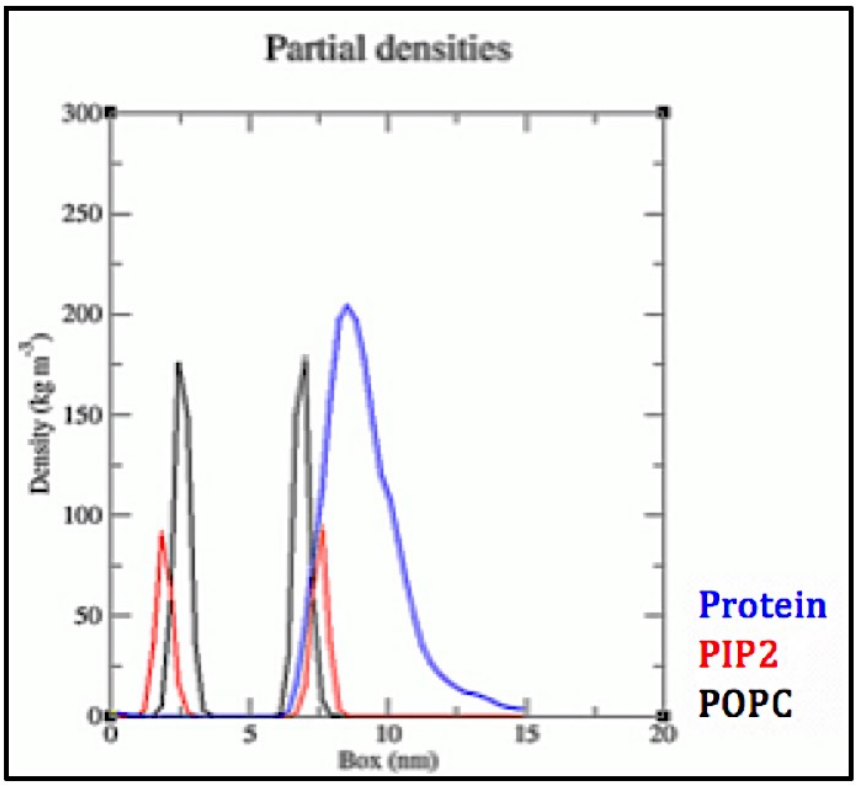

Graph 24 Density plot shown from a 10-protein simulation. As shown, the same relationship between POPG and the protein but it's not as close as that of the protein with PIP2. Colour code is as in graph 23.

G-density analysis of a POPG and PIP2 10-protein simulations confirmed lipid specificity. Graphs 23 shows that, as the density of either lipid increases, so does the density of the protein. When comparing the two graphs, it appears that there is a closer relationship between the protein and PIP2. This is shown by the closeness of the two curves and how, when the PIP2 density reached its peak, so did the protein density.

Further examinations of lipid specificity, protein lipid contacts tests were carried out. Those were done by using a locally written script that analysed the simulation trajectory by looking at contacts the protein made with the membrane. The results from the script were plotted using Microsoft Excel and, indeed, they confirmed that the protein did seem to prefer to bind to the negatively charged PIP2 lipids. Below is a graph showing lipid contact analysis for one of the 5 protein simulations:

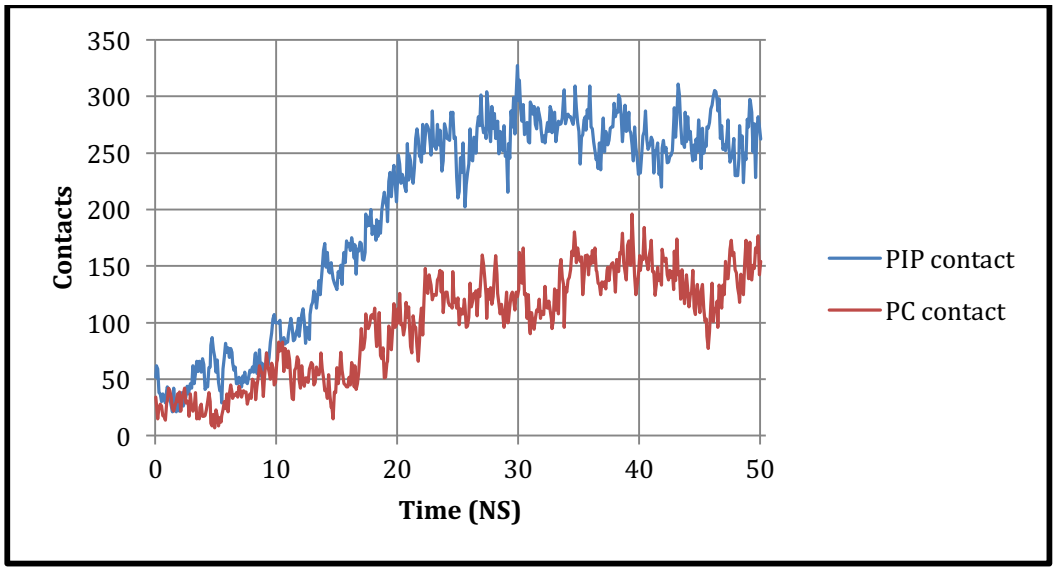

Graph 25 It shows lipid-protein contacts. The graph plots the number of contacts throughout a whole 50 ns 10-protein simulation.

From analyzing the frame where an 8-protein cluster was membrane associated, there were 263 contacts made with a PIP2 lipid as compared to 127 contacts with POPC. This accounted for 67% of total contacts at the one point. This was a significant proportion particularly when considering that there were twice as many PC lipids as PIP2 lipids.

The difference in contact is highlighted when fewer proteins are interacting with the membrane. For example, Graph 26 below describes the lipid contact analysis of one of the 5 protein simulations.

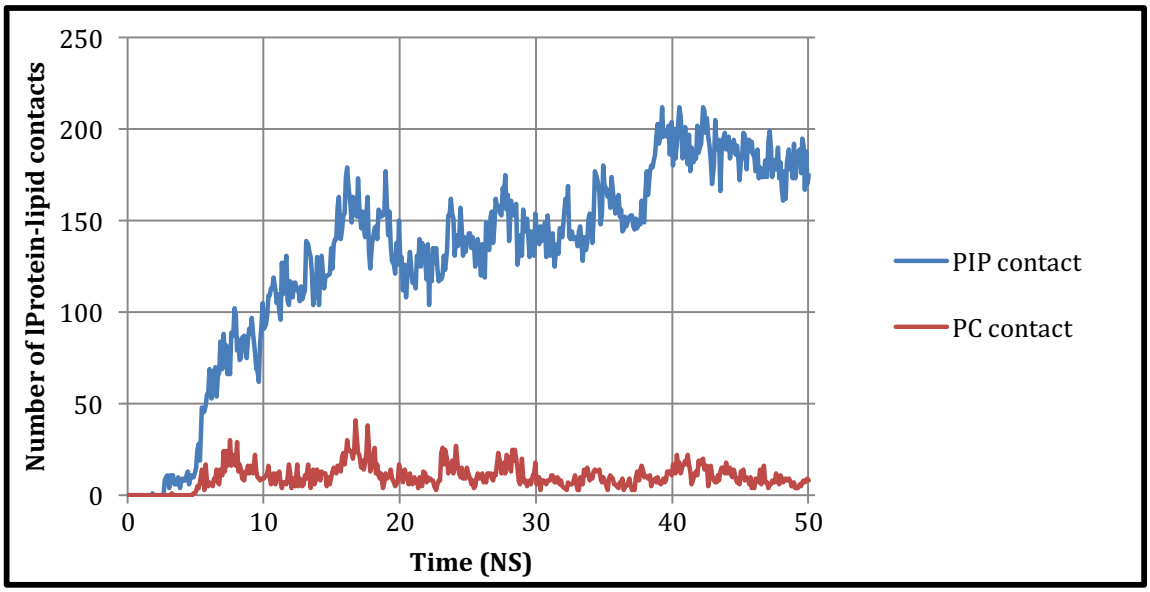

Graph 26 It shows lipid-protein contacts. The graph plots the number of contacts throughout a whole 50 ns 5-protein simulation.

Visually, it is obvious that the protein has a marked preference for PIP2 head groups. However, numerically if we take the point where a 3-protein cluster became membrane associated, we find that 179 contacts were made with a PIP2 head group and only 30 contacts made with a POPC lipid. Namely, 85% of total contacts were made with PIP2.

Therefore, lipid contact results support the evidence in showing that HCV peptides are attracted to negatively charged lipids. Then, it is clear that membrane association is driven electrostatically where positively charged amino acids within the peptide structure facilitate membrane association.

10.5 PIP2 vs. POPG contact

There are vast amounts of literature with findings that HCV protein has specificity towards PI4P. In these simulations, when I compare contact data between POPG and PIP2, I find that HCV has a marked preference for the structurally similar PIP2 lipid. Graph 27 below plots data relating to POPG and PIP2 simulations from 2 simulations with 5 proteins.

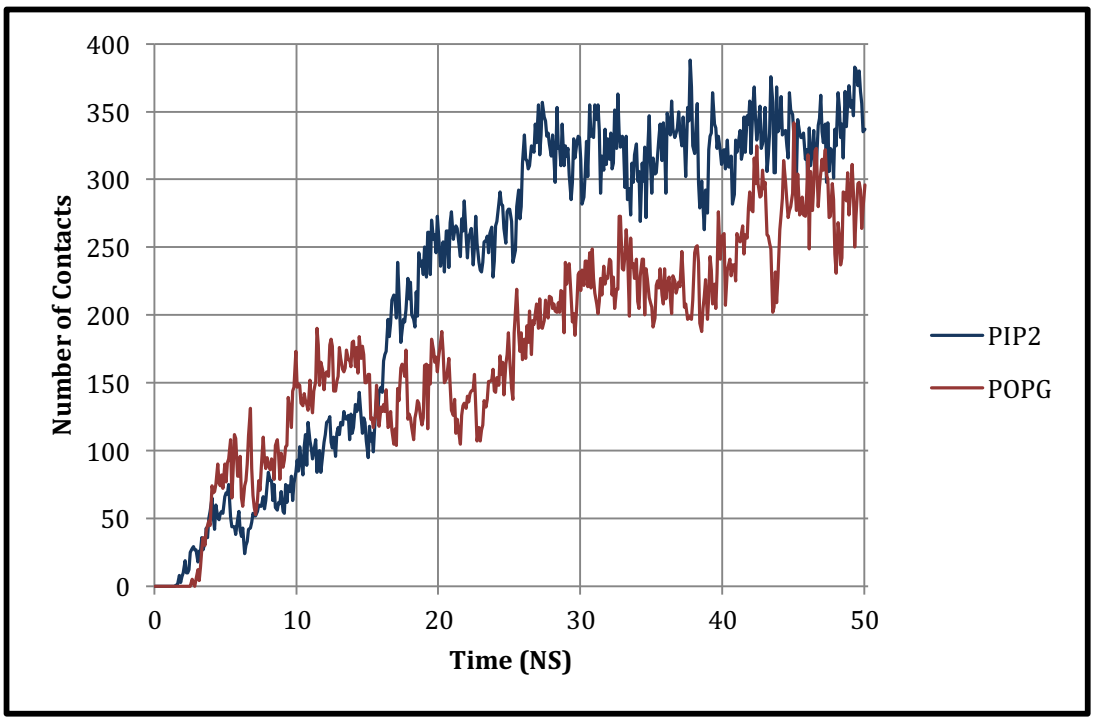

Graph 27 **It shows lipid-protein contacts. The graph compares the numbers of PIP2 and POPG contacts as seen through two 50 ns 5 protein simulations.**

Although contact with these two lipids is similar, it can be concluded that there is a marginal preference to PIP2 as compared to POPG. These results compare data from two simulations where the lipid of interest formed a membrane with POPC in the ratio of 2:1. Consequently, perhaps extrapolation of conclusions from these results may not reflect truly which of the two lipids HCV prefers. To be convinced that this is indeed the case, it may be worthwhile building a membrane with all three lipids and running simulations.

Graph 28 below looks at two simulations with 10 proteins. As can be seen, the first simulation showed that contact with the two lipids was more or less the same with PIP2 having a marginal advantage. However, when running the same simulation for a third trial (the purple and orange lines), there was observed a marked difference in contacts. The difference in contacts between the two lipids is very significant. In order to know conclusively how much more HCV favors PIP2 over POPG, I believe it would be important to carry out simulations that put all the lipids in one membrane so that we can observe how the protein clusters associate with the new membrane.

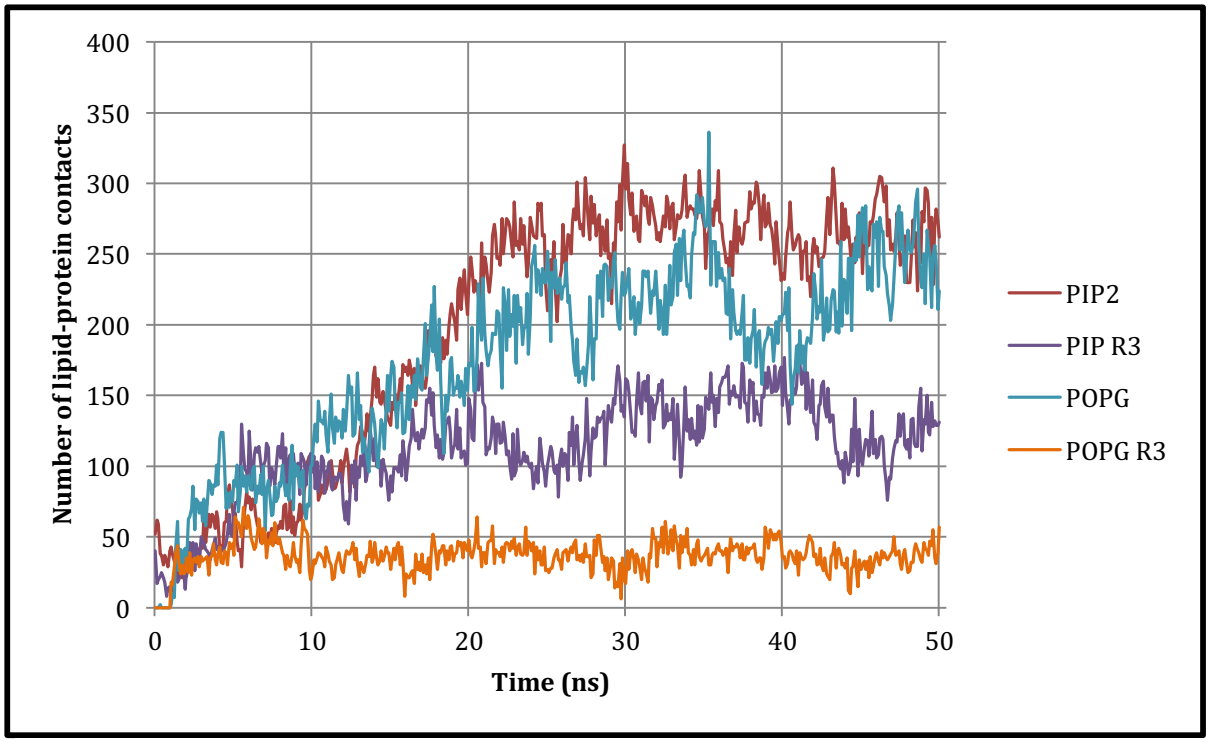

Graph 28 **It shows lipid-protein contacts. The graph compares the numbers of PIP2 and POPG contacts as seen through four 50 ns 10-protein simulations.**

10.6 Future simulation possibilities

The membrane bilayers used here is relatively small in size and, consequently, could have restricted the space in which the proteins had to work as well as the curvature. It would be good to simulate the same concentrations of protein in larger membranes to see if the same result, particularly in relation to the curvature, was observed since predictions would dictate that it ought to be more prominent with a larger membrane.

Another direction, which the simulations can take, is to try to mimic a liver cell membrane since the hepatitis virus tends to affect mainly liver cells. The liver cell has unique lipid composition in comparison to other body cells and, therefore, it would be interesting to see how the interaction with liver cell composition differs from that of POPC/POPG membrane.

Liver cell membrane composition:

- Neutral lipids
- Phospholipids:
- Phosphatidycholine
- Phosphatidylethanolamine
- Sphingomyetin
- Glycolipids
- Cholestrol
- Some free fatty acids

Quite a few papers have agreed that this was the composition of liver cell membranes. Although they differed on the relative amounts of these lipids, most agreed that the negatively charged phospholipids were relatively the most abundant lipids on a liver cell membrane. Perhaps, this explains why the hepatitis virus tends to attack liver cells (22, 23, 24).

Appendices

List of References

References: Dermaseptin

1. Davies, J., Davies, D. Origins and evolution of antibiotic resistance. Microbiol Mol Biol Rev. 2010;74(3):417-33.

2. Coelho, J.F., Ferreira, P.C., Alves, P., Cordeiro, R., Fonseca, A.C., Góis J.R. et al. Drug delivery systems: Advanced technologies potentially applicable in personalized treatments. EPMA J. 2010;1(1):164-209.

3. Rao, A.G. Conformation and antimicrobial activity of linear derivatives of tachyplesin lacking disulfide bonds. Arch Biochem Biophys. 1999;361(1):127-34.

4. Prestinaci, F., Pezzotti, P., Pantosti, A. Antimicrobial resistance: a global multifaceted phenomenon. Pathog Glob Health. 2015:2047773215Y0000000030

5. Rayamajhi, M., Humann, J., Penheiter, K., Andreasen, K., Lenz, L.L. Induction of IFN-alphabeta enables Listeria monocytogenes to suppress macrophage activation by IFN-gamma. J Exp Med. 2010;207(2):327-37.

6. Jenssen, H., Hamill, P., Hancock, R.E. Peptide antimicrobial agents. Clin Microbiol Rev. 2006;19(3):491-511.

7. Papp-Wallace, K.M., Endimiani, A., Taracila, M.A., Bonomo, R.A. Carbapenems: past, present, and future. Antimicrob Agents Chemother. 2011;55(11):4943-60.

8. Power, E. Impact of antibiotic restrictions: the pharmaceutical perspective. Clin Microbiol Infect. 2006;12 Suppl 5:25-34.

9. Levy, S.B., Marshall, B. Antibacterial resistance worldwide: causes, challenges and responses. Nat Med. 2004;10(12 Suppl):S122-9.

10. Yeaman, M.R., Yount, N.Y. Mechanisms of antimicrobial peptide action and

resistance. Pharmacol Rev. 2003;55(1):27-55.

11. Zdziarski, P., Simon, K., Majda, J. Overuse of high stability antibiotics and its consequences in public and environmental health. Acta Microbiol Pol. 2003;52(1):5-13.

12. Phoenix[1], D.A.,Dennison1, S.R., Harris2, F. Antimicrobial Peptides: Antimicrobial Peptides: Their History, Evolution, and Functional Promiscuity2013.

13. Witte, W. Medical consequences of antibiotic use in agriculture. Science. 1998;279(5353):996-7.

14. Paphitou, N.I. Antimicrobial resistance: action to combat the rising microbial challenges. Int J Antimicrob Agents. 2013;42 Suppl:S25-8.

15. Duclohier, H. Bilayer lipid composition modulates the activity of dermaseptins, polycationic antimicrobial peptides. Eur Biophys J. 2006;35(5):401-9.

16. Frecer, V., Ho, B., Ding, J.L. De novo design of potent antimicrobial peptides. Antimicrob Agents Chemother. 2004;48(9):3349-57.

17. Costelloe, C., Metcalfe, C., Lovering, A., Mant, D., Hay, A.D. Effect of antibiotic prescribing in primary care on antimicrobial resistance in individual patients: systematic review and meta-analysis. BMJ. 2010;340:c2096.

18. Sköld, O. Sulfonamide resistance: mechanisms and trends. Drug Resist Updat. 2000;3(3):155-60.

19. Sitaram, N., Nagaraj, R. Host-defense antimicrobial peptides: importance of structure for activity. Curr Pharm Des. 2002;8(9):727-42.

20. Castiglione-Morelli, M.A., Cristinziano, P., Pepe, A., Temussi, P.A. Conformation-activity relationship of a novel peptide antibiotic: structural characterization of dermaseptin DS 01 in media that mimic the membrane environment. Biopolymers. 2005;80(5):688-96.

21. Nikaido, H. Prevention of drug access to bacterial targets: permeability barriers and active efflux. Science. 1994;264(5157):382-8.

22. Janeway, C.A. How the immune system works to protect the host from infection: a personal view. Proc Natl Acad Sci U S A. 2001;98(13):7461-8.

23. Kim, J., Mosior, M., Chung, L.A., Wu, H., McLaughlin, S. Binding of peptides with basic residues to membranes containing acidic phospholipids. Biophys J. 1991;60(1):135-48.

24. Silvus J.R. S. Thermotropic Phase Transitions of Pure Lipids in Model Membranes and Their Modifications by Membrane Proteins. Lipid-Protein Interactions, John Wiley & Sons, Inc, New York. 1982:239–81.

25. Sum, A.K., Faller, R., de Pablo, J.J. Molecular simulation study of phospholipid bilayers and insights of the interactions with disaccharides. Biophys J. 2003;85(5):2830-44.

26. Giangaspero, A., Sandri, L., Tossi, A. Amphipathic alpha helical antimicrobial peptides. Eur J Biochem. 2001;268(21):5589-600.

27. Nagle JF, Tristram-Nagle S. Structure of lipid bilayers. *Biochimica et biophysica acta*. 2000;1469(3):159-195.

28. Spooner, M.J., Gale, P.A. Anion transport across varying lipid membranes--the effect of lipophilicity. Chem Commun (Camb). 2015;51(23):4883-6.

29. Epand, R.F., Savage, P.B., Epand, R.M. Bacterial lipid composition and the antimicrobial efficacy of cationic steroid compounds (Ceragenins). Biochim Biophys Acta. 2007;1768(10):2500-9.

30. Salton MR, Kim KS (1996). Baron S, et al., eds. *Structure.* In: *Baron's Medical Microbiology* (4th ed.). Univ of Texas Medical Branch. ISBN 0-9631172-1-1.

31. Ganz, T., Lehrer, R.I. Antibiotic peptides from higher eukaryotes: biology and applications. Mol Med Today. 1999;5(7):292-7.

32. Reddy, K.V., Yedery, R.D., Aranha, C. Antimicrobial peptides: premises and promises. Int J Antimicrob Agents. 2004;24(6):536-47.

33. Shai, Y. Mode of action of membrane active antimicrobial peptides. Biopolymers. 2002;66(4):236-48.

34. Hancock RE. Cationic peptides: effectors in innate immunity and novel

antimicrobials. Lancet Infect Dis. 2001 Oct;1(3):156-64.

35. Izadpanah A, Gallo RL. Antimicrobial peptides. J Am Acad Dermatol. 2005;52(3 Pt 1):381-90; quiz 91-2.

36. Zasloff, M. Antimicrobial peptides of multicellular organisms. Nature. 2002;415(6870):389-95.

37. Herce, H.D., Garcia, A.E. Cell penetrating peptides: how do they do it? J Biol Phys. 2007;33(5-6):345-56.

38. Patriksson, A., van der Spoel, D. A. Temperature predictor for parallel tempering simulations. Phys Chem Chem Phys. 2008;10(15):2073-7.

39. Bahar, A.A., Ren, D. Antimicrobial peptides. Pharmaceuticals (Basel). 2013;6(12):1543-75.

40. Guilhelmelli, F., Vilela, N., Albuquerque, P., Derengowski. LaS., Silva-Pereira, I., Kyaw, C.M. Antibiotic development challenges: the various mechanisms of action of antimicrobial peptides and of bacterial resistance. Front Microbiol. 2013;4:353.

41. Saberwal, G., Nagaraj, R. Cell-lytic and antibacterial peptides that act by perturbing the barrier function of membranes: facets of their conformational features, structure-function correlations and membrane-perturbing abilities. Biochim Biophys Acta. 1994;1197(2):109-31.

42. Clark, K.S., Svetlovics, J., McKeown, A.N., Huskins, L., Almeida, P.F. What determines the activity of antimicrobial and cytolytic peptides in model membranes. Biochemistry. 2011;50(37):7919-32.

43. Seo M. D., Won H. S., Kim J. H., Mishig-Ochir T. & Lee B. J. Antimicrobial peptides for therapeutic applications: a review. Molecules 17, 12276–12286 (2012).

44. Hancock RE, Powers JP The relationship between peptide structure and antibacterial activity. Peptides. 2003 Nov;24(11):1681-91.

45. Balayssac, S., Burlina, F., Convert, O., Bolbach, G., Chassaing, G., Lequin, O. Comparison of penetratin and other homeodomain-derived cell-penetrating

peptides: interaction in a membrane-mimicking environment and cellular uptake efficiency. Biochemistry. 2006;45(5):1408-20.

46. Redondo-Morata, L., Giannotti, M.I., Sanz F. Influence of cholesterol on the phase transition of lipid bilayers: a temperature-controlled force spectroscopy study. Langmuir. 2012;28(35):12851-60.

47. Eeman M, Deleu M. From biological membranes to biomimetic model membranes. *Biotechnol Agron Soc Environ* 2010 14(4), 719-736. 2010;14:719-36.

48. Sengupta, D., Leontiadou, H., Mark, A.E., Marrink, S.J. Toroidal pores formed by antimicrobial peptides show significant disorder. Biochim Biophys Acta. 2008;1778(10):2308-17.

49. Pálffy, R., Gardlík, R., Behuliak, M., Kadasi, L., Turna, J., Celec, P. On the physiology and pathophysiology of antimicrobial peptides. Mol Med. 2009;15(1-2):51-9.

50. Peters, B.M., Shirtliff, M.E., Jabra-Rizk, M.A. Antimicrobial peptides: primeval molecules or future drugs? PLoS Pathog. 2010;6(10):e1001067.

51. Peschel, A., Sahl, H.G. The co-evolution of host cationic antimicrobial peptides and microbial resistance. Nat Rev Microbiol. 2006;4(7):529-36.

52. Strandberg, K.L., Richards, S.M., Tamayo, R., Reeves, L.T., Gunn, J.S. An altered immune response, but not individual cationic antimicrobial peptides, is associated with the oral attenuation of Ara4N-deficient Salmonella enterica serovar Typhimurium in mice. PLoS One. 2012;7(11):e49588

53. McPhee, J.B., Bains, M., Winsor, G., Lewenza, S., Kwasnicka,A., Brazas, M.D. et al. Contribution of the PhoP-PhoQ and PmrA-PmrB two-component regulatory systems to Mg2+-induced gene regulation in Pseudomonas aeruginosa. J Bacteriol. 2006;188(11):3995-4006.

54. Andrä, J.; Goldmann, T., Ernst C.M., Peschel, A., Gutsmann, T. Multiple peptide resistance factor (MprF)-mediated Resistance of Staphylococcus aureus against antimicrobial peptides coincides with a modulated peptide interaction with artificial membranes comprising lysyl-phosphatidylglycerol.

J Biol Chem. 2011;286(21):18692-700.

55. Kristian, S.A., Datta, V., Weidenmaier, C., Kansal, R., Fedtke, I., Peschel, A. et al. D-alanylation of teichoic acids promotes group a streptococcus antimicrobial peptide resistance, neutrophil survival, and epithelial cell invasion. J Bacteriol. 2005;187(19):6719-25.

56. Saar-Dover, R., Bitler, A., Nezer, R., Shmuel-Galia, L., Firon, A., Shimoni, E. et al. D-alanylation of lipoteichoic acids confers resistance to cationic peptides in group B streptococcus by increasing the cell wall density. PLoS Pathog. 2012;8(9):e1002891.

57. McBride, S.M., Sonenshein, A.L. The dlt operon confers resistance to cationic antimicrobial peptides in Clostridium difficile. Microbiology. 2011;157(Pt 5):1457-65.

58. Peschel, A., Otto, M., Jack, R.W., Kalbacher, H., Jung, G., Götz, F. Inactivation of the dlt operon in Staphylococcus aureus confers sensitivity to defensins, protegrins, and other antimicrobial peptides. J Biol Chem. 1999;274(13):8405-10.

59. Sperandio, B., Regnault, B., Guo, J., Zhang, Z., Stanley, S.L., Sansonetti, P.J. et al. Virulent Shigella flexneri subverts the host innate immune response through manipulation of antimicrobial peptide gene expression. J Exp Med. 2008;205(5):1121-32.

60. Islam, M.R., Nagao, J., Zendo, T., Sonomoto, K. Antimicrobial mechanism of lantibiotics. Biochem Soc Trans. 2012;40(6):1528-33.

61. Chan, C., Burrows, L.L., Deber, C.M. Helix induction in antimicrobial peptides by alginate in biofilms. J Biol Chem. 2004;279(37):38749-54.

62. Schmidtchen, A., Frick, I.M., Andersson, E., Tapper, H., Björck, L. Proteinases of common pathogenic bacteria degrade and inactivate the antibacterial peptide LL-37. Mol Microbiol. 2002;46(1):157-68.

63. Sieprawska-Lupa, M., Mydel, P., Krawczyk, K., Wójcik, K., Puklo, M., Lupa, B. et al. Degradation of human antimicrobial peptide LL-37 by Staphylococcus aureus-derived proteinases. Antimicrob Agents Chemother.

2004;48(12):4673-9.

64. Poole, K. Efflux pumps as antimicrobial resistance mechanisms. Ann Med. 2007;39(3):162-76.

65. Tzeng, Y.L., Ambrose, K.D., Zughaier, S., Zhou, X., Miller, Y.K., Shafer, W.M. et al. Cationic antimicrobial peptide resistance in Neisseria meningitidis. J Bacteriol. 2005;187(15):5387-96.

66. Tzeng, Y.L., Stephens, D.S. Antimicrobial peptide resistance in Neisseria meningitidis. Biochim Biophys Acta. 2015;1848(11 Pt B):3026-31.

67. Warner, D.M., Shafer, W.M., Jerse, A.E. Clinically relevant mutations that cause derepression of the Neisseria gonorrhoeae MtrC-MtrD-MtrE Efflux pump system confer different levels of antimicrobial resistance and *in vivo* fitness. Mol Microbiol. 2008;70(2):462-78.

68. Frick, I.M., Akesson, P., Rasmussen, M., Schmidtchen, A., Björck, L. SIC, a secreted protein of Streptococcus pyogenes that inactivates antibacterial peptides. J Biol Chem. 2003;278(19):16561-6.

69. Hancock, R.E. Peptide antibiotics. Lancet. 1997;349(9049):418-22.

70. Khandelia, H., Langham, A.A., Kaznessis, Y.N. Driving engineering of novel antimicrobial peptides from simulations of peptide-micelle interactions. Biochim Biophys Acta. 2006;1758(9):1224-34.

71. Lehrer, R.I., Ganz, T. Antimicrobial peptides in mammalian and insect host defence. Curr Opin Immunol. 1999;11(1):23-7.

72. Ganz, T. The role of antimicrobial peptides in innate immunity. Integr Comp Biol. 2003;43(2):300-4.

73. Nicolas, P., El Amri, C. The dermaseptin superfamily: a gene-based combinatorial library of antimicrobial peptides. Biochim Biophys Acta. 2009;1788(8):1537-50.

74. Vouille, V., Amiche, M., Nicolas, P. Structure of genes for dermaseptins B, antimicrobial peptides from frog skin. Exon 1-encoded prepropeptide is conserved in genes for peptides of highly different structures and activities.

FEBS Lett. 1997;414(1):27-32.

75. Savoia, D., Guerrini, R., Marzola, E., and Salvadori, S. (2008) Synthesis and antimicrobial activity of dermaseptin S1 analogues. *Bioorg. Med. Chem. 16*, 8205–8209.

76. Strahilevitz, J., Mor, A., Nicolas, P., and Shai, Y. (1994) Spectrum of antimicrobial activity and assembly of dermaseptin-B and its precursor form in phospholipid membranes. *Biochemistry 33*, 10951–10960.

77. La Rocca, P., Shai, Y., Sansom, M.S. Peptide-bilayer interactions: simulations of dermaseptin B, an antimicrobial peptide. Biophys Chem. 1999;76(2):145-59.

78. Mor, A., and Nicolas, P. (1994) The NH2-terminal R-helical domain 1-18 of dermaseptin is responsible for antimicrobial activity. *J. Biol. Chem. 269*, 1934–1939.

79. Pouny, Y., Rapaport, D., Mor, A., Nicolas, P., Shai, Y. Interaction of antimicrobial dermaseptin and its fluorescently labeled analogues with phospholipid membranes. Biochemistry. 1992;31(49):12416-23.

80. Galanth C, Abbassi F, Lequin O, Ayala-Sanmartin J, Ladram A, Nicolas P, and Amiche M (2009) Mechanism of Antibacterial Action of Dermaseptin B2: Interplay between Helix−Hinge−Helix Structure and Membrane Curvature Strain *Biochemistry* 2009 *48* (2), 313-327 DOI: 10.1021/bi802025a

81. Lequin, O., Bruston, F., Convert, O., Chassaing, G., Nicolas, P. Helical structure of dermaseptin B2 in a membrane-mimetic environment. Biochemistry. 2003;42(34):10311-23.

82. Shai, Y. Mechanism of the binding, insertion and destabilization of phospholipid bilayer membranes by alpha-helical antimicrobial and cell non-selective membrane-lytic peptides. Biochim Biophys Acta. 1999;1462(1-2):55-70.

83. Noinville, S., Bruston, F., El Amri, C., Baron, D., Nicolas, P. Conformation, orientation, and adsorption kinetics of dermaseptin B2 onto synthetic supports at aqueous/solid interface. Biophys J. 2003;85(2):1196-206.

84. El Amri, C., Lacombe, C., Zimmerman, K., Ladram, A., Amiche, M., Nicolas, P. et al. The plasticins: membrane adsorption, lipid disorders, and biological activity. Biochemistry. 2006;45(48):14285-97.

85. Gallo, R.L. In defense of skin: antimicrobial peptides have their day. Interview by Hannah Branch. Future Microbiol. 2013;8(7):829-31.

86. El Amri, C., Lacombe, C., Zimmerman, K., Ladram, A., Amiche, M., Nicolas, P. et al. The plasticins: membrane adsorption, lipid disorders, and biological activity. Biochemistry. 2006;45(48):14285-97.

87. Zemel, A., Ben-Shaul, A., May, S. Perturbation of a lipid membrane by amphipathic peptides and its role in pore formation. Eur Biophys J. 2005;34(3):230-42.

88. Joanne, P., Galanth, C., Goasdoué, N., Nicolas, P., Sagan, S., Lavielle, S. et al. Lipid reorganization induced by membrane-active peptides probed using differential scanning calorimetry. Biochim Biophys Acta. 2009;1788(9):1772-81.

89. Khandelia, H., Kaznessis, Y.N. Molecular dynamics investigation of the influence of anionic and zwitterionic interfaces on antimicrobial peptides' structure: implications for peptide toxicity and activity. Peptides. 2006;27(6):1192-200.

90. Schweizer, F. Cationic amphiphilic peptides with cancer-selective toxicity. Eur J Pharmacol. 2009;625(1-3):190-4.

91. Mader, J.S., Hoskin, D.W. Cationic antimicrobial peptides as novel cytotoxic agents for cancer treatment. Expert Opin Investig Drugs. 2006;15(8):933-46.

92. Gaspar, D., Veiga, A.S., Castanho, M.A. From antimicrobial to anticancer peptides. A review. Front Microbiol. 2013;4:294.

93. van Zoggel, H., Carpentier, G., Dos Santos, C., Hamma-Kourbali, Y., Courty, J., Amiche, M. et al. Antitumor and angiostatic activities of the antimicrobial peptide dermaseptin B2. PLoS One. 2012;7(9):e44351.

94. Coates AR, Halls G, Hu Y. Novel classes of antibiotics or more of the same? British Journal of Pharmacology. 2011;163(1):184-194. doi:10.1111/j.1476-

5381.2011.01250.x.

95. Saunders, M.G., Voth, G.A. Coarse-graining methods for computational biology. Annu Rev Biophys. 2013;42:73-93.

96. Tanaka, S., Scheraga, H.A. Medium- and long-range interaction parameters between amino acids for predicting three-dimensional structures of proteins. Macromolecules. 1976;9(6):945-50.

97. Marrink, S.J., Mark, A.E. Molecular dynamics simulation of the formation, structure, and dynamics of small phospholipid vesicles. J Am Chem Soc. 2003;125(49):15233-42.

98. Tanaka, S., Scheraga, H.A. Medium- and long-range interaction parameters between amino acids for predicting three-dimensional structures of proteins. Macromolecules. 1976;9(6):945-50.

99. Miyazawa S, Jernigan R.L. Estimation of effective interresidue contact energies from protein crystal structures: Quasi-chemical approximation. Macromolecules 1985, 18,534

100. Tirion, M.M. Large Amplitude Elastic Motions in Proteins from a Single-Parameter, Atomic Analysis. Phys Rev Lett. 1996;77(9):1905-8.

101. Marrink, S.J., Tieleman, D.P. Perspective on the Martini model. Chem Soc Rev. 2013;42(16):6801-22.

102. Marrink, S.J., Risselada, H.J., Yefimov, S., Tieleman, D.P., de Vries, A.H. The MARTINI force field: coarse grained model for biomolecular simulations. J Phys Chem B. 2007;111(27):7812-24.

103. Marrink, S.J., Lindahl, E., Edholm, O., Mark, A.E. Simulation of the spontaneous aggregation of phospholipids into bilayers. J Am Chem Soc. 2001;123(35):8638-9.

104. Marrink, S.J., de Vries, A.H., Harroun, T.A., Katsaras, J., Wassall, S.R. Cholesterol shows preference for the interior of polyunsaturated lipid membranes. J Am Chem Soc. 2008;130(1):10-1.

105. Marrink, S.J., de Vries, A.H., Tieleman, D.P. Lipids on the move: simulations of

membrane pores, domains, stalks and curves. Biochim Biophys Acta. 2009;1788(1):149-68.

106. Marrink, S.J., Periole, X., Tieleman, D.P., de Vries, A.H. Comment on "On using a too large integration time step in molecular dynamics simulations of coarse-grained molecular models" by M. Winger, D. Trzesniak, R. Baron and W. F. van Gunsteren, Phys. Chem. Chem. Phys., 2009, 11, 1934. Phys Chem Chem Phys. 2010;12(9):2254-6; author reply 7-8.

107. Marrink, S.J., Risselada, J., Mark, A.E. Simulation of gel phase formation and melting in lipid bilayers using a coarse grained model. Chem Phys Lipids. 2005;135(2):223-44.

108. Baaden, M., Marrink, S.J. Coarse-grain modelling of protein-protein interactions. Curr Opin Struct Biol. 2013;23(6):878-86.

109. Wassenaar, T.A., Ingólfsson, H.I., Böckmann, R.A., Tieleman, D.P., Marrink, S.J. Computational Lipidomics with insane: A Versatile Tool for Generating Custom Membranes for Molecular Simulations. J Chem Theory Comput. 2015;11(5):2144-55.

110. Fiser, A., Sali, A. Modeller: generation and refinement of homology-based protein structure models. Methods Enzymol. 2003;374:461-91.

111. Jensen Frank (1999). *Introduction to Computational Chemistry*. England: John Wiley and Sons Ltd.

112. Verlet, Loup (1967). "Computer "Experiments" on Classical Fluids. I. Thermodynamical Properties of Lennard–Jones Molecules" Physical Review 159: 98–103. doi:10.1103/PhysRev.159.98. .

113. Skeel, R. D., "Variable Step Size Destabilizes the Stömer/Leapfrog/Verlet Method", BIT Numerical Mathematics, Vol. 33, 1993, p. 172–175.]

114. Berendsen H. J. C., Postma J. P. M., van Gunsteren W. F., DiNola A., and Haak J. R (1984) Molecular dynamics with coupling to an external bath, The Journal of Chemical Physics 81, 3684

115. Silhavy, T.J., Kahne, D., Walker, S. The bacterial cell envelope. Cold Spring Harb Perspect Biol. 2010;2(5):a000414.

116. Humphrey, W., Dalke, A. and Schulten, K. (1996) VMD: Visual molecular dynamics, J Mol Graphics 14, 33-&)

117. Barnoud, J., Rossi, G., Monticelli, L. Lipid membranes as solvents for carbon nanoparticles. Phys Rev Lett. 2014;112(6):068102.

References: HCV peptide.

1. Dvory-Sobol, H. , Pang,P.S. and Glenn,J.S. "The Future of HCV Therapy: NS4B as an Antiviral Target." *Viruses* 2.11 (2010): 2481–2492. *PMC*. Web. 11 Mar
2. Elazar, M., Liu, P., Rice, C. M. and Glenn, J. S. (2004). An N-terminal amphipathic helix in hepatitis C virus (HCV) NS4B mediates membrane association, correct localization of replication complex proteins, and HCV RNA replication. J Virol *78*, 11393-11400.
3. Liefhebber, J.M., Brandt, B.W., Broer, R., Spaan, W.J., van Leeuwen, H.C. Hepatitis C virus NS4B carboxy terminal domain is a membrane binding domain. *Virology Journal* 2009;6:62. doi:10.1186/1743-422X-6-62.
4. Wuthier,R.E.: Two-dimensional chromatography on silica gel-loaded paper for the microanalysis of polar lipidsJ. Lipid Res. 1966 7:(4) 544-550
5. Gao, L., Aizaki, H., He, J. W. and Lai, M. M. (2004). Interactions between viral nonstructural proteins and host protein hVAP-33 mediate the formation of hepatitis C virus RNA replication complex on lipid raft. J Virol *78*, 3480-3488.
6. Stansfeld,P.J, Hopkinson,R., Ashcroft, F.M. and Sansom,M.S.P. PIP2-Binding Site in Kir Channels: Definition by Multiscale Biomolecular Simulations *Biochemistry* 2009 *48* (46), 10926-10933
7. Marrink, S. J., de Vries, A. H. and Mark, A. E. (2004) Coarse grained model for semiquantitative lipid simulations, J Phys Chem B 108, 750-760.
8. Bond, P. J. and Sansom, M. S. (2006) Insertion and assembly of membrane proteins via simulation, J Am Chem Soc 128, 2697-2704.
9. Carpenter, T., Bond, P. J., Khalid, S. and Sansom, M. S. P. (2008) Self-assembly of a simple membrane protein: Coarse-grained molecular dynamics simulations of the influenza M2 channel, Biophysical Journal 95, 3790-3801).
10. Berendsen, H. J. C., Postma, J. P. M, van Gunsteren,W.F., DiNola, A. and Haak, J.R. 1984. Molecular dynamics with coupling to an external bath. J. Chem. Phys. 81:3684–3690.)
11. Humphrey, W., Dalke, A. and Schulten, K. (1996) VMD: Visual molecular dynamics, J Mol Graphics 14, 33-&)

12. Gao, L., Aizaki, H., He, J. W. and Lai, M. M. (2004). Interactions between viral nonstructural proteins and host protein hVAP-33 mediate the formation of hepatitis C virus RNA replication complex on lipid raft. J Virol *78*, 3480-3488.
13. Palomares-Jerez, M. F., Nemesio, H., Franquelim, H. G., Castanho, M. A., Villalain, J.N-terminal AH2 segment of protein NS4B from hepatitis C virus. Binding to and interaction with model biomembranes, Biochimica Et Biophysica Acta, 1828 (2013) 1938-1952.
14. Ashworth Briggs1, E.L., Gomes1,2,R., Collier1,W., Findlow1,I.S., McCormick2*, C.J., Philip T.F., Williamson1. Interaction between the NS4B amphipathic helix, AH2, and charged lipid Head groups alters membrane morphology and AH2 oligomeric state - implications for the Hepatitis C Virus life cycle.
15. Christie,W.W.: Rapid separation and quantification of lipid classes by high performance liquid chromatography and mass (light-scattering) detection. J. Lipid Res. 1985 26:(4) 507-12
16. Van der Spoel, D., Lindahl, E., Hess, B., Groenhof, G., Mark, A. E., and Berendsen, H. J. C. (2005) Gromacs: Fast, Flexible, and Free, J Comput Chem 26, 1701-1718.
17. Berendsen, H. J. C., Vanderspoel, D. and Vandrunen, R. (1995) Gromacs - a Message-Passing Parallel Molecular-Dynamics Implementation, Comput Phys Commun 91, 43-56.
18. Hess, B., Kutzner, C., van der Spoel, D. and Lindahl, E. (2008) GROMACS 4: Algorithms for highly efficient, load-balanced, and scalable molecular simulation, J Chem Theory Comput 4, 435-447.)
19. Marrink, S. J., Risselada, H. J., Yefimov, S., Tieleman, D. P. and de Vries, A. H. (2007) The MARTINI force field: coarse grained model for biomolecular simulations, J Phys Chem B 111, 7812-7824.).
20. Stahelin, R. V, Membrane Binding and Bending in Ebola VP40 Assembly and Egress, Frontiers in Microbiology, volume 5, 2014
21. Godoy, P., Hewitt, N.J., Albrecht, U. et al. Recent advances in 2D and 3D in vitro systems using primary hepatocytes, alternative hepatocyte sources and non-parenchymal liver cells and their use in investigating mechanisms of hepatotoxicity, cell signaling and ADME. *Archives of Toxicology* 2013;87(8):1315-1530. doi:10.1007/s00204-013-1078-5.
22. Tapas, K. R., Vladimir, P., Skipski, M.B., Essner,E. and Archibald,F.M.: Lipid

Composition of Rat Liver Plasma Membranes. *J. Biol. Chem. 1969, 244:5528-5536.*

23. Sklan, E.H., Glenn, J.S. HCV NS4B: From Obscurity to Central Stage. In: Tan SL, editor. Hepatitis C Viruses: Genomes and Molecular Biology. Norfolk (UK): Horizon Bioscience; 2006. Chapter 8. Available from: http://www.ncbi.nlm.nih.gov/books/NBK1633/
24. Egger, D., Wolk, B., Gosert, R., Bianchi, L., Blum, H. E., Moradpour, D. Bienz, K. (2002). Expression of Hepatitis C Virus Proteins Induces Distinct Membrane Alterations Including a Candidate Viral Replication Complex. J Virol *76*, 5974-5984.